Faculdade de Engenharia da Universidade do Porto

Departamento de Engenharia Mecânica

Condition Monitoring of Motor Bearing Faults with Vibration and Current Signals

João Pedro Ferreira Araújo

Master's Degree Dissertation presented to

Faculdade de Engenharia da Universidade do Porto

Dissertation supervised by

Professor José Dias Rodrigues — Associate Professor at FEUP

Engineer Carina Freitas — Researcher at Siemens

Porto, 2017

LaTeX

FEUP-U.PORTO

João Araújo

2017

In memory of Carmen Marques.

Acknowledgments

As this Master's Degree Thesis comes to a conclusion, it is an appropriate time to mention some people who helped me in this final project.

I would first like to express my most sincere appreciation to my supervisor, Eng. Carina Freitas, for guidance provided during the development of this work and her admiring persistence when problems came along.

I also show my esteem to Dr. José F. D. Rodrigues for encouraging me to pursuit excellence.

A special thank you to all of Siemens PLM (Research Technology and Development) for the support: Jacques Cuenca for the inspiration he conveyed; Thomas D'Hondt for adding some interesting insights; Alexandre Maurício for being a very patient and supporting research colleague; Andrea Renno for his unique friendship; and every one else for creating an excellent environment around me.

At the end of the Master's Degree in Mechanical Engineering, a special reference to Faculdade de Engenharia da Universidade do Porto for these incredible years and resources put at the disposal of its students in order to provide them a superior education, professional and personally.

On a more personal note, I express my gratitude to my girlfriend Tânia Vilarinho, for her love, understanding and dedication. Also to the very good friends I have made in college over the past few years, with a special greeting to João Ramos, a friend who has unconditionally been on my side.

Last, but not least, my family, who always encouraged me to pursue my dreams. A special note to my mother, Manuela Ferreira, without whom I would not be who I am today. My deepest gratitude and I hope to make you proud.

Keywords

Condition Monitoring

Bearing Faults

Induction Motors

Vibration Signals

Cyclic Spectral Correlation

Envelope Analysis

Palavras-Chave

Monitorização de Condição

Defeitos em Rolamentos

Motores de Indução

Sinais de Vibração

Cyclic Spectral Correlation

Envelope Analysis

Abstract

Manufacturing equipments in industrial plants are often expensive. By ensuring their proper functioning can be a way of reducing repair-related costs along with unnecessary stoppage time of the production unit. Consequently, corporates all over the world have started to dedicate some of their investigation to maintenance programs that would allow to reduce these costs. Hence the recent growth of the Condition Monitoring field.

Induction motors are broadly used different production units, and bearing faults are known to account for most of their failures. There are some developments in describing motor's operation condition by vibration analysis.

Vibration analysis is one of the most often used techniques as a means of diagnostic in the condition monitoring field. In late years electrical current signal analysis has been an emerging force as well, with the advantage of being a less intrusive method. However, in the literature there are mixed opinions regarding which is the best method and which relevant diagnostic information can be obtained differently from one another.

Following this line of reasoning, the focus of this dissertation will be to analyse both types of signals for diagnostic purposes on two induction motors: one healthy reference and one with an unknown bearing fault.

For this analysis, several signal processing techniques were studied and applied to the measured signals. Bearing fault diagnosis has been performed by envelope analysis for decades and is still proven to be the most effective procedure. The challenge presented for this work was to process signals subject to severe electromagnetic interference. Still, the Cyclic Spectral Correlation proved to be an effective tool in determining an appropriate frequency band for demodulation to be performed.

A semi-automated processing procedure was established for vibration signals. At this stage current signals did not reveal relevant diagnostic information.

Resumo

Equipamentos industriais de unidades produção são frequentemente caros. Assegurando o seu funcionamento adequado é uma boa forma de reduzir custos associados à sua reparação, bem como tempo de paragem da unidade desnecessário. Consequentemente, empresas por todo o mundo têm dedicado parte da sua investigação a programas de manutenção para reduzir estes custos. Daí o recente crescimento do ramo de *Condition Monitoring*.

Motores de indução são de uso comum nestas unidades de produção, e além disso, é sabido que defeitos em rolamentos são responsáveis por uma parte significativa das suas falhas. Existem já alguns desenvolvimentos em análise de vibrações no que toca a descrever a condição de operação de motores.

Análise de vibrações é um dos métodos mais frequentemente empregues como meio de diagnóstico em *condition monitoring*. Recentemente, também a análise de sinais de corrente elétrica tem surgido como uma força emergente no ramo, com a vantagem de ser um método menos intrusivo. Contudo, na literatura existente as opiniões são mistas no que toca à distinção do melhor método, bem como à informação relevante que se pode extrair, diferente de cada um, em termos de diagnóstico.

Seguindo este raciocínio, o foco desta dissertação incidirá sobre a análise comparativa de ambos os tipos de sinais provenientes de dois motores: um de referência dita "saudável", e outro com um defeito de rolamento indeterminado.

Para esta análise, várias técnicas de processamento de sinal foram estudadas e aplicadas aos sinais medidos. Diagnóstico de defeitos em rolamentos tem vindo a ser feito há várias décadas por *Envelope Analysis*, e continua provado que é o procedimento mais eficaz para o efeito. O principal desafio do presente trabalho passou pelo processamento de sinais sob condições de severa interferência eletromagnética. Apesar deste factor, o *Cyclic Spectral Correlation* provou ser uma ferramenta eficaz na deteção de uma banda de frequência apropriada para efetuar desmodulação do sinal.

A partir da análise efetuada, foi possível estabelecer um procedimento semi-automatizado para processar sinais de vibração. Nesta fase, os sinais de corrente não revelaram informação relevante para efeitos de diagnóstico.

Nomenclature

Latin characters

Variable	Description	Units
A	Loop Area	m^2
A_i	Magnitude of i_{th} component	-
a_n, b_n	Fourier coefficients	-
B	Magnetic flux density	T
$BPFI$	Ball Pass Frequency in the Inner race	Hz
$BPFO$	Ball Pass Frequency in the Outer race	Hz
BSF	Ball-Spin Frequency	Hz
B_w	Bandwidth	Hz
C	Cepstrum	-
d	Rolling element diameter	m
D	Pitch diameter	m
E	Expected value	-
e_{ind}	Induced voltage	V
F	Force	N
$\mathcal{F}$	Fourier transform	-
f_{abc}	Three-phase voltage (or current) signal	V (or A)
f_{bf}	Bearing fault characteristic frequency	Hz
F_c	Centre frequency	Hz
f_{dq0}	Three-phase voltage (or current) signal in dq coordinates	V (or A)
f_i	Frequency of i_{th} phenomenon	Hz
f_r	Rotation frequency	Hz
f_s	Supply frequency	Hz
FTF	Fundamental Train Frequency	Hz
H	Magnetic field intensity	A● turns/m

i_n	Electric current of n_{th} phase	A
I	Electric current intensity	A
k	Generic integer	-
K_c	Factor dependent on the machine's construction	-
k_f	Frequency modulation index	-
K_S	$dq0$ transformation matrix	-
l	Coil segment	m
m	Unbalanced mass	Kg
n	Sample number	-
N	Total number of samples	-
$n(t)$	Stationary noise signal	-
N_c	Number of turns in the coil	-
n_i	Rotation speed of i_{th} component	rad/s
n_P	Number of poles in the motor	-
n_r	Number of rolling elements	-
P	Power	W
$p(t)$	Periodic signal	-
r	Radius	m
R	Electrical resistance	Ω
R_{xx}	Autocorrelation function of signal x	-
s	Motor slip	-
$S(f, \tau)$	Short time Fourier transform	-
S_{xx}	Spectral correlation function of signal x	-
t	Continuous time	s
T, T_P	Time periods	s
T_s	Sampling period	s
v	Velocity vector	m/s
V	Voltage	V
$W(a, b)$	Wavelet transform	-
$w(t)$	Window moved along the signal	-
X	Frequency-domain signal	-
x_i	Time-domain signal of i_{th} phenomenon	-

Greek characters

Variable	Description	Units
α	Cyclic frequency	Hz
μ	Magnetic permeability	-
Φ	Magnetic flux	Wb
φ	Contact angle	rad
$\phi(f)$	Phase function	-
ϕ	Phase angle	rad
ψ	Mother wavelet	-
$\mathcal{T}$	Torque	N•m
τ	Time-lag	s
θ	Angle	rad
ϑ	Phase angle	rad
σ	Damping ratio	-
ω_i	Angular velocity of i_{th} component	rad/s

Note: The variables units are presented according to the International System of Units (SI). Throughout the text other units may be used to allow an easier interpretation.

List of Acronyms

Acronym	Description
AC	Alternate Current
AE	Acoustic Emission
ANC	Adaptive Noise Cancellation
BPFI	Ball Pass Frequency in Inner race
BPFO	Ball Pass Frequency in Outer race
BSF	Ball-Spin Frequency
CBM	Condition-Based Maintenance
CBMS	Condition-Based Maintenance Strategies
CI	Condition Indicators
CM	Condition Monitoring
CS1	1^{st}-order Cyclostationary
CS2	2^{nd}-order Cyclostationary
CSC	Cyclic Spectral Correlation
DC	Direct Current
DFT	Discrete Fourier Transform
EMI	Electromagnetic Interference
EPRI	Electric Power Research Institute
ESA	Electrical Signature Analysis
FFT	Fast Fourier Transform
FRF	Frequency Response Function
FT	Fourier Transform
FTF	Fundamental Train Frequency
HT	Hilbert Transform
IEEE	Institute of Electrical and Electronics Engineers

IFFT	Inverse Fast Fourier Transform
IGBT	Insulated-Gate Bipolar Transistor
MED	Minimum Entropy Deconvolution
MFS	Machine Fault Simulator
PWM	Pulse-Width Modulation (or Modulated)
SANC	Self-Adaptive Noise Cancellation
SISW	Siemens Industry Software
SK	Spectral Kurtosis
SQ	SpectraQuest
STFT	Short Time Fourier Transform
SVM	Space Vector Modulation
SVPWM	Space Vector Pulse-Width Modulation
TBF	Time Between Failures
TSA	Time Synchronous Average
VA	Vibration Analysis
VFD	Variable Frequency Drive

Contents

List of Figures

List of Tables

CHAPTER 1

Introduction

1.1 Condition Monitoring

According to the ISO definition

> "Condition monitoring: Detection and collection of information and data that indicates the state of a machine"[1].

Simply put, it refers to a condition-based maintenance strategy in order to prevent machine failure. It requires continuous monitoring of the machine system. As such, maintenance can be performed at a more appropriate time, as the intervention is only required when some indicator is given that the system's "health" is not at 100 %. As a consequence, this type of maintenance will lead to increase of reliability and reduction of maintenance-related costs.

Maintenance Strategies

Throughout the history of mechanical systems, maintenance techniques have also been improving, as the systems themselves. When the first mechanical systems were originated, technology wasn't as advanced as it is today, so the machines would run, developing faults with time, until they achieved a (catastrophic) failure state and they would then need to be replaced. Eventually, this Run-to-Failure type of maintenance became quite inconvenient, as it leads to large stoppage times of production units for replacement of the whole system (and consequent loss of productivity), not to mention major maintenance-related costs that would easily be prevented with experienced technicians that could determine the state of the machine by touch and sound. As technology evolved, so did the machines and maintenance techniques.

Time-based preventive maintenance takes this experience into account and stipulates that minor periodic checks of the machines' components should be performed in order to prevent a major machine breakdown. These periodic verifications would usually reflect the life of the component at which it could operate without sustaining significant damage, resulting in an overall expansion of the machine's remaining life. In other words the timespan between verifications would be shorter than the expected time between failures (TBF).

In recent decades, this strategy has also proven to have some disadvantages. It would sometimes require unit downtime without any kind of damage to attend to, as well as ex-

cessive consumption of resources, as parts would be replaced irrespective of their condition. In addition, dismounting and remounting machine components is time costly as it also requires recalibration of the machine and, when not performed properly, could introduce some misalignment or other underlying condition that could lead to improper operating conditions.

Nowadays, industrial competition is as fierce as ever and the tinniest stoppage of the production unit can cause major losses. With that in mind, many companies started adopting a condition monitoring-based maintenance (CBM), also called predictive maintenance, strategy as a way of maximizing their productivity and reducing unnecessary unit downtime to a minimum.

Based on continuous monitoring of mechanical systems, this maintenance strategy accounts for greater safety for personnel, prevention of routine shut-downs, and also a more profitable production process. It also allows for detection of machine faults at an early stage and, with proper intervention, extension of equipment life [1]. An example of the economic advantages of CMBS can be observed in Figure 1.1. It refers to the company ALcontrol and the difference in maintenance-related costs, concerning their evolution since they included oil analysis as a CBM strategy.

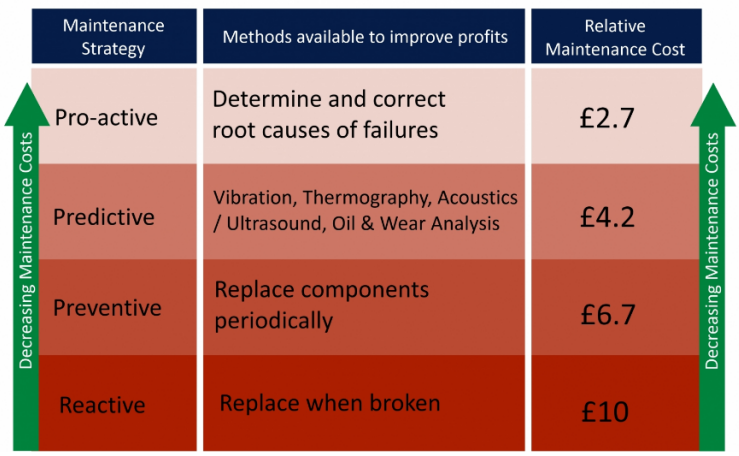

Figure 1.1: Economic Benefits of CBM [2].

Despite its advantages, predictive maintenance requires thourough analysis of the measured signals. Knowledge of the specific processing techniques is fundamental for proper interpretation of the results and performing correct diagnosis on the condition of the machine. Advantages of CBM strategy are evident when compared to a run-to-failure strategy, and even to a preventive one.

A preventive approach can be effective when the system or its components deteriorate at a predictable rate, that can be calculated if the system operates at a steady regime [3]. However, for complex machinery it is impossible to ensure that every component will have the exact same lifetime. As such, the time between repairs usually comprises the lifespan of most components, with a small percentage only being replaced after their estimated operating life, possibly leading to failure that would have otherwise never occurred. On the other hand, there are components which do not fall under this particular category: their operating lifetime cannot be precisely estimated due to some sort of randomness in their behaviour. This is the case of rolling element bearings which are one of the most common components in rotating machinery, and therefore, correct diagnosis of their condition is

essential to ensure proper operating condition of the mechanical system.

Other Maintenance Strategies

The present work will focus on vibration and electric current signature analysis as the main ways for fault detection in a three-phase induction motor's bearings. The concept behind this approach states that in the presence of a fault the rotating machinery will produce some periodic or quasi-periodic signature visible in those signals, whether we refer to the measured raw signals or the processed ones.

Nevertheless, several types of analysis can be included in CBM strategy, such as chemical analysis, vibration analysis, wear debris, thermography, performance analysis, acoustic emission (AE) or ultrasound, which may also be useful analysis tools, depending on the case.

Nowadays, the most common approaches refer to vibration and lubricant analysis. The latter consists of analysing the circulating lubricant in the machine in search of wear debris or chemical contaminants that could give some indication on the machine's "health". A combined analysis of *ferrography* and *spectrography* with a *chip detector* (for retention of metallic debris) allows the characterization of the quantity, type, shape and dimension of particles in the lubricant as well as measurement of its viscosity [3]. These techniques are, so far, the ones that provide solid diagnosis information on the mechanical system's condition at earliest stages, and therefore, the most reliable ones for determining possible underlying conditions that may affect the machine's operational condition in the future.

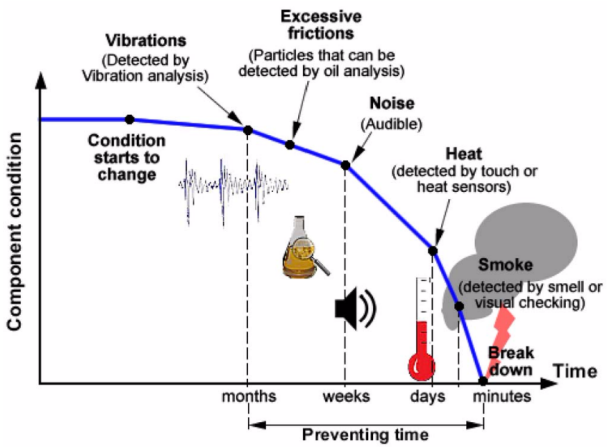

Figure 1.2: CBM strategies vs machine lifetime [1].

Electrical signature analysis (ESA) is a very recent method to integrate the vast span of techniques included in CBM strategies. Electric motors are core components of most industrial units and so, it is important to ensure their operation in proper conditions. ESA has been introduced as a tool capable of identifying existing and developing motor faults by continuous monitoring of the motor's supply current and voltage. Three-phase current supplied to the motor was measured by means of current probes installed in the supply input (one probe per phase). Those signals, as well as the acceleration ones' analysis will be discussed in further chapters.

1.2 Problem Statement and Objectives

Rolling element bearings are fundamental components present in every rotating machinery. Their failure is often of random nature and accounts for a large percentage of machine failure in industry. This topic has proven to be of particular interest, specially in core pieces of industrial machinery such as electric motors. These often operate continuously for long periods of time, with part of, or even the entire unit dependent on their operation.

The present work will investigate vibration and electric current signals as means of diagnosing bearing faults in an electric motor. Several signal processing techniques will be approached for discussion, as well as advantages of the proposed methods.

As main objectives set for the current work, we can enumerate the following:

- Understanding the fundamentals of CBM, the techniques that make it a more effective maintenance strategy and the current state of technology for performing the required types of analysis.
- Clarify the use of vibration and electric current analyses, and how they can reflect a machine's current condition for diagnosis purposes.
- Review knowledge on bearing diagnosis, specifically for medium speed regime, mechanism of fault propagation and possible influential factors.
- Understand the importance of proper procedures for dismounting and remounting machinery, as human error is often a major factor of influence in these operations. Evaluate importance of standard procedures for performing measurements correctly with minimal external influence.
- Study and apply different signal processing techniques for better assessment of the measured signals, and consequently, of the machine's condition.

1.3 Document Outline

The present text is structured in six chapters.

Chapter 2, exposes induction motors and variable frequency drives theoretical principles of operation, common issues related to their application.

Chapter 3, discloses fundamental theory on condition monitoring, namely on vibration analysis, rotating machines and the types of signals that are studied in this field. It also refers to rolling element bearings' applications and common defects.

Chapter 4, explains in detail several signal processing techniques and procedures of common use in condition monitoring. This chapter culminates in the section where, the adopted analysis procedure is presented, based on the previously discussed techniques.

Chapter 5 refers to the analysis of the results obtained for some analysis cases conducted on the measured signals.

At last but not least, chapter 6 exposes conclusions of the present work, as well as suggestions for future developments of the conducted investigation.

CHAPTER 2

Induction Motors and Variable Frequency Drives Fundamentals

2.1 Induction Motors

2.1.1 AC Machinery Fundamentals

Induction motors are very common in nowadays industrial applications. This section aims to expose the basics of alternate current (AC) machinery, as an introductory approach to understanding induction motors operation.

AC machinery consist of generators that convert mechanical energy to AC electrical energy and of motors that operate by doing the opposite conversion. There are 2 major types of AC machinery: *synchronous machines*, which magnetic field currents are supplied by distinct direct current (DC) power sources; *induction machines* which field current is supplied by magnetic induction into the field winding (usually placed on the rotor for both types of machines).

To better understand the basics of motor operation, observe the example given by figure 2.1 where a single coil is rotating inside a uniform magnetic field, B, generated by a large stationary magnet, and examine how voltage is induced.

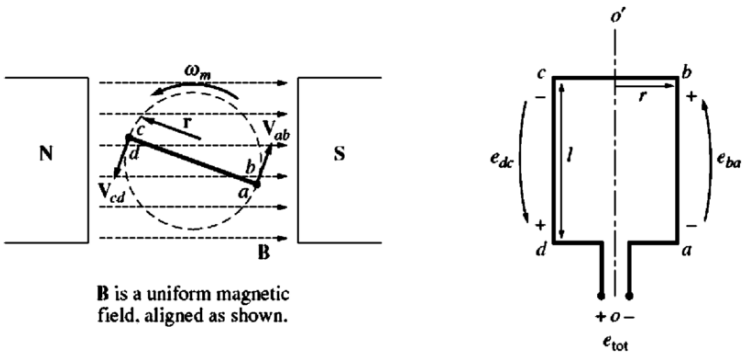

Figure 2.1: Single loop in uniform magnetic field: (a) Front view; (b) View of coil [4].

The rotating part of the machine will from henceforth be referred to as *rotor*, and the stationary part as *stator*.

To determine the voltage on the loop we need to examine how the voltage is induced in each segment. For that, let us consider equation 2.1.

$$e_{ind} = (v \times B) \bullet l \tag{2.1}$$

In this equation e_{ind} is the induced voltage, v the velocity vector, B the stator's magnetic field and l the length of the loop segment. Suppose that segments ab and cd are perpendicular to the page plane and that segments bc and da are parallel to said plane.

1. *Segment ab.* In this segment, the velocity vector is tangential to the rotation path, with B pointing from left to right as shown in the previous figure. $v \times B$ will result in a vector pointing from a to b, which will consequently be the direction of the induced voltage e_{ba}.

$$e_{ba} = vBl \ sin \ \theta_{ab} \tag{2.2}$$

2. *Segment bc.* For this case, segment l is in the page plane. As such, it is perpendicular to the $v \times B$ vector at each of its extremities. So, by equation 2.1 we can conclude that $e_{cb} = 0$.

3. By analogy, we can infer that the case of segment cd will be similar that of ba and that the case of segment da will be analogous to that of segment cb.

Considering that $e_{ind} = e_{ba} + e_{cb} + e_{dc} + e_{ad}$ and that from the trigonometric identity $sin \ \theta = sin(180° - \theta)$, since $\theta_{ab} = 180° - \theta_{cd}$, we can conclude that the induced voltage on the single coil will be given by:

$$e_{ba} = 2vBl \ sin \ \theta \tag{2.3}$$

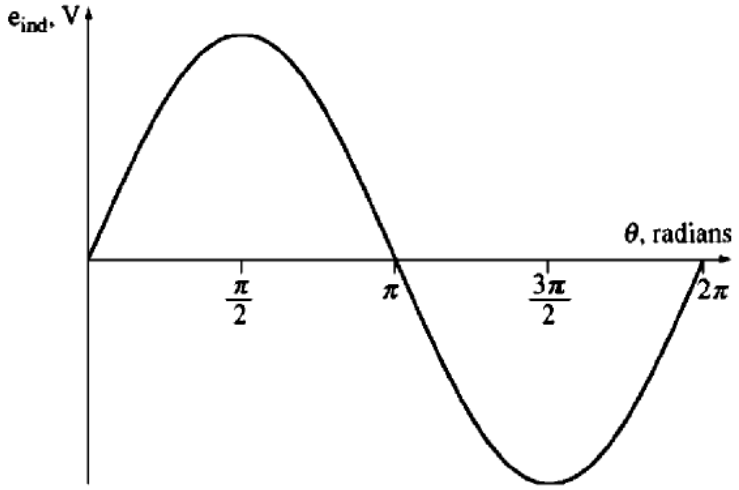

Figure 2.2: Plot of e_{ind} vs θ [4].

where $\theta = \omega t$. Considering r as the radius of the loop, measured from the rotation axis to the coil's outer segment, and ω as the angular velocity, the tangential one can be expressed as:

$$v = r\omega \tag{2.4}$$

Considering the area of the loop as $A = 2rl$, and substituting it as well as the previously determined velocity term in equation 2.3, we reach the expression:

$$e_{ind} = AB\omega \ sin \ \omega t \tag{2.5}$$

The term AB refers to a quantity known as *magnetic flux*. Note that the flux through the coil is maximum when it is perpendicular to the magnetic flux density lines, so that $sin\theta = 1$:

$$\Phi_{max} = AB \tag{2.6}$$

So, the initial equation 2.1 can finally be rewritten as:

$$e_{ind} = \Phi_{max}\omega \ sin \ \omega t \tag{2.7}$$

or, in the case of a real AC machine,

$$e_{ind} = N_C\Phi_{max}\omega \ sin \ \omega t \tag{2.8}$$

where N_C designates the number of turns of the wire of the inductor.

Hence, the voltage induced on the coil is a sinusoid with amplitude equal to the product of the magnetic flux that passes through the coil and the rotational speed of the machine.

From this point, it is now possible to examine how the machine's torque is produced. Consider that a current i is flowing inside the loop, from a to d, and that the coil is positioned at an arbitrary angle θ (such as in figure 2.1), respective to the magnetic field. To assess the torque's direction and magnitude, the Lorentz force on each segment should be calculated.

The Lorentz force can be determined by the following expression.

$$F = i(l \times B) \tag{2.9}$$

The torque on each segment is then given by:

$$\begin{aligned} \mathcal{T} &= (\text{force}) \times (\text{perpendicular distance}) \\ &= (F) \times (r \ sin \ \theta) \\ &= Fr \ sin \ \theta \end{aligned} \tag{2.10}$$

where θ is the angle between vectors r and F.

The torque direction will be dependent on vectors r and F. Figure 2.3 illustrates how the force is generated in each segment of the coil.

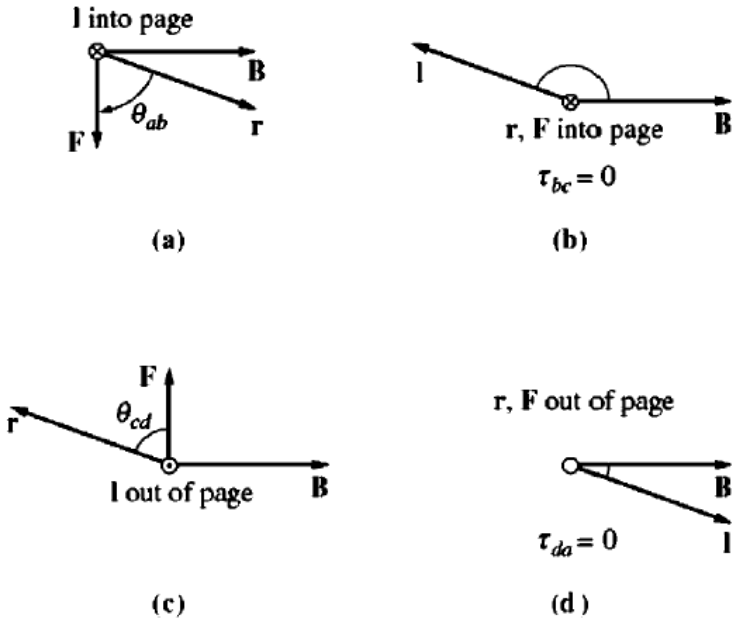

Figure 2.3: Derivation of induced force and torque on segments: (a) ab; (b) bc; (c) cd; (d) da [4].

1. For segment ab, the current is flowing into the page and the magnetic field B is pointing to the right, resulting in the Lorentz force vector, F, pointing down. So, by 2.10, the torque $\mathcal{T}_{ab}$ will be:

$$\mathcal{T}_{ab} = Fr\ sin\ \theta_{ab} \tag{2.11}$$

   in the clockwise direction.

2. In segment bc, the current is flowing in the same direction as that of the page plane, with B pointing to the right, but also in the same plane, with the resulting force, F pointing into the page, same as r. In this case, as r and F are parallel, the resulting torque will be 0.

$$\begin{aligned} \mathcal{T}_{bc} &= Fr\ sin\ \theta_{bc} \\ &= 0 \end{aligned} \tag{2.12}$$

3. As we did before for the induced voltage e_{ind}, we can infer by analogy what forces and torques will be induced on the other half of the segments. For segment cd, since l points in the opposite direction as it did for segment ab, the induced force F will now instead point upwards. Also r is symmetric to the one of that case, respective to the rotation axis. As such, the induced torque, $\mathcal{T}_{cd}$ will be in the clockwise direction, and given by:

$$\mathcal{T}_{cd} = Fr\ sin\ \theta_{cd} \tag{2.13}$$

   Concluding our comparison, the case of segment da is similar to that of cb, though this time r and F are pointing out of the page, but still parallel, resulting in a null torque.

$$\begin{aligned} \mathcal{T}_{da} &= Fr\ sin\ \theta_{da} \\ &= 0 \end{aligned} \tag{2.14}$$

By summing all the previously calculated components, and considering that $\theta_{ab} = \theta_{cd}$ we obtain:

$$\begin{aligned} \mathcal{T}_{ind} &= \mathcal{T}_{ab} + \mathcal{T}_{bc} + \mathcal{T}_{cd} + \mathcal{T}_{da} \\ &= 2rliB\ sin\ \theta \end{aligned} \tag{2.15}$$

Note that, analogous to the induced voltage e_{ind}, the torque can be expressed as a function of θ, reaching its maximum when the loop's plane is parallel to the magnetic field, and having null values when that plane is perpendicular to B.

For real AC machinery, the torque is usually expressed not only as a function of θ, but also dependent on 3 other factors:

1. Strength of the rotor's magnetic field.
2. Strength of the stator's magnetic field.
3. A constant referent to the machine's geometry.

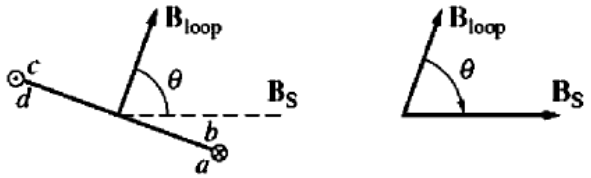

Figure 2.4: Derivation of induced torque: (a) B_{loop} produced by the loop's current, perpendicular to B_s of the stator ; (b) Geometric relation between stator and rotor's magnetic flux densities [4].

Equation 2.15 can be rewritten as:

$$\mathcal{T}_{ind} = K_c B_{loop} B_s\ sin\ \theta \tag{2.16}$$

where K_c is a factor dependent on the machine's construction, B_{loop} refers to the magnetic flux density produced by the current flowing inside the loop and is perpendicular to the loop's plane (in a real case, it would correspond to B_r, produced by current flowing in the rotor's coil), and B_s referring to the magnetic flux produced by the stator, with θ the angle between the latter two. Note that it can be confirmed that this θ, by trigonometric identities corresponds exactly to the one we had previously. So, equation 2.16 becomes:

$$\mathcal{T}_{ind} = K_c B_{loop} \times B_s \tag{2.17}$$

thus proving the dependence of the induced torque on the four aforementioned factors [4].

2.1.2 Operation principles

In the previous section we have seen that the interaction between two magnetic fields present in a machine will induce a torque that will tend to align the rotor's magnetic field with that of the stator. Should there be a way to make the stator's magnetic field rotate, the induced torque on the rotor would cause it to continuously try to "catch up" to the magnetic field of the stator. This is the basic principle behind induction motor operation. The question remains: how is the stator's magnetic rotation feasible? This fundamental principle basically builds on the assumption that if a set of three-phase currents, of equal magnitude and with 120° of difference between each, flowing in a three-phase winding, it will produce a rotating magnetic field of constant magnitude. Simply put, the three-phase winding is a set of three windings separated by a 120 electrical degrees difference, around the stator's surface [4].

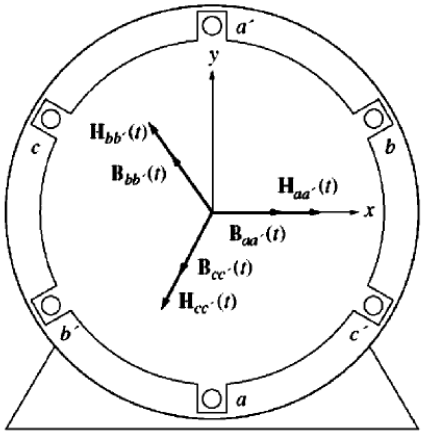

Figure 2.5: Three-phase stator [4].

Figure 2.5 shows a simple three-phase stator, with three coils separate at 120° each. This winding only produces one north and one south pole, hence it is a two-pole winding. Now, let us apply the previously mentioned set of currents on this winding and analyse what happens at each instant. The three-phase currents are given by:

$$i_{aa'} = I_M \ sin \ \omega t \ [\text{A}] \tag{2.18}$$

$$i_{bb'} = I_M \ sin \ (\omega t - 120°) \ [\text{A}] \tag{2.19}$$

$$i_{cc'} = I_M \ sin \ (\omega t - 240°) \ [\text{A}] \tag{2.20}$$

In coil *aa'*, for instance, the current flows from *a* to *a'*, producing a magnetic field intensity:

$$H_{aa'}(t) = H_M \ sin \ \omega t \angle 0° \ [\text{A} \bullet \text{turns/m}] \tag{2.21}$$

Direction of $H_{aa'}(t)$ is determined by the right hand rule, i.e. if the fingers curl in the direction of the current flow, the direction of the vector will be that pointed by the thumb. It can also be noted that the magnetic field intensity is a sinusoidal function in time, but it's direction is constant. The same happens for the other two windings *bb'* and *cc'*, though in their case we have to consider the same relative angles as we did previously for their currents.

$$H_{bb'}(t) = H_M \ sin \ (\omega t - 120°) \angle 120° \ [\text{A} \bullet \text{turns/m}] \tag{2.22}$$

$$H_{cc'}(t) = H_M \ sin \ (\omega t - 240°) \angle \ 240° \ [\text{A} \bullet \text{turns/m}] \tag{2.23}$$

Since the flux density of a magnetic field is given by:

$$B = \mu H \ [\text{T}] \tag{2.24}$$

it is only logical to assume that the equations that characterize it for each winding will assume the same form as equations 2.21-2.23. Note that μ refers to the magnetic permeability of the material.

Presented with this, we are now able to calculate the net magnetic flux density, by adding the ones respective to each coil. For the time instant in which $\omega t = 0$ we then obtain the following:

$$\begin{aligned} B_{net} &= B_{aa'} + B_{bb'} + B_{cc'} \\ &= 0 + \left(-\frac{\sqrt{3}}{2} B_M\right) \angle \ 120° + \left(\frac{\sqrt{3}}{2} B_M\right) \angle \ 240° \\ &= 1.5 B_M \angle \ -90° \end{aligned} \tag{2.25}$$

where $B_M = \mu \times H_M$. Now let us suppose that the magnetic field has rotated to a position in which $wt = 90°$. The currents for each phase will now be:

$$i_{aa'} = I_M \ sin \ 90° \ [\text{A}] \tag{2.26}$$

$$i_{bb'} = I_M \ sin \ (-30°) \ [\text{A}] \tag{2.27}$$

$$i_{cc'} = I_M \ sin \ (-150°) \ [\text{A}] \tag{2.28}$$

But, because the coils are in a fixed position we need to consider the variation of the current phase, and so:

$$B_{aa'} = B_M \angle 0° \tag{2.29}$$

$$B_{bb'} = B_M \ sin \ (-30°) \angle \ 120° \tag{2.30}$$

$$B_{cc'} = B_M \ sin \ (-150°) \angle \ 240° \tag{2.31}$$

Adding all these components we finally lead to:

$$\begin{aligned} B_{net} &= B_{aa'} + B_{bb'} + B_{cc'} \\ &= B_M \angle 0° + (-0.5 B_M) \angle 120° + (-0.5 B_M) \angle 240° \\ &= 1.5 B_M \angle 0° \end{aligned} \tag{2.32}$$

thus proving that though the position of stator's magnetic field is constantly changing (rotating in a counter-clockwise direction), its magnitude remains constant in time.

We have seen so far that the induction motor's operation is based on a rotating magnetic field (of the stator) that "forces" that of the rotor to try to keep up with it, by inducing a torque. The rotor speed however will never match that of the stator's magnetic field, otherwise both magnetic fields would be aligned and the induced torque on the rotor would be null. This phenomenon is characteristic of induction motors. Because the rotor is powered by the induction phenomenon, if both magnetic fields were aligned, the time

derivative of the magnetic flux would be null, and thus, the induced voltage would be null as well. Ultimately, there would be no current circulating in the rotor circuit and consequently, there would be no induced torque. For this reason, it is often referred to the concept of *rotor slip* or its *slip speed*.

The slip speed is given by:

$$n_{slip} = n_{sync} - n_m \tag{2.33}$$

where n_{slip} is the rotor's slip speed, n_{sync} is the speed of the magnetic fields if they were aligned (synchronous speed), and n_m the mechanical speed of the motor (rotor). The motor slip can also be expressed in percentage as in equation 2.34.

$$\begin{aligned} s &= \frac{n_{slip}}{n_{sync}} (\times 100\%) \\ &= \frac{n_{sync} - n_m}{n_{sync}} (\times 100\%) \\ &= \frac{\omega_{sync} - \omega_m}{\omega_{sync}} (\times 100\%) \end{aligned} \tag{2.34}$$

From the previous equations, we can also express the mechanical speed as a function of the synchronous speed and of the slip

$$n_m = (1 - s) n_{sync} \tag{2.35}$$

or

$$\omega_m = (1 - s) \omega_{sync} \tag{2.36}$$

This concept also applies when we want to determine the frequency of the rotor. Consider equation

$$n_{sync} = \frac{120 f_s}{n_P} \tag{2.37}$$

that gives us the motor's synchronous speed as a function of the supply frequency, f_s and the number of poles of the motor, n_P. The rotor frequency can finally be calculated as [4]:

$$\begin{aligned} f_{rotor} &= s f_s \\ &= \frac{n_{sync} - n_m}{n_{sync}} f_s \\ &= (n_{sync} - n_m) \frac{n_P}{120 f_s} f_s \\ &= \frac{n_P}{120} (n_{sync} - n_m) \end{aligned} \tag{2.38}$$

2.1.3 Construction

In the previous sections, we have seen the basic principles of operation of an induction motor. In the present one, we are going to elaborate on the induction motor's construction and some of it's basic components.

Stator

The stator of the induction motor refers to its outer stationary part. An example of this component is presented in figure 2.6. It comprises three main parts:

1. **Outer cylindrical frame:** Often made of cast iron or aluminium alloys, or welded sheet steel. It usually includes feet or a flange, dependent of the type of mounting of the motor.
2. **Magnetic path:** Consists of a series of slotted alloy steel laminations placed into the outer cylindrical frame. It is laminated on purpose, in order to minimize eddy current losses and heating.
3. **Insulated windings:** In a three-phase motor, the stator circuit possesses three sets of coils, separated by 120° (one for each phase). These coils are connected to a three-phase power supply and placed inside the slots of the magnetic path.

Figure 2.6: Typical induction motor stator [4].

Rotor

There are two different types of induction motor rotor windings: squirrel-cage rotor and wound rotor. Their main components are essentially the same, in the way that both of them comprise a set of slotted laminations of electromagnetic substance (special core steel) that are pressed together in form of a cylinder. These thin sheets are insulated from one another by means of varnish. The slots form the electric circuit, whereas the cylindrical electromagnetic substance constitutes a magnetic path [5]. Both types of rotors are presented in figure 2.8.

The squirrel-cage rotor consists of a set of copper or aluminium bars placed around its perimeter and connected on both ends to end rings. The rotor conductors are embedded in the slots. This allows for a very sturdy construction.

On the other hand, the wound rotor conductors consist of a set of windings that mirrors that of the stator. When connected at the end, they are not shorted by the end ring. Instead, the winding terminals are brought out and shorted by brushes of slip rings mounted on the shaft. This allows us to access rotor currents on the stator brushes and examine them, or add extra resistance to the rotor circuit in case we wish to alter the torque-speed characteristic of the motor. An example of the latter case is given in figure 2.7.

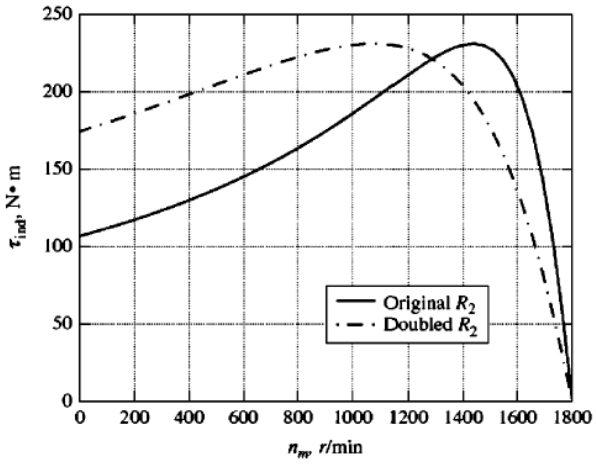

Figure 2.7: Induction motor torque-speed characteristic curve. One case for given R_2 of the rotor, and another for twice that resistance [4].

Other than the aforementioned main parts, the induction motor also comprises others such as:

- **End flanges:** One at each end for supporting the motor bearings.
- **Bearings:** There are two sets of them at each end of the motor, for supporting the motor's shaft.
- **Shaft:** Usually made of steel. It is used to transmit torque to the coupled load.
- **Cooling fan:** Often located at the opposite end as the load's. Allows for cooling of the stator and the rotor.
- **Terminal box:** Located either on the top or the side of the stator's cylindrical frame to receive external connections [5].

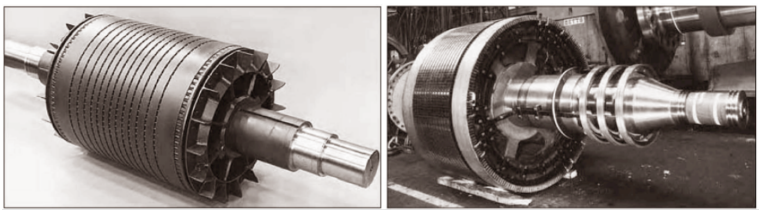

Figure 2.8: Induction motor rotors: (a) Squirrel-cage rotor; (b) Wound rotor [4].

2.1.4 Power Flow and Losses

An induction motor can be regarded as a component that transforms electrical power into mechanical, in order to supply torque to a given load for any number of applications. As such, energetic efficiency is a topic of interest, as there are several factors that may influence power losses in a motor.

There are four main types of power losses in an induction motor:

1. Electrical (or copper) losses;

2. Core losses;
3. Mechanical losses;
4. Stray load losses.

Electrical losses refer to losses related to resistive heating by Joule effect. They occur in both the stator and the rotor, and can be calculated separately once the field (rotor) and armature (stator) currents are known by the following formula:

$$P_{loss} = 3I^2R \tag{2.39}$$

where I and R can designate either stator or rotor currents and resistances, respectively, depending on the case.

Core losses are the ones caused by hysteresis and eddy currents. This hysteresis is basically due to the fact that a ferromagnetic material does not follow its saturation curve linearly (segment *ab* in figure 2.9) when it is not in the presence of the magnetic field any more, with a residual flux present in the metal's core (it follows instead segment *bc*). To force the magnetic flux back to zero a coercive magnetomotive force is required. The smaller the magnetomotive forces applied on the core metal, the smaller will be the the loop area, thus resulting in smaller core losses. This phenomenon can be observed in figure 2.9.

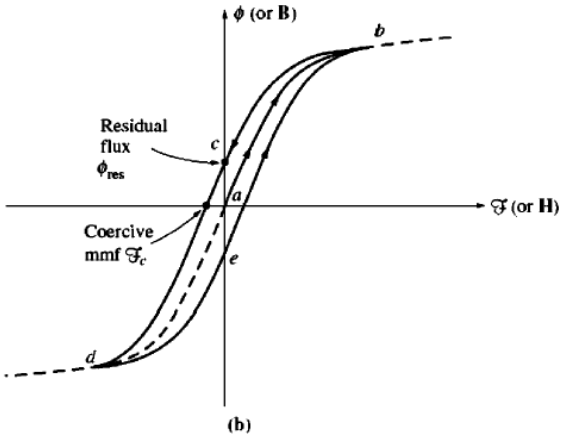

Figure 2.9: Hysteresis loop in ferromagnetic materials caused by an alternate current [4].

Eddy currents also account for part of core losses. Their generation mechanism is quite simple in fact. Suppose a time-variant magnetic flux inducing oscillating voltages in a ferromagnetic core. The same would happen to a wire wrapped around the core. These voltages account for the generation of *eddy currents* inside the core. Because these currents are circulating in a resistive material, they account for a core loss: their dissipated energy goes to heating the metallic core. The amount of energy loss depends on the length of their path inside the core. For this reason, ferromagnetic cores subject to alternating fluxes are often broken down into very thin laminations and insulated from one another.

Mechanical losses are caused by two main effects: *friction* and *windage*. Friction losses occur on the bearings that support the motor's shaft, and if present, at the brushes of the slip ring (in case of a wound rotor). Windage on the other hand refers to friction between the motor's moving parts and the surrounding air (inside the motor's casing). These losses can also be lumped together with core losses and named *no-load rotational loss*. At no-load

conditions, the input power of the motor must overcome these losses, and measuring it is a good way to estimate these losses.

Stray losses or miscellaneous losses are the ones that cannot be classified in any of the previous categories. No matter how meticulously losses are accounted for, there are always some others that will not be included in the aforementioned categories. They are generally assumed, by convention, to represent 1% of the full load.

We can observe the power flow diagram in figure 2.10 where losses are represented at each stage of the power flow in the induction motor.

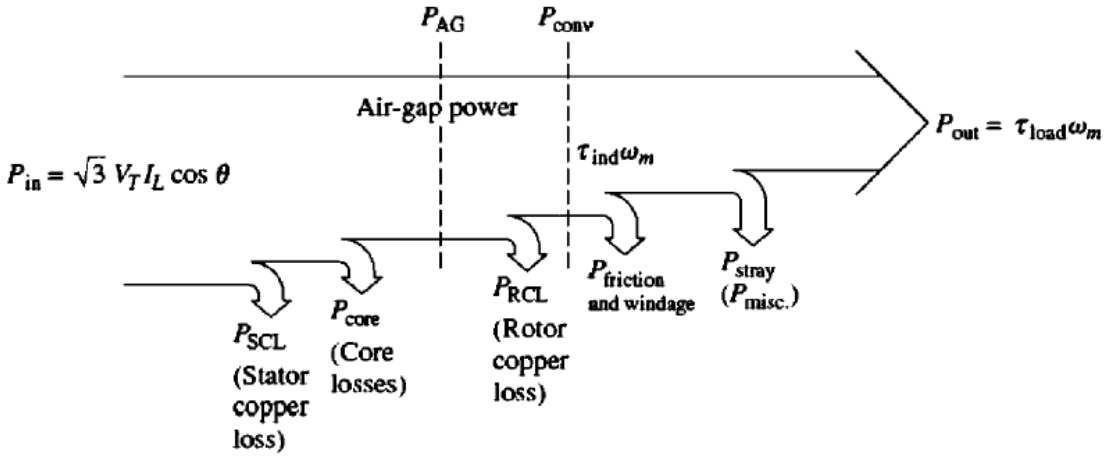

Figure 2.10: Power flow diagram of an induction motor [4].

Notice that P_{in} is represented in the form of three-phase set of currents and voltages, and the stator and rotor copper losses refer to resistive heating in the respective components. The air-gap power represents the power that from that point on is transferred from the stator to the rotor across the air-gap. Finally, $P_{conv} = \mathcal{T}_{ind}\omega_m$ is the power converted from the electrical form to the mechanical one [4].

2.1.5 Faults: Causes and Effects

Induction motors are very common in everyday applications. They are sturdy, low maintenance, able to perform with good efficiency and with a reasonably accessible power supply. They are sufficiently reliable in their operation, but also subject to various types of faults during their operating life. Induction motor faults can be classified in different types:

- **Electrical-related faults:** These may consist of unbalanced supply voltage or current, over or under voltage or current, reverse phase sequence, insulation-related faults (e.g. earth fault or inter-turn short-circuit), or overload.
- **Mechanical-related faults:** Can be any number of faults related to the mechanical parts or operation such as broken rotor bar, unbalance or misalignment, air-gap eccentricity, bearing faults, rotor or stator winding failures or soft foot.
- **Environmental-related faults:** Faults may occur due to environmental conditions such as extreme temperatures, excessive moisture, high vibration levels due to improper installation or foundation. These factors can affect the motor's performance.

Studied by	Bearing fault (%)	Stator fault (%)	Rotor fault (%)	Others (%)
IEEE	42	28	8	22
EPRI	41	36	9	14

Table 2.1: Fault occurrence studies in induction motors [5]

Studies conducted on the reliability of induction motors were performed by two separate entities - IEEE and EPRI (Electric Power Research Institute) and the results regarding the most frequent faults and percentage of occurrence are shown in table 2.1.

This classification however, is not very clear as the faults that occur either on the stator or the rotor may be of several different kinds, as the ones that were previously listed. In the present section we will elaborate on some of the faults, culminating on bearing faults, whose detection is the focus of the present work.

Broken Rotor Bar

In a squirrel-cage induction motor, if a rotor bar is cracked or completely broken, we are in the presence of the fault. There are various reasons for this fault to occur, but probably the main one is due to manufacturing defects that may cause rotor asymmetry. It could also be that non-uniform stresses occur during the brazing process in the cage assembly, or even the presence of heavy end rings in the rotor that generate large centrifugal forces during operation, and cause additional stress on the rotor bars. The breaking or cracking of a rotor bar will lead to an asymmetrical distribution in the rotor currents. If the bar is cracked, overheating will take place at that region which may lead to the breaking of the bar. Additionally, the side bars will carry higher currents, possibly inducing higher thermal and mechanical stresses that may also lead to cracking or breaking of several bars. The main causes for this fault are listed as follows:

- Manufacturing defects;
- Thermal stresses;
- Mechanical stresses due to bearing faults;
- Frequent starts of the motor and long start-up time;
- Fatigue of the rotor bar's metal.

Effects of this fault can be measured in the spectrum of the stator's current signals, as it produces side-bands at frequencies given by 2.40:

$$f_{brb} = f_s(1 \pm 2ks) \tag{2.40}$$

where f_s is the supply frequency, s is the slip and k is an integer.

Rotor Mass Unbalance

It is known that in the case of a healthy motor, the rotor rotates co-axially inside the stator. This implicates that the air-gap between the two parts is uniform, thus resulting in a uniform electromagnetic pull induced on the rotor. In case there is a mass unbalance

on the rotor, or if the rotor is bowed, this will result in air-gap eccentricity, and the electromagnetic pull on the rotor will no longer be uniform - the rotor side located on the smaller air-gap will be subject to a stronger electromagnetic pull, whereas the opposite will happen for its opposite side. In extreme cases the rotor will grind on the stator, resulting in extensive damage for both parts. This fault usually causes some noise and vibrations during motor operation.

The main causes for this type of fault are usually:

- Manufacturing defect;
- Internal misalignment or shaft bending;
- It may occur after extended operation periods, if there is uneven mass addition or subtraction, respective to its rotation axis.

Mass unbalance in the rotor causes dynamic eccentricity that lead to an oscillation in the air-gap length. The latter will result in variation of the air-gap flux density, and consequently, in the induced voltage on the rotor winding. The fluctuations of the induced voltage will produce currents at frequencies determined by the air-gap flux density harmonics, given by:

$$f_{unb} = f_s \left[\frac{k\,(1-s)}{2n_P} \right] + 1 \tag{2.41}$$

where f_s is the supply frequency, n_P is the number of poles of the motor, s is the slip of the motor and k is an integer.

Stator Winding Insulation Fault

As the title of the section suggests, this type of fault occurs due to an absence of insulation that causes a short-circuit on the stator winding. There are several types of short-circuits that can occur: between two turns of the same phase (turn-to-turn short), between two coils of the same phase (coil-to-coil short), between turns of two different phases (or even between all phases), between winding conductors and the stator core (coil to ground short), or even open-circuit fault (when the winding breaks and there is no current flow in it). Some of these faults are visible in figures 2.11 and 2.12.

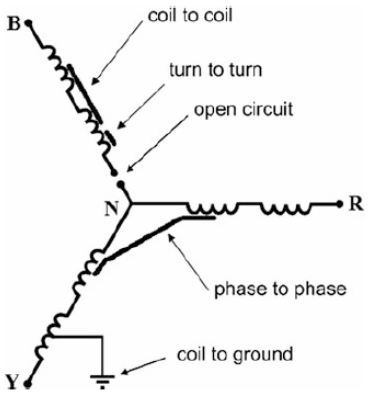

Figure 2.11: Schematics of winding insulation faults [5].

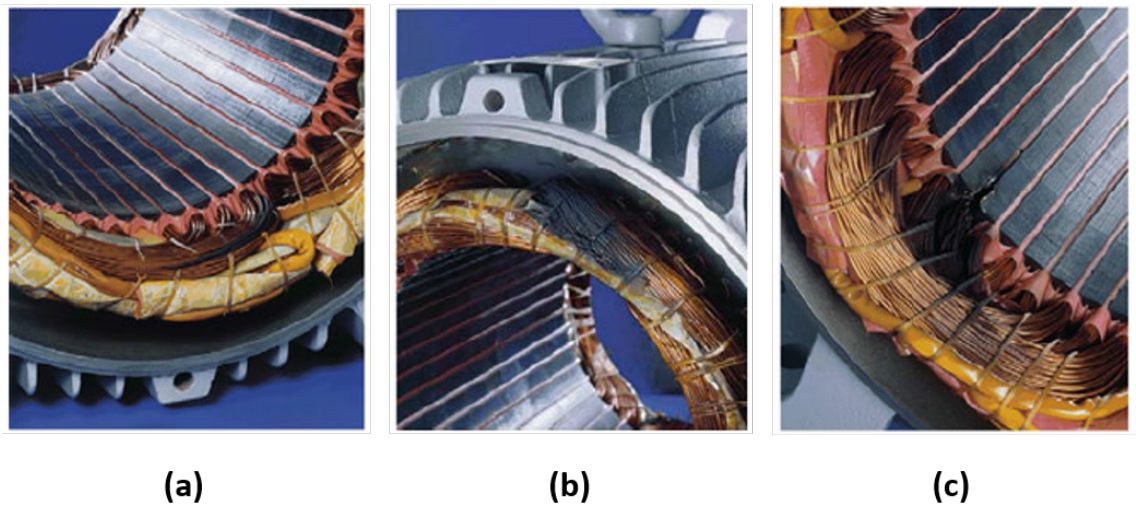

Figure 2.12: Winding insulation faults: (a) Turn-to-turn short; (b) Phase-to-phase short; (c) Coil-to-ground short [5].

Stators are constantly under stresses of various origins during their operation. These stresses can be mechanical, electrical, thermal or environmental. Eventually they will lead to the same faults in this case, but their origin is quite different and explained as follows:

- **Mechanical Stresses:** These have two main causes: either by stator coil movement or by the rotor striking the stator. Stator coil movement can occur due to the forces induced by current, and since the force is proportional to the current's square, it may lead to looseness of the top sticks and damage to the copper conductor. Striking of the stator by the rotor can occur when there is a severe misalignment between the two parts. It can also occur when there is shaft deflection or bearing failure. In this case the hits will cause the stator laminations to puncture through the coil's insulation leading to coil-to-ground short. Also related to mechanical stresses, high vibration levels may cause the stator winding to disconnect resulting in open-circuit fault.

- **Electrical Stresses:** Occur essentially because of existing voltage transients. These transients can derive from different faults: phase-to-phase short, coil-to-ground, or three-phase short. These faults on the other hand may originate from opening and closing of circuit breakers, variable frequency drives (VFDs) or even lightning. Voltage transients reduce winding lifetime and may lead, in extreme cases, to insulation faults.

- **Thermal Stresses:** Are among the main causes for insulation faults on stator windings. Thermal stresses may arise due to current overflow resultant from overload or sustained fault, high ambient temperatures, unbalanced supply voltage, lack of ventilation, among others. The rule of thumb on this matter state two facts: winding temperature increases 25% in presence of 3.5% of voltage unbalance, for the phase of highest current; and that for every $10°C$ rise above the stator winding's temperature limit, insulation lifetime will be reduced by 50%. Another factor that may contribute for thermal stresses, for instance, are constant motor start-ups in a short time span.

- **Environmental Stresses:** These stresses often occur when the motor is set up in an unsuitable environment, i.e., subject to extreme temperatures, high moisture or humidity levels, or excessive dust or other foreign materials. The latter ones may

cause reduced heat dissipation or reduced ventilation effectiveness, resulting in an excessive temperature rise that may damage the winding insulation during motor operation.

Single Phasing Fault

Single phasing fault is related to a defective power supply. It occurs when one of the phases for powering the motor is absent.

It can arise from:

- A power line that is down, or a blown fuse.
- Failure of equipment in the supply system.
- Short-circuit in one of the motor phases.

Single phasing can affect motor operation by:

- Overheating the motor winding due to the flow of negative sequence current.
- Overloading healthy phases (in case the fault occurs during motor operation), as the induced torque is defined by the load demand, and thus overheating the motor system.
- The motor will not start if there is a persistent fault on the power supply.

Single phasing can also be prevented by phase failure relays. These devices detect the lack of one (or multiple) phases in the supply and when that happens, they open a switch, cutting the power to the motor.

Bearing Faults

Induction motors possess two sets of bearings, one at each end of the rotor. Their application purpose is mainly for supporting the motor shaft, holding the rotor in place during the motor operation, letting the shaft rotate freely and reducing friction. When mounted on a motor, usually the inner race of the bearing is coupled to the shaft, with the load being transmitted by the rolling elements. This mode of operation together with the application of lubricant between the races helps to reduce friction. Physical damage sustained by any part of the bearing can be designated a bearing fault. These faults produce a distinct signature during the motor operation that will be discussed later on. In the present section we will focus on the mechanisms of fault generation. To what concerns induction motor failure, bearings are their weakest component and the ones accountable for most failure occurrences in motors, according to the revealed studies presented in table 2.1.

Bearing fault causes and effects can be described as follows:

- Excessively tight fits, and high temperature or load conditions. All these factors contribute to degradation of the bearing's lubricant. When the elastic limit of the bearing material is surpassed by the load, brinelling takes place.
- Fatigue failure occurs when the bearings are subject to extensive operation periods. It results in fragmentation of small particles of the races or rolling elements. It is a progressive process and once it takes place it spreads during the operation, resulting in increase of noise and vibration levels.

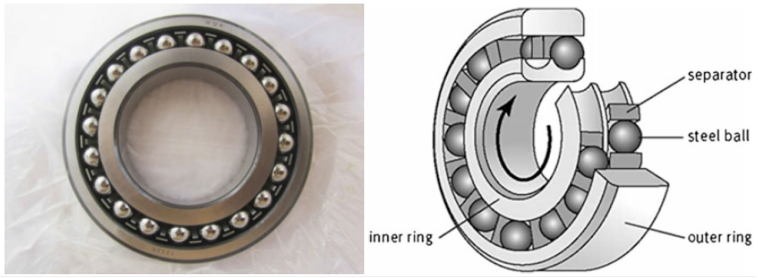

Figure 2.13: Typical ball bearings: (a) Real bearing; (b) Dissected ball bearing [5].

- Corrosion sets in if the bearing is operating in an improper environment (e.g. with a corrosive atmosphere). This type of environment may also lead to deterioration of the lubricant properties. Early fatigue can take place on the corroded bearings.
- Lubricant failure can occur if the flow is limited or in the presence of high temperatures, resulting in overheating of the bearing. This heat generation will contribute for degrading lubricant properties. Degradation of the lubricant may result in excessive wear of the bearing parts.
- Misalignment of the bearings can take place due to improper installation or operating conditions. Continuous operation under this condition contributes to developing uneven wear of the bearing parts, temperature rise and higher vibration levels.
- Electrically induced fluting (a.k.a. Electrical Discharge Machining) occurs when an electrical current flows between the bearing races and through the rolling elements. Current spikes at the interfaces etch a fluting pattern on the bearing surfaces. This is a particular problem in motor bearings where usually variable frequency drives (VFDs) are present and known to cause this effect due to their large voltage transients. This issue can be partially prevented by using electro-conductive grease or installing a shaft grounding system [6].

Examples of faults generated by these mechanisms are shown on figure 2.14. For further reading on the subject of induction motors and faults, the reader is suggested to consult references [1], [4], [5], [6], [7].

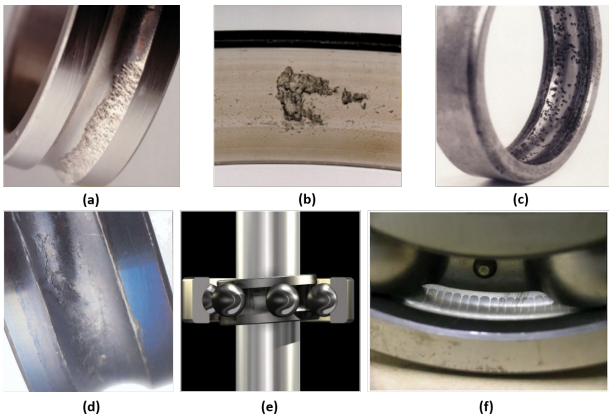

Figure 2.14: Bearing damage by different causes: (a) Overloading; (b) Fatigue; (c) Corrosion; (d) Lubricant failure; (e) Bearing misalignment; (f) Electrically induced fluting [1], [7].

Other Faults

There are several other types of faults that we will refer in this section, though they might not be as relevant, in terms of possibility of occurrence as the aforementioned ones. Over and under voltages for instance may appear due to relevant changes in voltage supply levels. Over voltage induces additional stresses on the insulation, whereas under voltage leads to excessive line currents resulting in overheating of the winding. Overload often occurs due to an excess of mechanical load. When this happens, the motor cannot develop sufficient torque and the rotor gets blocked. Overload will lead to excessive current levels in the windings which may also result in overheating. It can be prevented by means of a fuse. Crawling is an electromechanical fault of the motor. It causes the motor to run at a speed near to one-seventh of its synchronous speed. It occurs when the air-gap flux is not sinusoidal in time due to odd harmonic content that will affect the generated torque. In the presence of this condition, the motor, even under loaded condition will not accelerate past that speed, and stator current and vibration levels will increase. Its effect can be minimized by selecting an appropriate number of rotor slots when designing the motor.

2.2 Variable Frequency Drives

Variable Frequency Drives are quite common components in electrical motors, as they permit a simple way of regulating the motor's rotational speed. In this section the basic operation principles of this component will be described, along with possible advantages and disadvantages of its use.

2.2.1 Operation Principles

The functioning of these drivers is based on a simple concept called *pulse-width modulation* (PWM). PWM refers to the process of varying the pulses' width, in a pulse train, in direct proportion respective to a voltage control signal - the greater the control voltage, the wider the pulses will become. By applying a sinusoidal waveform of the desired frequency for the control voltage, it is possible to obtain a high power waveform whose average power varies sinusoidally in an adequate manner for driving AC motors.

A basic single-phase PWM circuit is shown on figure 2.15(a). T_1 through T_4 represent insulated-gate bipolar transistors (IGBT) which are basically switches that allow high frequency switching in an electrical circuit, combined with great efficiency. The state of these switches is controlled by two comparators. *Comparators* are devices that compare their input voltage to a reference one, turning the switches on or off according to the comparison result. The voltage reference signals for this application are typically sawtooth or triangle waveforms. As an example, observe figure 2.15(b), where comparator A compares the input voltage $V_{in}(t)$ with its input reference $V_x(t)$. When the first is higher than the latter, switch T_1 will be turned on, and T_2 will be turned off, and vice-versa. For the next step, lets examine how PWM signals are generated according to their input voltage $V_{in}(t)$. For this purpose, consider a constant null input voltage, intersecting $V_x(t)$ and $V_y(t)$ at the x axis. In this case $V_u(t)$ and $V_v(t)$ will be identical and since the voltage at the load's terminals results from $V_{load}(t) = V_v(t) - V_u(t)$, the voltage at its terminals will be zero. Now, if a constant positive voltage is applied, of half of the reference voltages' maximum, the resulting output voltage applied to the load will be a pulse-train with a 50% duty-cycle. Finally, taking this analysis one step further, a real single-phase case will be presented, in which the reference input voltage is a sinusoidal waveform. The width of the generated

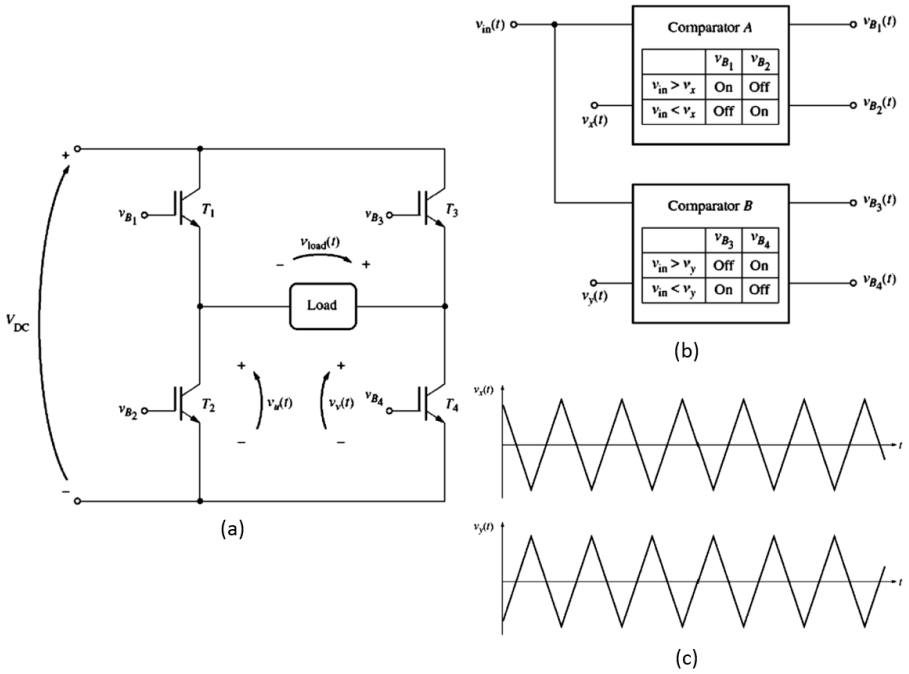

Figure 2.15: PWM basic concepts: (a) PWM single-phase circuit; (b) Comparators for transistors' control; (c) Voltage reference signals [4].

pulse-train for the output voltage varies sinusoidally according to the control voltage signal. The outcome in this case is a high-power waveform whose average voltage is directly proportional to that of the control signal, in a specific time interval. The *fundamental frequency* of the output signal will be the same as the one of the control signal. Some harmonic content is also present, though it doesn't present a significant limitation for this particular application. It might cause heating of the driven motor, but this fact can be compensated with a particular motor design that favours cooling, or by derating a common motor (running it at an inferior power than its full rated one). The given examples of the PWM signal generation can be seen in figures 2.16 and 2.17. For a three-phase motor, the signal generation mechanism is basically the same. The most significant difference in this case relates to the fact that the VFD comprises three comparators, one for each phase, as the control voltages will be three sinusoidal waveforms with a 120° phase shift between each of them [4]. Nowadays, reference voltage signals in VFDs can range from 1 kHz up to 20 kHz.

In the case of a real VFD, the control voltage fed into the comparators' circuits is achieved by means of a microcomputer placed on the circuit board of the PWM motor controller. The digital control signal generated by the microcomputer allows for a much more refined control than that that we have seen thus far. The microcomputer makes it possible to vary the control voltage to different amplitudes or frequencies defined by the user. It allows for implementation of acceleration and deceleration ramps or current limits, by setting these parameters in this components' software.

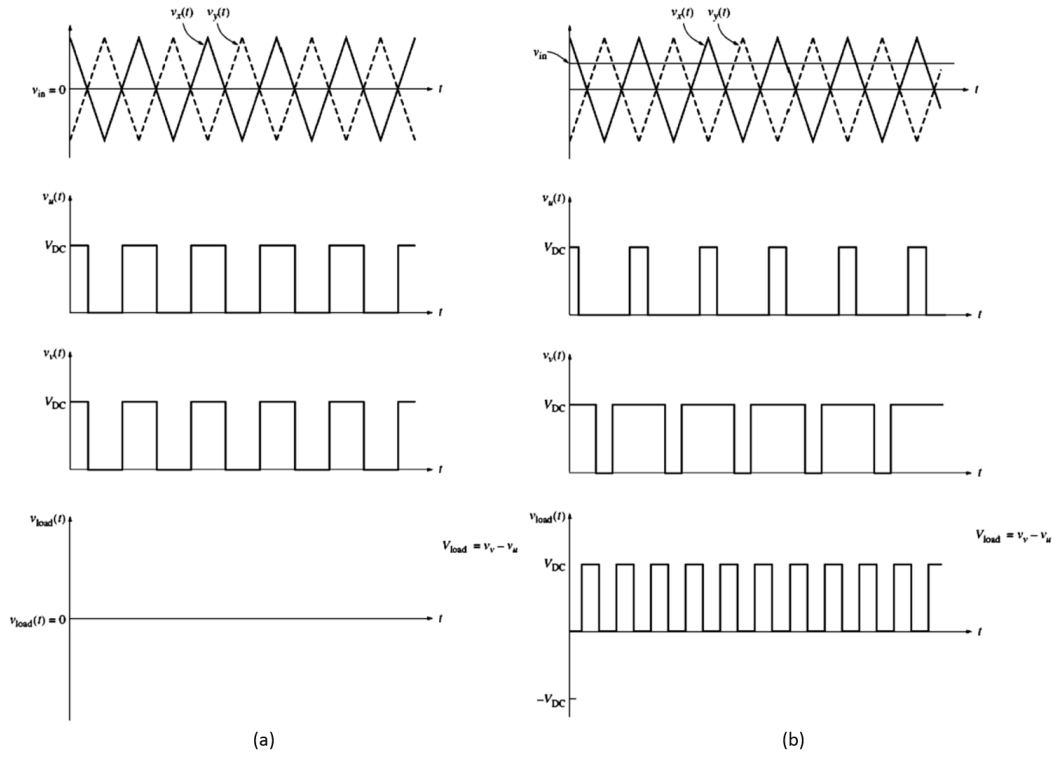

Figure 2.16: PWM basic signals: (a) Constant null control voltage; (b) Constant positive control voltage [4].

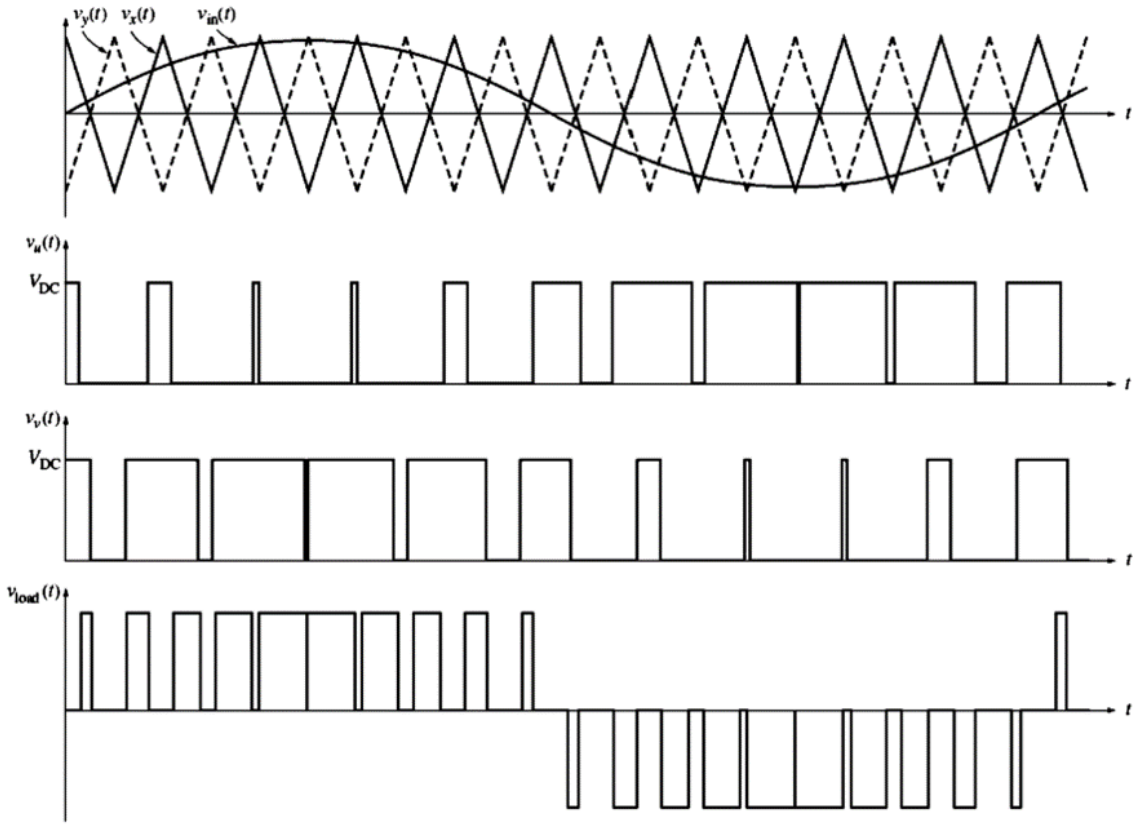

Figure 2.17: PWM basic signals with sinusoidal control voltage [4].

2.2.2 Application

In terms of application, VFDs are quite flexible, allowing for customized settings of several parameters. Referring to its inputs, they are able to perform both single and three-phase connections, at either 50 Hz or 60 Hz of supply frequency, with voltages ranging from 208 V to 230 V. Regarding their output signals, in the case of an induction motor, these signals will be a set of three-phase voltages, with frequencies ranging from 0 Hz to 120 Hz, and amplitudes ranging from 0 V to the rated voltage of the motor at full load. Both output frequency and voltage levels can be set independently by the afore seen PWM mechanism. Though the parameters are controlled independently, the drive's control ensures the output rms voltage level is constant. Hence, the voltages' peaks will remain constant in magnitude, with the rms value being controlled by the fraction of time in which the pulses occur, while the frequency is determined by the rate at which the pulses' polarity switches.

Speed Adjustment

Regarding the speed adjustment, VFDs allow for an external control, whether it is done manually on the driver cabinet's control, or remotely by an external voltage or current signal. This flexibility in adjusting the drive's output frequency is very important, as it grants the equipment the capability to adapt to external processes, and thus responding according to the plant's needs.

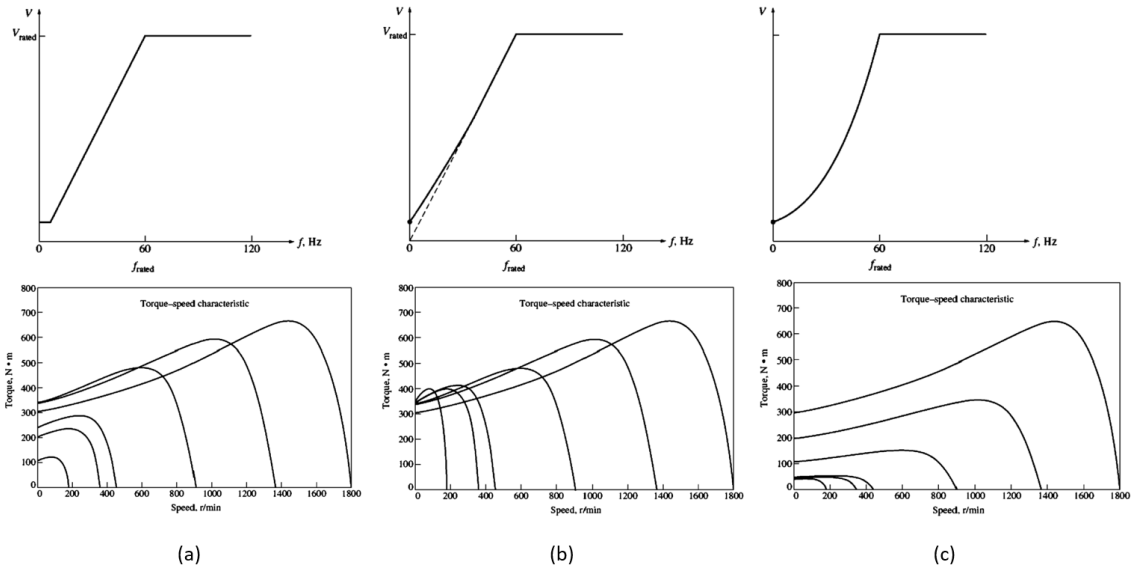

Figure 2.18: VFD voltage versus frequency patterns and resulting torque-speed characteristic curve of the motor: (a) Standard linear voltage-frequency variation; (b) Characteristic curves for loads with high starting torques; (c) Characteristic curves for soft-start loads [4].

Figure 2.18 presents different application cases that require different starting torques. In case (a) the most generic case can be observed, where the variation of voltage and frequency of the VFD occurs linearly, up to the base speed (above which the voltage level is held constant). At very low speeds a constant voltage level ensures a minimum starting torque for the motor. The torque-speed characteristic curves can be observed for several frequencies below the base speed. Case (b) is representative of loads that require high

starting torques. Notice that for any frequency below 30 Hz the output voltage is higher than that of the previous case. Consequently, the torque will be higher as it can be seen in the respective torque-speed characteristic, especially at low speeds. This torque gain occurs at the expense of higher magnetization currents (and thus, higher magnetic saturation). These are often acceptable for the short time spans required to start the heavy loads. Case (c) shows a voltage-frequency curve applied to loads with low starting torques (a.k.a. soft-start loads). The voltage level varies parabolically with the output frequencies below the base speed. As such, for any given speed below 60 Hz, the output voltage (and hence the output torque) will be lower to those of the standard case, helping to provide a smooth start for low-torque loads. It can also be noted that the starting torques present lower values when compared to those of case (a).

When it is desired to vary the motor's operating speed, from 400 to 1000 rpm for instance, if the speed variation is sudden, the drive does not force the motor to take that 'leap' instantaneously. Instead, it will progressively increase the motor speed, limited to a safe level implemented by built in circuits of the drive. The case would be the same for decelerating the motor, in the sense that the speed variation does not occur instantaneously [4].

2.2.3 VFD signals

As we have seen thus far, VFDs allow for a simple but effective control of induction motors. In fact, power electronic components such as this type of drives are so flexible that they are now responsible for the control of 50 to 60 percent of power systems in developed countries' industry. Consequently, these systems' behaviour will be strongly influenced by the drives that control them.

One major issue of interest in VFD applications is the harmonic content of their voltage and current signals, induced in the power system they control. This phenomenon occurs due to some switching transients in the controller circuits. The harmonics increase the current flow (mainly in the neutral line of a three-phase system), leading to an increase of losses as well as additional heating, and consequently, to the need of larger equipment to supply the same total load.

Should we consider the case of two wye-connected motors where one is directly connected to the power supply and another one is being controlled by a VFD. The spectra of the current signals can be observed in 2.19. The phase spectrum of the motor connected directly to the supply presents just the fundamental frequency, whereas the same spectrum for the motor controlled by the VFD presents the fundamental frequency along with all of its odd harmonics. The current in the neutral is zero for the first motor, while for the second one it is not, presenting some odd harmonic components in the spectrum [4].

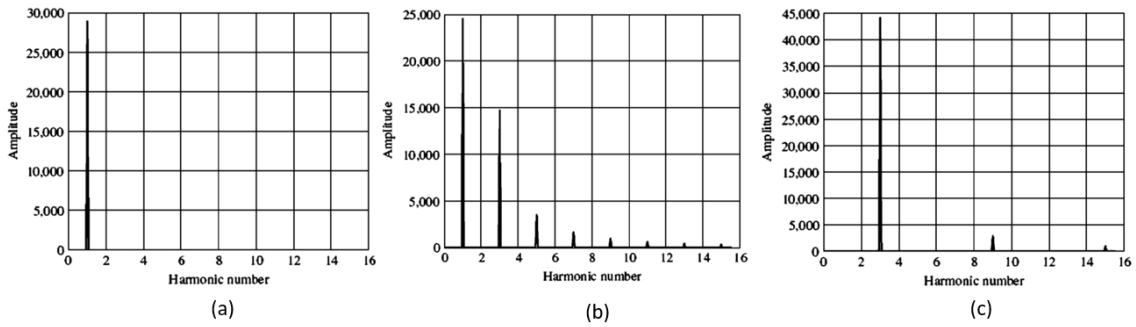

Figure 2.19: Induction motor current spectra: (a) Phase current in motor without a VFD; (b) Phase current in motor controlled by a VFD; (c) Neutral current in motor controlled by a VFD [4].

According to the literature, the spectrum content of these signals appears to be very clear, in the cases we know which frequencies to look for. However, the most common case is when you would get a VFD from a manufacturer with no knowledge of the parameters that were previously implemented in the drive. This makes the analyst's task much more difficult when the goal is to determine frequencies of interest in the spectrum, such as those of the input parameters implemented on the VFD. It is also possible to observe in figure 2.20 that by simulating a simple PWM signal for a single phase, that the signal's spectrum is not that clear, presenting overall broadband impulsiveness.

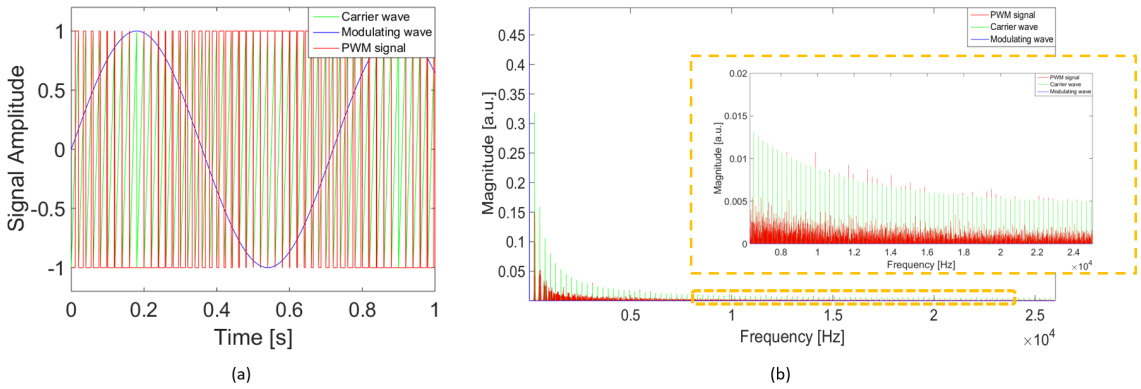

Figure 2.20: PWM simulated signal for a single phase: (a) Signal generated by the VFD; (b) Fourier spectrum of each signal component.

Space Vector Modulation

Space Vector Modulation (SVM) is an advanced PWM control algorithm for generating multi-phase AC. Nowadays it is regarded as the best alternative performance-wise.

Figure 2.21 shows a generic three-leg inverter which is a commonly implemented circuit for three-phase voltage PWM inverter. It converts a DC voltage supply, via a series of switches, into a three-phase supply for the load (e.g. a three-phase induction motor).

The switches must be operated in such a way that they do not allow for two switches of the same leg to be activated at the same time, otherwise the DC supply would be shorted.

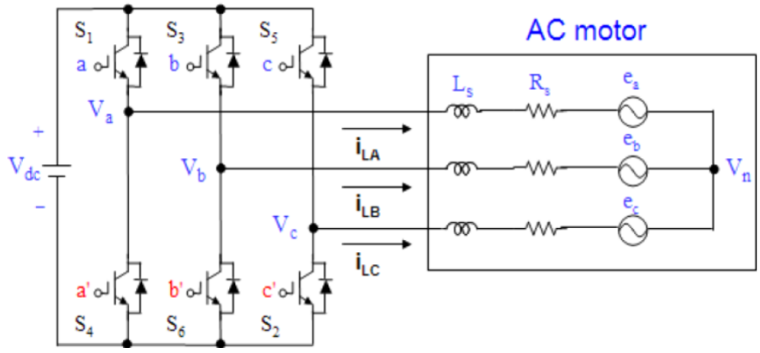

Figure 2.21: Generic PWM inverter circuit connected to a three-phase motor [8].

This can be ensured with complementary operations within each leg (e.g. if switch S_1 is on, switch S_4 is off, and vice-versa). Considering these operations along with all possible switches combinations, we obtain eight possible switching vectors listed in table 2.2.

Voltage Vectors	Switching Vectors						V_{ab}	V_{bc}	V_{ca}	Vector Type
	S_1	S_3	S_5	S_4	S_6	S_2				
V_0	0	0	0	1	1	1	0	0	0	Zero Vector
V_1	1	0	0	0	1	1	$+V_{dc}$	0	$-V_{dc}$	Active Vector
V_2	1	1	0	0	0	1	0	$+V_{dc}$	$-V_{dc}$	Active Vector
V_3	0	1	0	1	0	1	$-V_{dc}$	$+V_{dc}$	0	Active Vector
V_4	0	1	1	1	0	0	$-V_{dc}$	0	$+V_{dc}$	Active Vector
V_5	0	0	1	1	1	0	0	$-V_{dc}$	$+V_{dc}$	Active Vector
V_6	1	0	1	0	1	0	$+V_{dc}$	$-V_{dc}$	0	Active Vector
V_7	1	1	1	0	0	0	0	0	0	Zero Vector

Table 2.2: SVPWM switching vectors [8]

These vectors can also be represented in a direct-quadrature (dq) reference frame for simplified visualization, where d denotes the horizontal axis and q the vertical one. This reference frame is usually obtained by applying a $dq0$ transform. This matter will not be developed much further since this tool was merely used to simplify the understanding of the PWM signal generation. An example is shown in figure 2.22. Note that the switching vectors are expressed as a $\{S_1, S_3, S_5\}$ combination.

The active vectors V_1 through V_6 vary as a pulsed sinusoid, with each leg offset 120° from each other. The reference voltage V_{ref} is obtained by applying by applying a $dq0$ transform, as shown in equations 2.42 and 2.43, where f_{abc} denotes either a three-phase voltage or current and K_s is the matrix that relates both reference frames. The reference signal is then sampled at a sampling time period T_s and the actual signal is then synthesized by using a combination of the two adjacent active switching vectors and one (or both) zero vectors. Several strategies can be implemented for selecting the vectors' combination. These strategies may influence the harmonic content of the PWM synthesized signals [8].

$$f_{dq0} = K_s f_{abc} \tag{2.42}$$

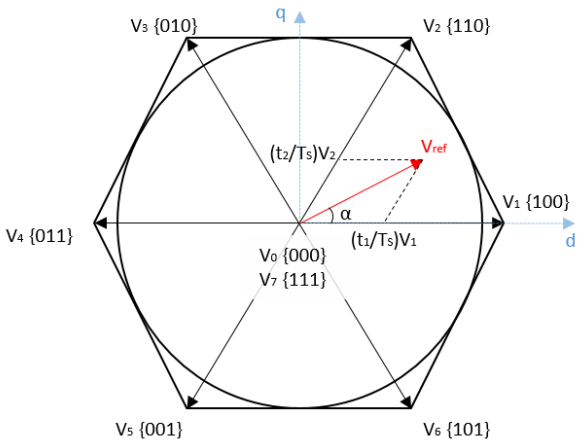

Figure 2.22: SVPWM switching vectors represented in a dq reference frame [8].

$$K_s = \frac{2}{3}\begin{bmatrix} 1 & -\frac{1}{2} & -\frac{1}{2} \\ 0 & \frac{\sqrt{3}}{2} & -\frac{\sqrt{3}}{2} \\ \frac{1}{2} & \frac{1}{2} & \frac{1}{2} \end{bmatrix} \tag{2.43}$$

CHAPTER 3

Vibration Signals

3.1 Vibration-based Monitoring

Mechanical systems are nowadays widely used, whether their application serves everyday use of regular people or, especially, in manufacturing facilities. The industrial equipments used in such facilities are often expensive, with their breakdown accounting for a severe cost to the plant. In chapter 1 we referred to Condition Monitoring (CM) strategies as a way of reducing such costs by monitoring the 'health state' of the machine. Vibration-based monitoring is nowadays the most commonly used method for this purpose since it is able to provide reliable information of a relatively recent faulty condition, allowing for proper maintenance to be performed long before machine failure takes place.

Vibration of a system can be regarded as an oscillation about an equilibrium position. This oscillation can then be plotted relative to that equilibrium position in each time instant, presenting itself as a time-domain waveform. Though this waveform carries crucial information regarding the machine's condition, it is often difficult to interpret as events of several components may be represented in the same signal, hence the need to represent our signal in other domains to unmask relevant information regarding the machine's condition.

Even when they are in good condition, rotating machines generate vibrations. These vibrations are often associated with periodic events, such as a shaft rotation, gear-teeth meshing, a fan rotation, among others. When these components' geometry is known, it is possible to associate the information retrieved from the vibration signals (usually, frequencies of interest) to events that correspond to the machine's operating signature, or, to a possible faulty condition. It is in this stage that CM techniques present added value to our cause, allowing us to separate our machine's signals in a healthy state, from the ones that could indicate a faulty state, often with the indication of the fault's source.

Periodic events that frequently appear masked in the time-domain signals become quite clear once represented in the frequency domain, hence its broad use by several techniques for diagnostic purposes. However, some events that occur in vibration signals do not have an exact periodicity associated to them. That is the case, for instance, of an internal combustion engine, where the vibration events are not periodical, but strictly related to the engine's cycle. Nevertheless, this allows us to distinguish between perfectly periodic events and non-periodic ones [3].

A predictive maintenance approach based on vibration analysis is supported on two main premises [9]:

1. All failure modes have distinct vibration frequency components that can be determined separately;
2. The amplitude of each of the aforementioned frequency components will remain constant unless a change occurs in the machine's operating dynamics (e.g. a possible fault).

Regardless of these primary assumptions, there are still some considerations to be made regarding vibration analysis (VA). As we previously referred the frequencies of interest we are looking for in the vibration signals for machine diagnosis are masked by other signal components, such as noise, other unrelated mechanical signals and the transmission path from the fault's source, through the structure, until our signal reaches the sensor where it is measured. Even though several algorithms are available to look for these frequencies of interest, they are not always easy to find, hence the need to use refined pre or post-processing techniques and take into account the sensors characteristics. These are some of the parameters that will ultimately influence the machine's diagnosis.

Other factors of influence to take into consideration for bearing diagnostics is the fact that the transducer is usually placed on the bearing's housing. However, there is relative vibration between the bearing and its housing. Also, with varying operational conditions such as load or speed, the analysis of our mechanical system may become of increasing complexity.

Advantages of Vibration Analysis

Vibration analysis is nowadays the prevalent method adopted by CBM strategies, as it offers several advantages. When compared to oil analysis, for instance, which may take considerable time between the collection of samples and their analysis, vibration responses can be measured instantly. Taking this comparison one step further, chemical analysis of the oil will usually indicate that many of the metals in bearing components are of the same chemical composition, whereas an increase in the vibration response will only be given by the faulty component, and thus give us more conclusive results. This is mainly due to the fact the oil analysis needs to be processed by specific equipment whereas vibration signals can be analysed on site. Another advantage to point out is that recent signal processing techniques now allow for the enhancement of weak impulses resulting from incipient faults, or fault signals buried under noise.

CBM strategies differ in many ways. Vibration analysis allows for both intermittent or permanent monitoring. Intermittent monitoring allows for a reduced cost in measurement equipment, and should be used in cases where the cost of the machine is outweighed by the cost of lost production. In spite of its advantages, this type of strategy should not be used in cases that could indicate high probability of unpredictable failure. On the other hand, by applying a permanent monitoring strategy, one can prevent these unpredictable failures. Still, it adds significant equipment-related cost and is only justifiable in certain cases of critical machines where their cost would be greater than that of lost production, or in cases as the aforementioned one of possibility of unpredictable failure occurrence. An example is given in [3] regarding such a case, where high-speed turbo-machines of a power generating plant, where proximity probes are permanently installed in the fans' shafts, to monitor vibration levels. If these are not within an acceptable range, an automatic shut-down of the machine can be set so that extensive damage to the system can be prevented and maintenance may take place as soon as possible.

This leads to one simple conclusion: a compromise between both strategies would represent

an ideal solution. If transducers are permanently mounted on a machine, both permanent and intermittent monitoring can be performed in parallel, with the 'health state' of the machine updated regularly. This would allow for detection of incipient faults weeks or even months in advance before a possible failure state is achieved. Consequently, if the machine were to continue operating with this incipient fault condition it would allow for enough time for production planning, as well as order the necessary spare parts and for minimum production downtime. The potential of this strategy is often costly for the plant. However, it can be economically justifiable for industrial applications if one is able to exploit the component's life and perform its replacement during a programmed maintenance stoppage of the unit [3].

3.2 Rotating Machinery

In order to perform a proper analysis of our measured vibration signals, one must first understand which components rotating machines comprise, what types of signals are generated by these components and what is actually measured by the transducers. This section along with the following sections of the present chapter are destined to that purpose.

3.2.1 Rolling Element Bearings

Rolling element bearings are broadly used in various types of equipment, whether we are referring to domestic or industrial use. Motors, pumps, compressors or practically every rotating machine comprises some kind of bearing. Its main function is to ensure the support of the rotating part of the system, and are therefore critical to ensure proper operation of the machine. This component is conceived to transfer forces of the rotating parts to the main supporting structure and ensure reduced friction during the machine's operation.

The two most common types of bearings are anti-friction (or rolling element) bearings and journal bearings. The latter ones operate based on hydrodynamic lubrication. The region between the journal and the sleeve is filled with lubricating oil characterized by a certain viscosity. When running at high speeds, fluid pressure builds up towards the centre of the sleeve. This pressure is then responsible for supporting the shaft load. When the machine is not operating, the journal sits on the sleeve, causing it to wear out in successive starts and stops. When the sleeve material wears out it can easily be replaced. Another aspect to take into account is that when loads are excessive in precision shafts, the pressure built up in journal bearings becomes inadequate for their proper functioning. A commonly implemented solution for this problem are hydrostatic bearings, where externally pressurized fluid is provided to the journal. This also helps to overcome our initial problem when, while the shaft was stopped, the journal would sit on the sleeve. In hydrostatic bearings, due to the presence of pressurized fluid, those components never come into contact with one another. One final consideration regarding this type of bearings is that due to the damping produced by the fluid in journal bearings, their vibration response can be controlled for several load and speed conditions, particularly when resonant vibration modes occur [10].

Rolling element bearings on the other hand are probably the most commonly used and will, from henceforth, be subject of study in the present text. Rolling element bearings are subject to very strict tolerances when manufactured. In spite of this fact, only about 10 to 20% of bearings reach their design life. As a consequence, they are often responsible for machine failure. This can occur due to a series of factors as improper lubrication

or lubricant choice, contamination with foreign particles, improper storage or shipping, excessive moisture in the surrounding environment, improper handling or installation, or inadequate operating conditions in a particular cases, among others. All these factors can contribute to the bearings' operating life reduction and special care to these factors must be taken [11].

Rolling element bearings comprise four main components. Two circular races (inner and outer) between which the rolling elements are held, along with the cage (or separator) to ensure adjacent rolling elements do not come into contact with each other. Sealing on both sides is applied to prevent intrusion of external particles into the bearing, so as to prevent both mechanical damage and lubricant contamination. These components can be seen in figure 3.1. For different types of bearings, rolling elements can differ in their geometry: these elements can be spherical rollers (symmetric or asymmetric), tapered, needle or cylindrical rollers, or most commonly, spherical balls. Rolling elements are often made of hardened steel and manufactured with extreme attention to what concerns surface finish, to be as round as possible. However, due to imprecisions that may occur during the manufacturing process, the rolling elements are not perfectly circular, with radial variations usually around a few microns. Nowadays, the best bearings manufactured in the world have radial imperfections of 3 to $5\mu m$. These imperfections would cause radial loads to oscillate during the machine's operation, making vibration signal analysis much more complex. The bearing's characteristic vibration signal would then be amplitude modulated at the shaft rotation frequency [10]. The existence of such manufacturing imperfections can eventually lead to a faulty condition if the bearing operates without proper maintenance.

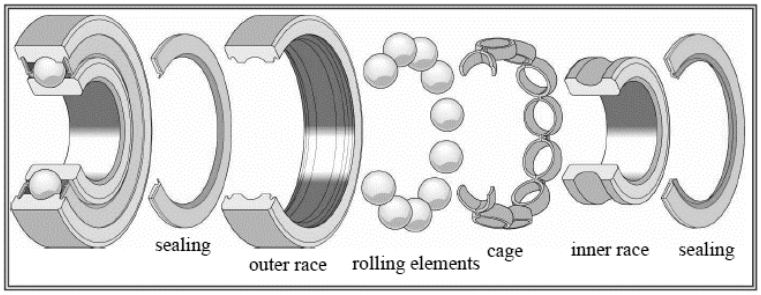

Figure 3.1: Ball Bearing Components [11].

3.3 Bearing Faults

Bearing faults generation mechanisms were already discussed in section 2.1.5 and these are important in terms of which factors must be taken into consideration during their use. However, when diagnosing a bearing through vibration analysis one must understand how they operate in order to assess their condition properly. In the previous section, manufacturing imperfections that could lead to an eventual fault were also referred. Bearing faults can occur on each of its components, as listed below:

- Outer race faults;
- Inner race faults;
- Ball (rolling element) faults;
- Cage faults.

For all intents and purposes, consider the case of a bearing, with a localised fault, operating in a machine. If vibration signals of such a bearing were analysed, what would we see? Figure 3.2 illustrates examples of localized faults in each component. What actually happens is that when the rolling element strikes a fault on one of the races, or a faulty rolling element strikes one of the races, a shock is induced, exciting high frequency resonances of the entire structure from the source (fault strike) to the sensor that measures the vibration signal. As the machine is rotating continuously, a series of broadband bursts is excited by these shocks. These bursts are subject to further amplitude modulation caused by two main factors:

- The bursts' strength depends on the load source of the bearing - hence, these bursts will be modulated by the rate at which the fault passes through the load zone;

- Depending on the location of the moving fault, the transmission path's transfer function will vary, respective to the fixed positions of the response transducers.

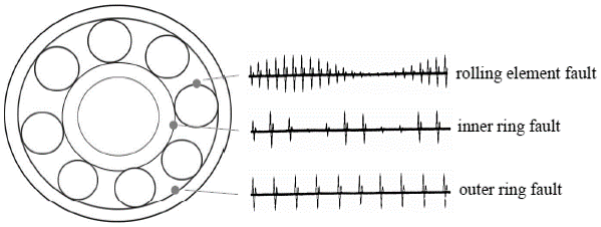

Figure 3.2: Bearing Fault Signals [11].

Under normal operating conditions, outer race faults are not subject to shaft speed modulation, whereas the opposite happens with an inner race fault. The rolling element fault is typically modulated at the cage frequency. However, further amplitude modulation can occur at the shaft rotating frequency in cases where unbalance and misalignment aggravate the vibration of the machine, under operation. Bearing defects commonly start as small pits or spalls and in early stages, give rise to sharp impulses that cover a wide frequency range (possibly even reaching an ultrasonic range around 100 kHz). On the other hand, when faults like brinelling occur, where the rolling elements indent one of the races causing plastic deformation, the entry and exit of the fault through the load zone does not give rise to such abrupt impulses, and thus the excited frequency band will not be as wide. It can also happen that, with wear, localised faults become smoothed, originating an extended fault region with lower vibration amplitudes, when compared to the initial fault condition. In this case, diagnostic information is more difficult to extract from signal analysis. It can sometimes be detected by the way this fault modulates other machine signals, such as those of a gear-mesh, if the gear in question were supported by this bearing. Such an example can be seen in figure 3.3, where an extended inner race fault modulates a gear signal. One advantage of analysing bearing signals is that their periodicity is not precise, having some small degree of randomness associated to them. Gear signals, on the other hand, are perfectly periodic, and appear as multiples of the shaft's rotation (and their respective number of teeth). The fact that the bearing signal is not perfectly periodic allows us to separate it from deterministic signals, such as those of gears.

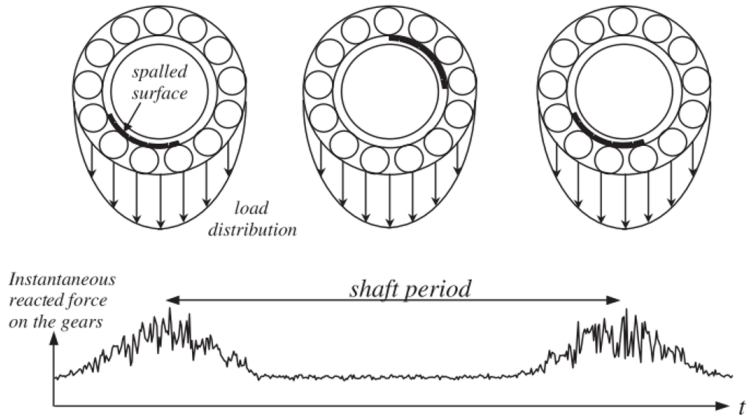

Figure 3.3: Modulatiton of an inner race fault on a gear signal [12].

Bearing Fault Frequencies

For analysing machine signals, their processing and visualization often becomes simpler when done in the frequency domain. Hence, it is important to understand what factors or frequencies of interest should be sought for performing diagnosis of the bearing's condition. Fortunately, these frequencies of interest can easily be calculated by kinematic relations. For bearings, these characteristic fault frequencies can be calculated by equations 3.1 through 3.4, and are listed below as follows:

- Ball-Pass Frequency in the Outer Race (BPFO) - Indicates an outer race fault;

$$BPFO = \frac{n_r f_r}{2}\left\{1 - \frac{d}{D}\cos\varphi\right\} \tag{3.1}$$

- Ball-Pass Frequency in the Inner Race (BPFI) - Indicates an inner race fault;

$$BPFI = \frac{n_r f_r}{2}\left\{1 + \frac{d}{D}\cos\varphi\right\} \tag{3.2}$$

- Ball-Spin Frequency (BSF) - Indicates a ball or rolling element fault;

$$BSF = \frac{d}{2D}\left\{1 - \left(\frac{d}{D}\cos\varphi\right)^2\right\} \tag{3.3}$$

- Fundamental Train Frequency (FTF) - Indicates a cage fault.

$$FTF = \frac{f_r}{2}\left\{1 - \frac{d}{D}\cos\varphi\right\} \tag{3.4}$$

In the latter equations, d represents the rolling elements' diameter, D represents the pitch diameter, φ the contact or load angle of the rolling elements measured from the radial plane, f_r the shaft rotation frequency (or speed) and n_r the number of rolling elements. Note that the BSF represents the frequency at which rolling elements strike the same race, therefore, it is possible for two impacts per period to occur.

Nonetheless, these formulae are purely theoretical and obtained exclusively from kinematic relations. During the bearing operation some degree of slip is always present due to the small clearance between moving components, as well as the presence of lubricant. The main contribution for the occurrence of slip is the constant variation of the load angle φ. This happens because the rolling elements' position is constantly changing due to variations of the local ratio of radial to axial loads. As a natural consequence, each rolling element is trying to roll at a different speed and will have a different effective rolling diameter. The presence of the cage reduces the elements deviation, causing random slip. In practical terms, this will result in an average $1-2\%$ deviation of the characteristic fault frequencies from the calculated ones. This random slip, although being quite small, allows us to prove the fact that bearing fault signatures are not exactly periodic, thus giving a fundamental change in their classification, and that is a key factor when performing bearing diagnosis [12].

Bearings, like any mechanical component, have a natural frequency associated to their mass and stiffness. These components are often designed so that this natural frequency will be higher than the operating frequencies of the mechanical structure which comprises them, so as to avoid resonances. However, incipient faults such as pits in the races tend to provoke sharp impacts that occur in an extremely short timespan, inducing high frequency and amplitude (or resonant) vibration. These are helpful when diagnosing incipient faults, since analysis in the frequency domain could go over the range of 6 kHz, making the excitation quite visible in the frequency domain [13].

There are other important considerations to take into account when diagnosing the condition of a rolling element bearing. First, let us consider a bearing with a faulty rolling element. In order for the measured vibration signal to possess viable diagnostic information, it is extremely important to ensure that during the bearing operation:

1. The rolling element is not stuck in any way. It must be rotating freely so that the fault zone strikes the races in order to produce measurable alterations in the vibration signal.

2. For retrieving relevant diagnostic information, it is important that the fault's strike on one of the races occurs when the rolling element is passing through the load zone.

It has been repeatedly stated throughout this text that bearing vibration signals can be easily masked by other signals of the rotating machine. Hence, if the strike occurs when the fault is passing through the load zone, the vibration produced by such strike will increase in amplitude, making it more distinguishable from other signal components such as gear meshing signals.

Moreover, when analysing the spectrum for frequencies of interest, for inner race faults, side-bands of the fault frequency usually appear modulated (spaced) at the shaft rotation frequency, whereas for a rolling element fault, these side-bands are spaced at the fundamental train frequency. Resorting to demodulation of these signals in the frequency domain (a.k.a. envelope analysis), valuable diagnostic information can be extracted. For both types of faults, bearing signals can be treated as cyclostationary. To better understand new concepts introduced in this last paragraph, the following section presents briefly what common types of signals are found in rotating machinery and how they are classified.

3.4 Signal Classification

Rotating machinery often comprise several different components. These components tend to produce vibration signals whose nature usually differs, depending on the components they originate from. The present section aims to give a better understanding of the signals generated by such components, which will ultimately prove quite useful when diagnosis of the machine state needs to be performed. It has been pointed out that bearing fault signals have some degree of randomness in their nature, whereas gear signals are perfectly periodic.

This is one major distinction to be made regarding the nature of the signals that will be analysed in the present text. Signal classification will often determine the methods applied for signal processing and analysis. Thus, proper signal classification constitutes an important primary step in the present work. Figure 3.4 presents a diagram that helps us gain a notion of how signals' natures vary.

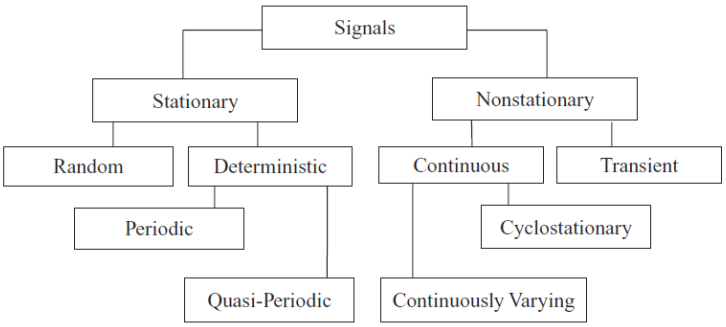

Figure 3.4: Types of Signals [3].

Howbeit, measured vibration signals from rotating machinery comprise all sorts of components, whether they are random, deterministic or cyclostationary. Applying the previous classification might not seem so obvious when faced with the issue of diagnosing a mechanical system. So, previous knowledge of the system or the nature of the signals that we want to analyse is often helpful for selection of appropriate analysis tools.

Deterministic signals represent physical phenomena whose behaviour can be exactly predicted. Gear signals are a good example, since the gear meshing is predetermined to occur a certain number of times per revolution of the shaft. As the teeth mesh together, vibration impulses are generated at constant time intervals (for a constant shaft rotation speed). These signals are also known as discrete frequency components, since the frequency of the gear-meshing is constant. When analysing the frequency Fourier spectrum, sharp peaks appear at the meshing frequency and its harmonics, if no other contribution is present in the signal. Fans, such as those present in electric motors are another good example. The blade-pass frequency is also a discrete frequency component, as it occurs at regular intervals (at constant speed) and can be easily obtained by multiplying the shaft rotation frequency by the number of blades of the fan.

Nonstationary signals on the other hand, are those whose behaviour is not exactly predictable. The aforementioned case of the bearing with a ball fault is a good example of this type of signal. To measure the fault's signature, one is dependent on several conditions coming together in the same instant. As such, the signature we wish to measure might not always be present in the signal, making its behaviour unpredictable even though mathematically proven that it can exist. Transient signals are also included in this category. These are often associated to impulses directly linked to the release of energy originating in certain

physical phenomena. Gear meshing, combustion of gas in internal combustion engines, exhaust of fluids in pumps, or even bearing faults originate transient signal components which often carry crucial information about the system's condition. These transients manifest themselves as decaying pulses with very short duration that excite resonant structural modes [14].

This classification is arguably unique. In spite of that, it is an important stepping stone to understand the nature of the analysis one should perform and to understand to what extent the applied tools are valid.

Stationary Deterministic Signals

Stationary deterministic signals are characterized by their waveform being perfectly repeatable in constant time intervals.

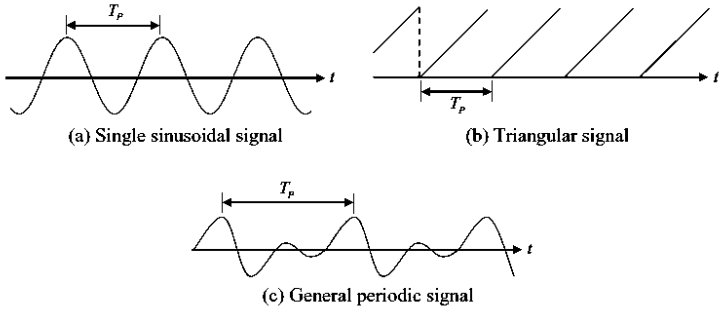

Figure 3.5: Examples of Periodic Signals [15].

Simple examples are shown in figure 3.5. Both the sinusoidal and the triangular waveforms are perfectly repeatable in time, at constant time periods T_P (in seconds). This period's representation may also be made in its reciprocal form, $1/T_P$. This frequency is represented in Hertz. The same considerations can be made for a more general case, such as the one illustrated in 3.5 (c).

Regardless of the waveform, the mathematical definition of periodic means that the wave's behaviour must be constant in time, as expressed in equation 3.5:

$$x(t) = x\left(t + kT_P\right); k = \pm 1, \pm 2, \pm 3, ... \tag{3.5}$$

Cases (a) and (b) can easily be described by mathematical expressions. Case (c) on the other hand is a bit more difficult to describe in such a way. It is more approximated to a measured signal of a physical phenomenon, such as the output of an accelerometer. A simpler approach to analyse this signal's components is to convert it to the frequency domain, where the periodic signal can be decomposed in discrete frequency components, thus revealing its periodicities. This transformation to the frequency domain can be made by applying a Fourier series, and will be further explained in chapter 4.

Figure 3.6 illustrates a frequency domain representation of a triangular waveform with period $T_P = 2$ seconds. The components that represent the signal in this domain are $1/T_P$ and other components which are "harmonically related" to the fundamental component ($2/T_P$, $3/T_P$, and so forth) [15]. It is known however that there are a number of factors contributing in the real world that make these periodicities less precise. As such, the term *quasi-periodic* has been used to characterize similar phenomena.

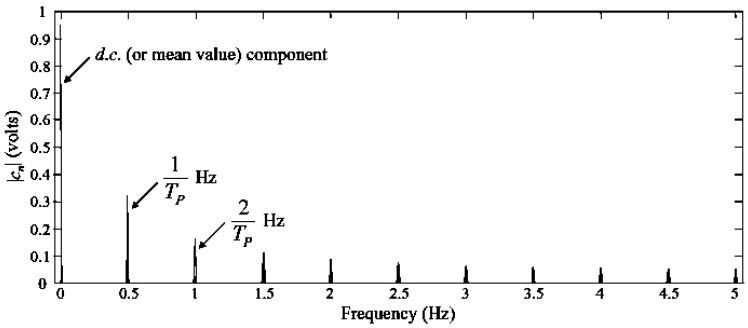

Figure 3.6: Frequency domain representation of a periodic signal [15].

Stationary Quasi-Periodic Signals

Quasi-periodic signals refer to signals whose behaviour may appear at first as if it were periodic, but, when closely observed, one can conclude that it is actually not. Even for simple situations, the sum of sine and cosine waves result in a waveform that never repeats itself. Consider the example of a signal described by equation 3.6:

$$x(t) = A_1 sin\,(2\pi p_1 t + \vartheta_1) + A_2 sin\,(2\pi p_2 t + \vartheta_2) \tag{3.6}$$

where A_1 and A_2 are amplitudes, p_1 and p_2 are frequencies of each sine component, and ϑ_1 and ϑ_2 represent phase angles. If the frequency ratio p_1/p_2 is a rational number, the signal $x(t)$ will be periodic, repeatable at every time interval of largest common period of both $1/p_1$ and $1/p_2$. If the ratio is irrational however, the signal $x(t)$ will never repeat itself. Thus it can be stated that the sum of two or more sinusoidal components is periodic only if the ratios of all frequency pairs are determined to be rational (i.e. ratio of integers) [15].

Transient Signals

The term 'transient' suggests some limitation regarding the duration of the signal. Generally, a transient signal possesses a property that states that $x(t) = 0$ when $t \to \pm\infty$. Some examples of transient signals are shown in figure 3.7. In vibration engineering, impact testing is usually done to estimate the frequency response function (FRF) of the structure. This test is usually performed with a hammer, with the input force being measured, as well as the vibration response of the structure (by measuring acceleration signals). Results for such a test performed on a cantilever beam are presented in figure 3.8.

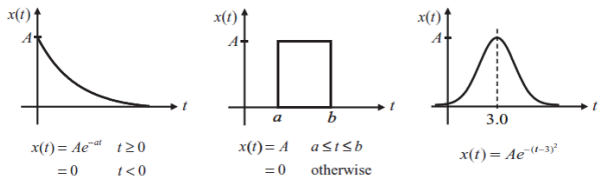

Figure 3.7: Theoretical Examples of Transient Signals [15].

The frequency characteristic of transient signals is very distinct from the Fourier series. Discrete frequency components are replaced by the concept of the signal comprising a continuum of frequencies. It should also be pointed out that the modal characteristics of the beam make it possible for the transient response to be modelled as a sum of decaying

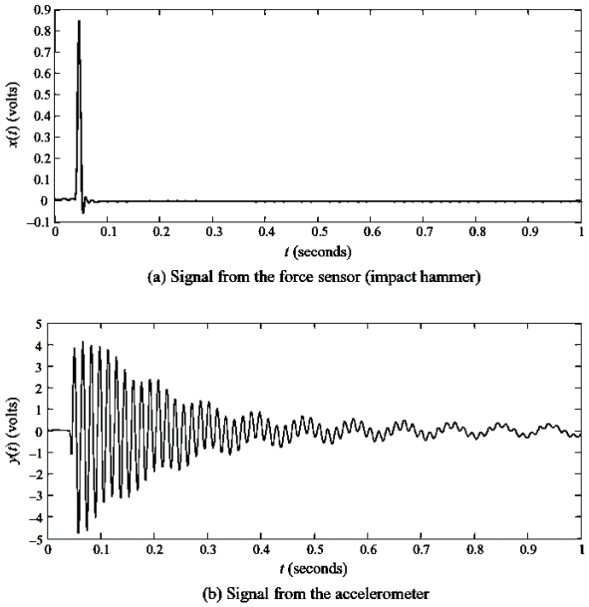

Figure 3.8: Practical Examples of Transient Signals [15].

oscillations, thus giving the possibility of estimating amplitudes, frequencies, damping and phases [15].

Cyclostationary Signals

Cyclostationarity characterizes a type of signal that inherently has a hidden periodicity, whether that hidden periodicity has a multiplicative or additive source. This classification includes stationary deterministic and random signals as particular cases, since stationary signals can be classified by having constant first order statistics in time. Repetitive transients and periodically modulated signals are also included [16].

Cyclostationarity might seem a rather abstract concept. Two common definitions of this concept are stated as follows:

- "Pure *nth*-order cyclostationarity refers to any hidden periodicity that can be evidenced by using a non-linear transformation of order n after all cyclostationary components of lower orders ($< n$) have been removed" [14].
- "For a signal to be cyclostationary of order n, its *nth*-order statistics must be periodic" [12].

Still, these definitions do not seem as obvious to what their added value would be in practical terms for performing analysis of the signals.

A primary approach usually consists of decomposing the signal into deterministic and random components, in order to separate their physical contributions. Since deterministic signals are a particular case of 1^{st}-order cyclostationarity (CS1), this first step allows for differentiating these components from the ones associated to high-order cyclostationary components. The periodic signal components can easily be analysed by conventional methods in the frequency domain, whereas the random part requires more specific analysis tools to reveal hidden periodicities [16]. Methodology for analysing such signals will be further developed in chapter 4.

More often than not, signals of interest produced by rotating machinery happen to be well described by their first two moments - their expected value and autocorrelation function. This means that most of the measured signals are either first or second-order cyclostationary (CS1 or CS2). This a particularly helpful concept to include in the analysis, since bearing fault signatures are CS2 cyclostationary components, hence the autocorrelation function should be a good way to enhance that specific component.

Some simple cases of cyclostationary will now be presented for clarification on the topic at hand. From this point forward, continuous time is designated t for simplicity.

Example 1: The simplest case to consider is a first-order cyclostationary signal. Such a signal, $x(t)$, would be composed of a periodic component $p(t)$ embedded in additive stationary noise $n(t)$, resulting in $x(t) = p(t) + n(t)$. Its first-order statistics, i.e. its expected value in the ensemble average sense then replicates the unaltered periodic component as presented in equation 3.7:

$$E\left[x(t)\right] = E\left[p(t) + n(t)\right] = p(t) \tag{3.7}$$

where the $E\left[x(t)\right]$ denominates the mean value of the signal $x(t)$, which is equal to the mean of the deterministic component $p(t)$, since the stationary random contribution is considered to be null.

Example 2: Analogously to our previous example, a second-order cyclostationary signal is one whose autocorrelation function (presented by equation 3.8) is periodic, i.e. the result of the signal's autocorrelation calculation is repeatable after a certain time period. Mathematically, it can be expressed as $R\left(t, \tau\right) = R\left(t + T, \tau\right)$, where τ denotes a certain time-lag and T the period at which the function repeats its values.

$$R_{xx}\left(t, \tau\right) = E\left[x(t - \tau/2)x(t + \tau/2)\right] = p(t) \tag{3.8}$$

A simple representative case can be given by a periodically amplitude modulated white noise (figure 3.9).

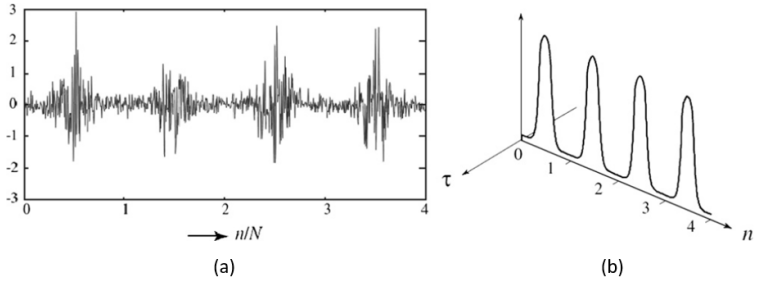

Figure 3.9: Example of amplitude modulated white noise: (a) Time signal composed of four periods; (b) Two-dimensional autocorrelation function (vertical axis) vs time (n) vs time-lag τ [15].

Note that the time representation is discrete, since n refers to a continuous number of samples and N is the total number of samples.

Despite the presence of a periodic modulation, the nature of the signal remains random. By virtue of the second-order non-linearity it introduces, the autocorrelation function is effective in revealing the hidden periodicity of the signal, as shown in 3.9 (b). For time-lag $\tau = 0$, the function returns the signal's instantaneous power following periodically as a

function of time. On the other hand, for other time-lag values, the function returns a null value because the carrier signal is white noise. Generally, any dependence on τ, when compatible with the autocorrelation function, will be possible, depending on the colour of the signal [12].

For practical purposes, analysis of first and second-order cyclostationary signals seems sufficient in order to extract information regarding the machine's condition. However, it will be proven later on that that was not the case in the present work, and thus further study of this topic on analysis of high-order cyclostationary signals should be required.

3.4.1 Common Signal Components

The aim of the present work was, ultimately, to diagnose bearing condition in an induction motor. This chapter aimed to inform the reader on what kind of signals are usually produced during rotating machinery operation. Discrete frequency components such as shaft rotation harmonics, or components produced by the motor fan are expected in the measured signals. Bearings tend to add a certain degree of randomness to the measured signals. However, there are certain operating conditions that can easily be diagnosed and enhance those discrete frequency components. This section describes two of those conditions briefly, as well as some of the consequences they can add, in terms of information for diagnosing the machine.

Unbalance

Unbalance is a common cause for excessive vibration levels. Simply put, it means the rotor system's centre of gravity does not coincide with the rotation axis. An unbalanced rotor system causes more vibration and generates excessive force in the bearing area thus reducing the life of the machine. A small degree of unbalance may be cause of severe damage in high speed rotating machines, causing critical parts to fail, such as bearings, seals and couplings. Overhung rotors are used in many engineering applications such as pump, fans, propellers and turbo machinery. The vibration signature of the overhung rotor is totally different from the centre-hung rotors. In practice, because of manufacturing errors, rotors can never be perfectly balanced. Some of those errors could be caused by porosity in casting, non-uniform density of material, manufacturing tolerances and gain or loss of material during operation. Consequently, centrifugal forces are generated and must be reacted against by bearings and supporting structures. The generated centrifugal force causes the rotor to rotate off its centre, inducing high vibration equivalent to one order of the shaft rotation [17].

$$F_{unb} = mr\omega^2 \tag{3.9}$$

An example can be seen in figure 3.10 (a), where r is the distance between the centre of gravity and the centre of rotation, m is the unbalanced mass, and ω the rotational speed. The centrifugal forces are determined by equation 3.9.

Misalignment

Misalignment occurs when two coupled shafts' rotational centres, driver and driven, are not in a straight line (parallel misalignment) or when there is an angle between them (angular misalignment). Usually this can happen due to differences in the elevation level.

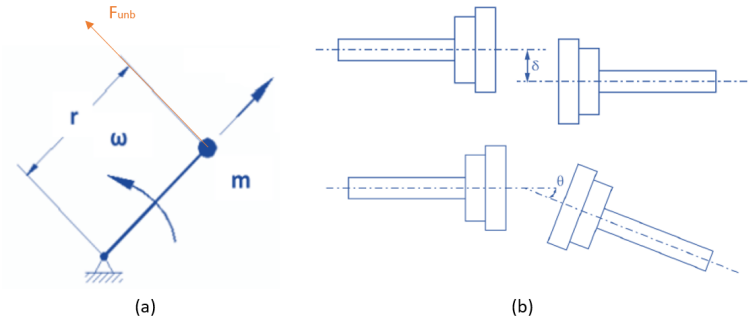

Figure 3.10: Schematic representations of: (a) Unbalance; (b) Misalignment [18], [10].

Both types of misalignments are presented in figure 3.10 (b). Note that in the case of parallel misalignment both shafts remain parallel to one another, but are laterally displaced, making it so that their centres of rotation do not coincide. On the other hand, when angular misalignment occurs, the shafts are no longer parallel with a clear angle between them. Similarly to unbalance, misalignment can lead to premature failure of machine components, by inducing bending deflections on the shafts, whose moments will have to be counteracted by reacting forces at the bearings and the machine's foundations. A misalignment condition may occur internally, corresponding to two (supposedly) co-axial bearings, or externally, in case when two machines are coupled together. Internal misalignment can occur due to a design error or mounting error, as the components responsible for this condition will essentially be the foundations and the bearings' housings.

Misalignment can generate an axial push and pull on the shafts, thus increasing axial vibration levels. This increase in vibration occurs at a frequency twice of the shaft's rotational speed, justified by the fact that an increase in misalignment will cause an increase in torque at twice the rotational speed. Flexible couplings can be used to minimize this effect. Depending on the type of coupling, these may also induce characteristic vibrations of their own. Alignment of the shafts should be performed in operating conditions to account for thermal expansion and deformations of the structure. This may cause some machines to run misaligned while cold [10].

CHAPTER 4

Signal Processing Techniques

Some concepts have been approached in the previous chapter referring to the Fourier spectrum or demodulations. Those are tools of common use in signal processing techniques. The present chapter will present some signal processing tools and techniques, culminating in the adopted procedure for the present work.

4.1 Basic Concepts

There are a number of algorithms already implemented to process signals measured by traditionally used sensors in industry, such as acoustic or acceleration signals that can be obtained by the use of microphones and accelerometers. The most common way of representing raw signals (term used to designate measured signals before any processing is done) is a waveform as a function of time, or, time-domain representation.

However, this representation is often not useful for extracting diagnostic information. For gears with broken teeth, the impacts are actually quite clear and can often be seen in this representation. Contrarily, bearing signals have much lower amplitudes and appear to be of random nature, being masked by other components. It has also been said that for analysing such signals it is useful to represent them in the frequency domain, where periodic components become much clearer.

Since the main goal of this work is to diagnose bearing faults, the main procedure consists of performing envelope analysis. This technique, which will be developed later on, focuses on demodulating the signal in a high frequency range, so that fault related information can be extracted. However, these modulations are often masked, and it is of the utmost importance to determine an appropriate filtering and so that fault signatures become visible in the frequency domain, at the end of the procedure. Other recently developed tools, such as cyclostationary analysis, have also proven quite useful when analysing signals such as those originating from bearings. It will be shown later on that this will be a major point of interest for the work developed in the present text, namely, for determining the aforementioned frequency bands of interest. For performing signal analysis, having a speed reference is often important, hence, tachometers are quite used for this purpose.

For starting our analysis, different forms of signal representations will be presented in this section.

4.1.1 Time Domain

Time-domain representations are the most simple form of representing a measured signal. It is important to understand which machinery components generate the different profiles of the signal. Time waveform representations are frequently unable to provide an analyst with relevant diagnostic information, as the components are represented in an additive way, generating an apparently random waveform. Amplitude and frequency modulations are also common occurrences when faced with such measured signals.

As an introductory step, it is good practice to visualize time-domain signals of isolated components. Figures 4.1 (a) and (b) present two waveforms. One low frequency signal, responsible for the amplitude modulation and a carrier signal. Carrier signals are high frequency signals, representative of the resonant modes of a mechanical structure and often excited by transients corresponding to impacts.

For better understanding of these basic concepts, the example given by the figure in (c) presents the interaction of two sinusoidal signals, where the one lower frequency signal modulates the high-frequency one in amplitude. By multiplying (a) by (b), we obtain the amplitude modulated signal in (c).

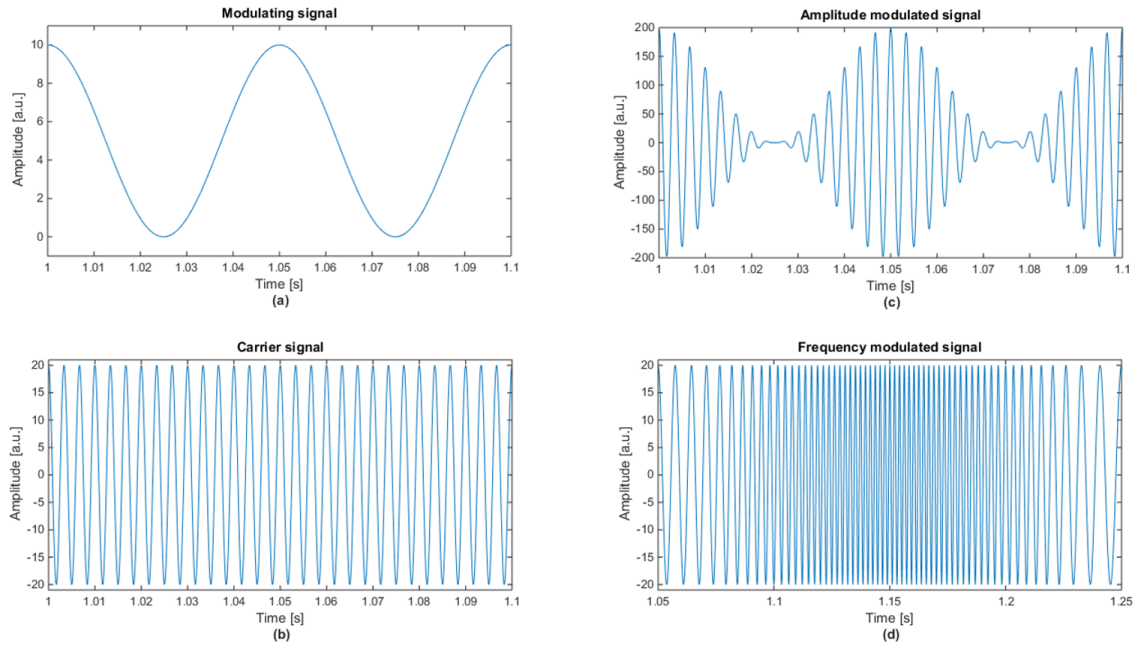

Figure 4.1: Example of Modulated Signals: (a) Modulating signal; (b) Carrier signal; (c) Amplitude modulated signal; (d) Frequency modulated signal.

These signals were simulated merely for clarification purposes. The carrier frequency is of 300 Hz, and the modulating one of 20 Hz.

Both of them can be expressed in the form of equations 4.1 and 4.2:

$$x_m(t) = A_m sin\ \omega_m t = A_m sin(2\pi f_m t) \tag{4.1}$$

$$x_c(t) = A_c sin\ \omega_c t = A_c sin(2\pi f_c t) \tag{4.2}$$

where the m index refers to the modulating signal and the c index refers to the carrier signal.

Another possible kind of modulation can occur, but in frequency. Though the concept might seem complex, the simplest form of exposing it is that: different frequencies can occur at different moments in time. Note that in (d) this modulation occurs without any change in the waveform's amplitude. The signal is generated based on the previous ones, though with slight changes in the formula. It can be expressed by equation 4.3:

$$x(t) = A_c sin\ \omega_c t = A_c sin\left[2\pi(f_c + k_f A_m sin\ \omega_m t)t\right] \tag{4.3}$$

where k_f is the frequency modulation index. For the signal to assume this continuous form, it should correspond to the ratio A_m/A_c.

Vibration signals originating in rotating machinery often comprise both types of modulations. The goal of the analysis is to determine the periodicity at which transients occur. For this purpose, demodulation techniques that allow for removal of carrier frequencies, such as the Hilbert transform, are applied in the envelope analysis stage.

In practice, signals do not have a purely sinusoidal behaviour. Instead, they take the form of decaying transients with a certain periodicity. These are designated damped impulses, as illustrated in figure 4.2 and expressed in equation 4.4.

The negative exponential behaves as the modulating wave and is, theoretically, repeatable at a determined frequency. The Hilbert transform allows the removal of carrier frequencies. The resulting signal (a.k.a. envelope) will then be composed, mainly, of the transients that originate in the bearing fault (represented by the orange dashed line in figure 4.2). More often than not, the frequency of the represented envelope (decaying amplitude of the transient) is much lower than the carrier frequency excited by the transient itself.

$$x(t) = A_m e^{\sigma t} sin(\omega_c t + \vartheta)\ , \quad \sigma < 0 \tag{4.4}$$

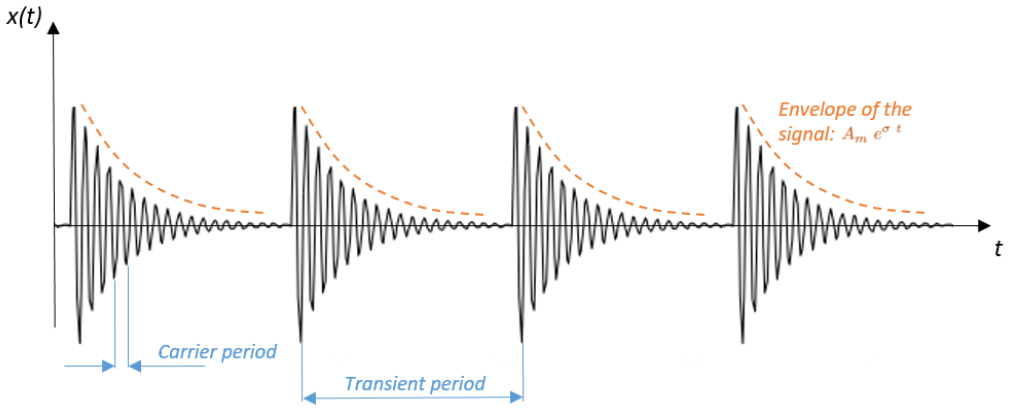

Figure 4.2: Example of a Transient Decaying Impulse [1].

Because events in rotating machinery tend to behave in a cyclic manner, their signals are constantly subject to amplitude or frequency modulations. Determining modulation frequencies helps to establish filter parameters.

Usually, signal processing algorithms seek to enhance these components, as they are often submerged in noise. Raw signal analysis however, often allows analysts to determine carrier frequencies, shaft components or other modulations.

4.1.2 Frequency Domain

Spectral analysis of signals is often used in a wide range of engineering problems. Spectral analysis allows for a simple representation of signals as a weighted sum of sinusoidal components, also called spectral components. Raw signals represented as time functions can be converted to frequency domain and decomposed into these spectral components. The function that weights this decomposition is represented as the density of each spectral component. This spectral density is also called spectrum. Representation of a signal by its spectrum can often give some insight on the signal's nature, namely its frequency content, that time-series do not provide [19].

In theory, any signal can be decomposed into a series of pure sine-waves contributions. The spectrum merely represents those components' frequencies, with their impact on the whole signal being given by each component's spectral density. A spectrum plot of a signal usually presents a series of vertical lines. Frequencies are represented in the spectrum's abscissa, whereas the amplitude of each component can be measured on the y-axis.

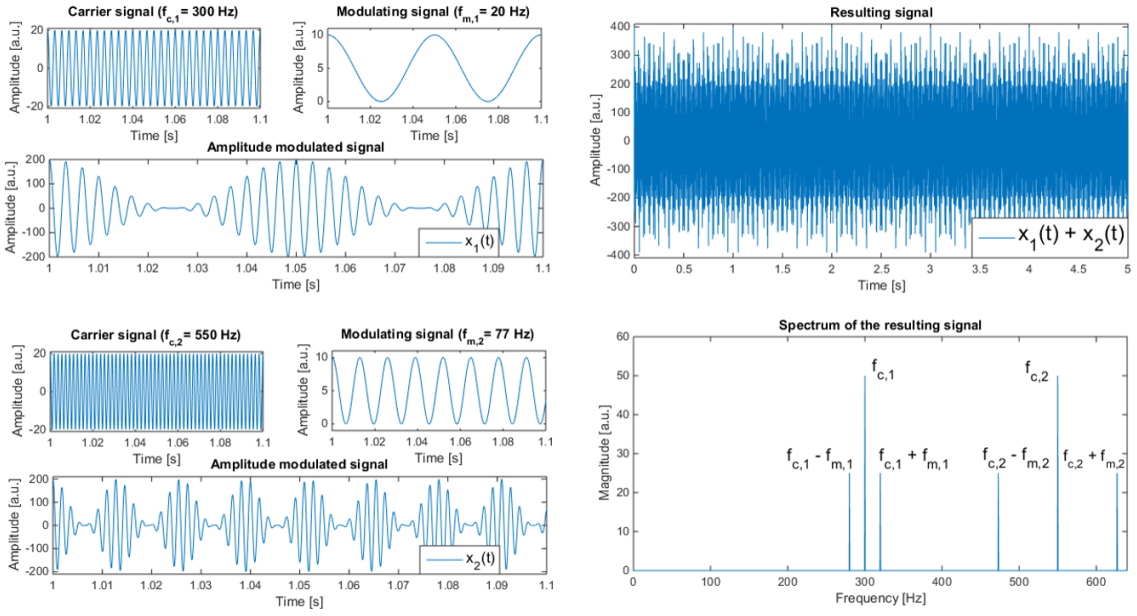

Figure 4.3: Example of an Amplitude Modulated Signal's Spectrum.

An example of this representation is given in figure 4.3, where two amplitude modulated signals, $x_1(t)$ and $x_2(t)$, are added to generate a third signal. This third signal is then represented by its spectrum, with the different frequency contributions quite clear.

Note that these signals are generated exactly as explained in the previous section. Their spectral components are quite clear, with their modulations appearing as side-bands of the respective carrier frequencies.

Frequency-domain data are obtained by converting time-domain signals using a mathematical technique referred to as Fourier transform (FT). Other representations such as in

the time-frequency domain or cyclic-spectral frequencies domain are also possible. These concepts will be further explained later on in the present chapter.

4.2 Pre-Processing Techniques

Now that some basic fundamental concepts for signal analysis were introduced, it is now possible to develop this topic with greater depth.

Pre-processing techniques are applied in a primary processing stage. Since bearing fault signatures are of a certain random nature, it is useful to separate them from discrete frequency components. In other words, periodic signals such as those of the shaft rotation frequency and its harmonics, possibly enhanced by a misalignment or unbalance conditions, gear-mesh frequencies or blade-pass frequencies can be reduced, or have their effects minimized by application of such techniques.

4.2.1 Cepstrum

The Cepstrum method was mainly explored in the 1960's. It was first introduced for studying seismic signals, aiming to isolate the influence of echoes from the remaining data. Back then, it was a superior method when compared to the application of the autocorrelation function in the determination of the echoes' delays.

The application of this technique in bearing diagnostics seeks to remove the aforementioned periodic components in the frequency spectrum, as well as their respective side-bands.

In conceptual terms, the Cepstrum detects periodicities in the frequency spectrum, whereas the spectrum itself detects periodicities in the time domain signal.

Analysing the quefrency domain is of great importance in condition monitoring applications. The first rahmonic of the cepstrum-edited signal directly indicates the spacing of harmonic content independently of its occurrence in the frequency spectrum. Other undetermined frequency components, such as those of bearings, can then be traced back to their sources. Recently, this first rahmonic has been identified as a stable trend parameter. The developing of this method is not simple, requiring a relative computational cost to the process, as well as some expertise in interpreting its results [20].

A common aspect of bearing and gear signals is that both have a harmonic series associated to their respective characteristic frequencies. When the side-band content becomes widely spread in the spectrum, the signal-to-noise ratio is often low. By applying the Cepstrum to the raw signal, one can try to recover relevant information, thus enhancing that ratio, and retrieve the time-domain signal [10].

The Cepstrum definition is rather complex. The most commonly used one is stated as: the inverse Fourier transform of the logarithmic spectrum of the signal. Figure 4.4 illustrates the functioning of the method.

There are some considerations to take into account when applying this technique. Noise level in the spectrum may affect the detection of a series of harmonic components. If the harmonics are somehow smeared by operational noise, the Cepstrum will not be able to detect them. Although various methods can be applied to enhance discrete frequency components, some precautions must be taken during measurements. For applying the Cepstrum, good harmonic/side-band resolution of the spectrum is often required. Hence,

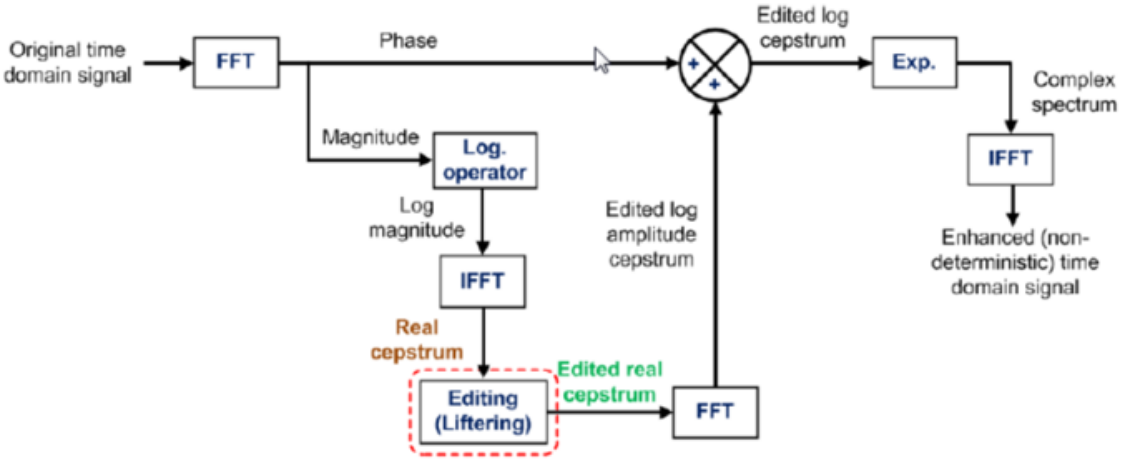

Figure 4.4: Schematic Representation of the Cepstrum Algorithm [21].

removal or minimizing of shaft frequency harmonics for separating them from other frequencies of interest (e.g. bearing fault frequencies or gear-mesh frequencies) is quite useful. Such harmonics can be enhanced due to a misalignment condition of the test bench. Therefore, its condition should be verified beforehand [3].

Other issues can arise when different frequency components are closely together in the spectrum which may cause harmonic content to cross over. This can happen if the filter characteristics or the components are not properly separated in the spectrum. One possible solution would be to improve spectral lines in the data collection. Another important aspect is the choice of the vibration parameters. The most common ones are velocity or acceleration, with displacement often being disregarded. The effect of choosing one of the first two is notorious, especially in the low quefrency, as the main difference between them is generally a slight change in the slope of the logarithmic spectrum, associated to the integration from acceleration to velocity [3].

Some new terms have been introduced in this section. This is due to the transformations performed by the Cepstrum method. A basic user should not be startled by its apparent complexity. Some simple terminology equivalences are established in table 4.1.

Frequency	**Quefrency**
Harmonic	Rahmonic
Filter	Lifter
Magnitude	Gamnitude
Phase	Saphe
Low-pass filter	Short-pass lifter
High-pass filter	Long-pass lifter

Table 4.1: Terminology in frequency and quefrency domains

On a final note for this section, the mathematical definition of the Cepstrum is going to be presented. Starting with its definition as the inverse FT of the logarithmic spectrum:

$$C(\tau) = \mathcal{F}^{-1}\ [log\,(X(f))] \tag{4.5}$$

$$X(f) = \mathcal{F}\,[x(t)] = A(f)e^{j\phi(f)} \tag{4.6}$$

where $X(f)$ represents the FT (or spectrum) of the time-domain signal. Expressing $X(f)$ of equation 4.6 in terms of amplitude and phase:

$$log\ X(f) = ln\ A(f)\ +\ j\phi(f) \tag{4.7}$$

When the term $X(f)$ is complex, the cepstrum provided by equation 4.5 is designated the complex cepstrum. When the power spectrum is applied instead of the spectrum $X(f)$, the resulting cepstrum is designated as the power cepstrum (or real cepstrum) and is given by equation 4.8.

$$C_{xx}(\tau) = \mathcal{F}^{-1}\ [2\ ln\ A(f)] \tag{4.8}$$

The phase function $\phi(f)$ must be unwrapped to a continuous function of frequency prior to calculating the complex spectrum. This can be a complex procedure, making the real cepstrum easier to use [3].

4.2.2 Angular Re-sampling

There are a number of situations when shaft speed fluctuations may occur. In such cases, it may be useful to represent our signal as a function of angle to isolate components related to specific moments of the machine's cycle. Hence, the signal is then presented in the Order domain, where we refer to orders as multiples of the shaft rotation, and the technique behind this is called order tracking (or angular re-sampling).

Application of angular re-sampling is particularly useful because speed fluctuations can cause smearing of discrete frequency components, or to see how harmonics' strengths vary along a wide range of speeds, as they pass through several resonances.

If a signal, which is synchronous with some phenomena of the machine's cycle, for instance the rotation of the shaft, is sampled at a fixed number of times per revolution, the digitally acquired samples are not separable from those of a sinusoid, meaning that we obtain a line represented in the spectrum. On the other hand, if regular temporal sampling is used, the signal's spectrum spreads over a wide range corresponding to the variation in the shaft speed, originaring smearing and leakage. This is due to the fact that the frequency component is not stationary on one spectral line. To apply this method, a sampling signal from a tachometer or shaft encoder is necessary to generate a sampling signal synchronous with the phenomena of interest (in this example, the shaft speed). However, this approach has a finite response in time and may not measure the slight random speed fluctuations along the cycle [3].

Due to the aforementioned limitations, it is often best to re-sample the measurement records uniformly according to angle of rotation. As a consequence of the speed variation as a function of time, the number of samples differs for each shaft revolution, resulting in the aforementioned smearing and leakage in the spectrum. As such, the measured signal is re-sampled at constant angle, but varying time, to avoid this issue and ensure the same number of samples per shaft revolution. Thus, angular re-sampling converts the time-domain data into the angular domain.

An example of how this method is implemented is shown in figure 4.5. Note that (a) as well as (b) illustrate the cyclic events with respect to time. On the other hand, (c) presents those events in the angular domain, at a constant angular reference.

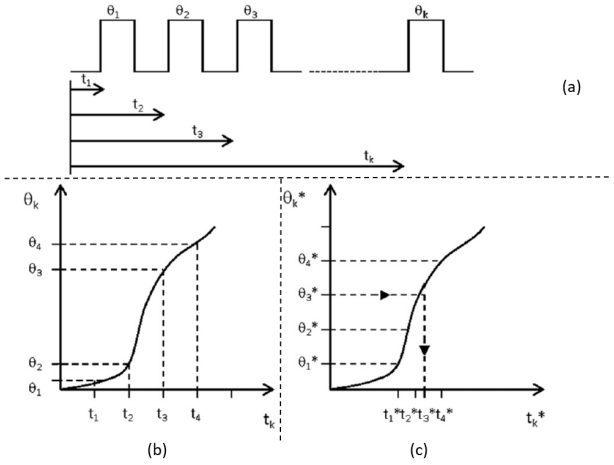

Figure 4.5: Schematic Representation of Angular Re-sampling [22].

4.2.3 Time Synchronous Averaging

The Time Synchronous Averaging (TSA) is a signal processing technique that is able to extract periodic signal components from a noisy dataset. This allows for variations in shaft speed to be corrected, so that the spreading of spectral energy into an adjacent bin can be minimized. As such, it is of common use as a de-noising method.

The tachometer signal is used as a speed reference, combined with the angular re-sampled one, to obtain an integer number of samples per revolution of the shaft using an interpolation method, granting this method the capability of filtering out asynchronous vibration and noise present in the signal.

This angular re-sampling of the signal is often implemented as a first step to correct slight variations in the machine's rotational speed, as well as the uneven number of samples acquired at the same angular positions. The method then averages the vibration over several revolutions of the shaft period. This has a significant effect in reducing asynchronous vibration components and zero-mean noise because as the number of revolutions gets larger, these components' values tend to approach zero, thus minimizing their influence and enhancing the signal-to-noise ratio (respective to periodic components).

Thus, TSA is a well suited method for gearbox analysis, as it enhances the vibration signature of a specific gear to be separated from other gears and noise sources in a gearbox that are not synchronous with that gear [23].

On one hand, it may not be a common method for analysing bearing fault signals. These are not of deterministic nature. Hence, their occurrence in time or angle can suffer slight variations. By averaging these signals in a large number of revolutions, it is possible for bearing fault information to be average to an insignificant value, thus accounting for the loss of relevant information. On the other hand, it is possible to include this method, if the signal resulting from the TSA is subtracted to the original signal. This allows to obtain a residual signal with the bearing fault component supposedly intact (if the bearing component of the signal is averaged out by the TSA).

Mathematically, it corresponds to a synchronous average of the signal, for a certain number of revolutions. Still, it can be expressed as a function of time, as the angular domain representation is basically just a different representation of the time-domain signal. As such, equation 4.9 accounts for a simple representation of this method.

$$x_a(t) = \frac{1}{K} \sum_{k=0}^{K-1} x(t \ + \ kT) \tag{4.9}$$

4.3 Processing Techniques and Analysis Domains

There are several other pre-processing techniques that can be applied to a signal. For bearing diagnostic purposes, it is often applied a technique to remove high-amplitude discrete frequency components that are capable of masking bearing signals, such as gears or shaft frequency harmonics (when subject to a misalignment or unbalance conditions), for instance. These procedures allow the extraction those periodic components, leaving the remaining signal with bearing fault information untouched. Other procedures such as Linear Prediction or Discrete-Random Separation can also be applied. Though they are not subject of the present text, references [3] and [12], as well as some of the others, provide some interesting information on the subject.

After removing masking discrete frequency components, our bearing fault signatures should become clearer. However, application of these signal processing techniques does not change the nature of the signal. As such, high-frequency resonances are still excited by the pulse-train generated by the faulty bearing under operation. The goal of this section is to enlighten the reader on some techniques that can be applied to identify these high-frequency bands that are excited in the resonant modes. After this identification is performed, filtering parameters can be established, and demodulation can be applied to retrieve the original frequencies of interest - the bearing's fault frequencies.

4.3.1 Frequency Domain

As seen in section 4.2.1, the representation in the frequency domain allows for complex machinery signals to be represented as discrete frequency peaks.

This representation can be obtained by applying a Fourier transform (FT) to the signal. The concept behind the Fourier series is that any finite length signal (with a few exceptions) can be decomposed into a series of periodic components.

So, a general periodic signal $x(t)$ can be described as in equation 4.11:

$$x(t) = x(t \ + \ kT) \tag{4.10}$$

$$x(t) = \frac{a_0}{2} + \sum_{n=1}^{\infty} a_n \ cos(n\omega_0 t) \ + \ \sum_{n=1}^{\infty} b_n \ sin(n\omega_0 t) \tag{4.11}$$

where k is any integer, ω_0 is the fundamental angular frequency in [rad/s] ($= 2\pi/T_0$). The fundamental frequency in Hz (f_0) equals $1/T_0$ and the coefficients of the cosine and sine terms can be obtained by correlating the latter with $x(t)$ as follows [3]:

$$a_n = \frac{2}{T} \int_{-T/2}^{T/2} x(t) \ cos(n\omega_0 t) dt \tag{4.12}$$

$$b_n = \frac{2}{T}\int_{-T/2}^{T/2} x(t)\ sin(n\omega_0 t)dt \tag{4.13}$$

The amplitude of a function at its n^{th} harmonic can be determined by resorting to equation 4.14.

$$A_n = \sqrt{a_n^2\ +\ b_n^2} \tag{4.14}$$

The Fourier series of a function may also be represented in the complex domain and it can be represented in either as real-imaginary parts or in a magnitude-phase format [10]. Phase information is often useful for determining misalignment or unbalance conditions of the machine. However, it does require for two accelerometers to be placed in the same component and displaced of a certain angle between them.

Discrete Fourier Transform

Measured signals for condition monitoring of a machine are often of different frequencies and characteristics, such that they cannot be described by a unique mathematical expression. Despite this fact, they can still be reconstructed in the time domain as modern digital equipment allow for high sampling frequencies, which means that data is regularly acquired in time, at very short time intervals. The Fourier integral can be estimated by equation 4.15:

$$X(k\ f) = t\sum_{n=0}^{N-1} x(n\ t)e^{-j2\pi k\ fn\ t} \tag{4.15}$$

where k is an index and N the total number of samples.

From equation 4.15 it is clear that the FT of a signal comprising N discrete data points, requires N^2 complex mathematical operations to be computed. When the discrete Fourier transform (DFT) was first implemented, computing resources were scarce and represented a computational challenge. A new computation algorithm was developed in the 1960's, where $Nlog10N$ operations were required instead of N^2. The application of this algorithm substantially reduced the required computation time to convert a measured signal to its frequency domain with its complex Fourier coefficients. The only requirement to meet would be that, for the $Nlog10N$ algorithm, the total number of data points N, required for computation should be a power of 2. That is, the total number of data points should be 128, 256, 512, 1024, 2048, 4096, and so on. This algorithm became a success and came to be known as the fast Fourier transform (FFT) [10].

Signal's Spectrum

As seen throughout this chapter, FFT allows time-domain signal components of a complex machinery to be represented in the spectrum as discrete frequency peaks. This is particularly helpful for an analyst. By visualizing a raw signal's spectrum, one can get a different insight on the signal's nature. As mentioned in the beginning of section 4.3, one of the main goals of signal analysis for condition monitoring is to detect high-frequency excited bands, where characteristic fault frequencies may be modulated.

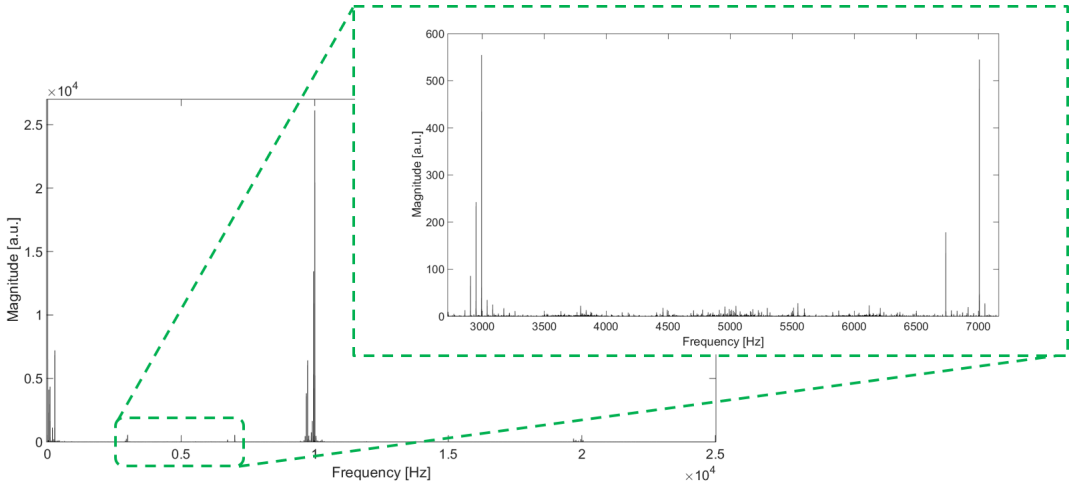

Figure 4.6: Spectrum of a measured acceleration signal.

Figure 4.6 shows the spectrum of a raw measured signal during the measurement campaign stage of this work. Note that there are clear excitations throughout the whole spectrum. However, smearing and leakage issues, along with the presence of masking components can make it quite difficult to retrieve diagnostic information at this stage, this step is common good practice, as one can get a sense of which main frequency components constitute the measured signals.

4.3.2 Time-Frequency Analysis

Frequency-domain representations are based on the theoretical assumption that signals are stationary. As such, the difficulty of leading with nonstationary or transient signals becomes increasing when the methods we have seen so far are based on such a conceptualization. In theory, the Fourier transform requires integration over all time. However, we are well aware that frequency changes can occur at different moments in time (e.g. in music). Therefore a representation that is able to capture the nature of time-varying frequency is often useful to analyse certain signals. It allows the analysis of determined behaviours in respect to time with precise frequency information which can be a good tool to understand when nonstationarities occur. This representation uses a two-axis coordinate system, where time is represented on the abscissa and frequency on the vertical axis. Magnitude information is commonly given by a certain colour. Various techniques employ this representation, which shows great potential in detection of bearing faults in complex rotating machinery, where the signal-to-noise ratio is very low and in the presence of several frequency components associated to many of the mechanical components [3].

Short Time Fourier Transform

One simple approach is given by the short time Fourier transform (STFT). It is based on moving a short-time window along the signal and then obtaining the spectrum as a function of the time-shift. Disadvantages of this technique, however, relate to the fact that frequency resolution is reciprocal of the effective time window length, and that the windows applied to the signal may overlap. Even so, the STFT is sometimes useful for tracking frequency variations with time, even with the restriction of resolution. This technique is described by the formula:

$$S(f,\tau) = \int_{-\infty}^{\infty} x(t)w(t-\tau)e^{-j2\pi ft}dt \tag{4.16}$$

where $w(t)$ is the window which is moved along the signal. Generally, the amplitude squared $|S(f,\tau)|^2$ is presented on a time–frequency diagram, also known as a spectrogram. The window could be of finite length, or, in theory, infinite as well, though in practice it must be truncated [3].

Wavelet Transform

Another possible approach to the analysis in the time–frequency domain is to decompose the signal as a family of 'wavelets' with a fixed shape, but that can be shifted and dilated in time. The formula for the Wavelet transform is given by equation 4.17.

$$W(a,b) = \frac{1}{\sqrt{a}} \int_{-\infty}^{\infty} x(t)\psi^* \left(\frac{t-b}{a}\right) dt \tag{4.17}$$

where the ψ^* is the mother wavelet's complex conjugate, which is translated by b and dilated according to the factor a. Since this definition corresponds in fact to a convolution, wavelets can be treated as a set of impulse responses of filters, which have constant percentage bandwidth properties due to the dilation factor. The dilation factor a is also designated as scale, but, through its inverse, represents log frequency, as well as for constant percentage bandwidth filters. Due to their characteristics, wavelets provide a better time localization at high frequencies, and thus, can be useful for detecting limited events in a signal.

Wavelet transform representations are able to provide information on speed fluctuations, transient events, and grant the possibility for verification of information obtained from time and frequency-domain signals, modulations, as it represents the evolution of the spectrum with time [3].

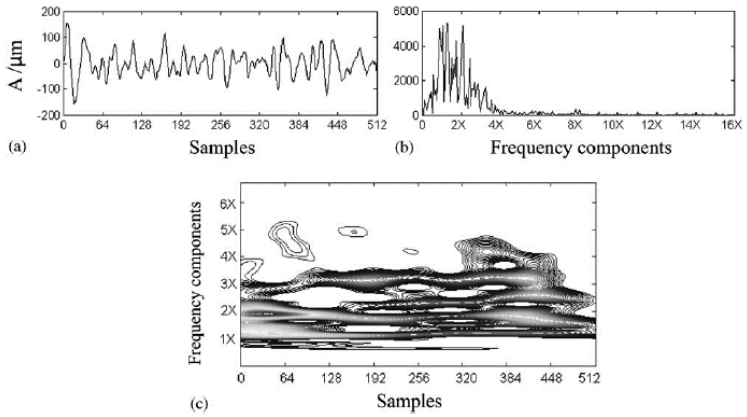

Figure 4.7: Example of time-frequency representation: (a) A non-stationary vibration time-domain signal; (b) Its frequency representation; (c) Its wavelet scalogram [24].

4.3.3 Cyclic Spectral Correlation

Over the past few years, cyclostationary analysis has been gaining some recognition in the Condition Monitoring field, mainly for analysis of vibration signals. This is due to

the fact that, though signals originating from rotating machinery might seem periodic, they are not exactly phase-locked to shaft rotational speeds, and consequently cannot be extracted after applying a discrete-random separation technique. Some examples are given by the combustion events in internal combustion engines, varying from cycle to cycle, and impulses from rolling element bearing faults, which are affected by a minor but randomly varying slip [25]. Benefits from the cyclostationary approach have been explored for over a decade, as research in this domain has culminated in a general methodology and analysis tools that have proven to be effective in analysing general rotating machinery vibration signals.

As aforementioned, a common approach in condition monitoring, mainly in bearing diagnostics, is to first separate signal components as periodic and random contributions. This can be regarded as an equivalent to separating the physical phenomena that originate these components. Cyclic Spectral Correlation (CSC) is a tool that has been developed and has proven to be quite efficient in the analysis of cyclostationary signals, namely in separating first from second or higher-order cyclostationary signal components.

The CSC is a recent, spectrum-based technique that has been successfully used to determine rotating machinery faults, as it takes advantage of the nonstationary nature of signals by defining them as cyclostationary instead.

According to Randall and Antoni [12], "an nth order cyclostationary signal is one whose nth order statistics are periodic". In other words, a cyclostationary signal can be defined as being of nth order cyclostationarity if it reveals a hidden periodicity after being subject to a nth order non-linear transformation, or even, by a probability density function that is periodically time-varying.

The simplest case is a first-order ciclostationary signal, x, the which is merely a periodic signal embedded in stationary noise n. Its first-order statistics (expected value) is therefore a periodic function as in equation 3.7, here presented as equation 4.18. Gear signals, due to their periodicity can be modelled as first-order cyclostationary.

$$E\left[x(t)\right] = E\left[p(t) + n(t)\right] = p(t) \tag{4.18}$$

In a similar manner, second-order cyclostationary signals are those whose autocorrelation function (given by equation 4.19) is a periodic function of time. These signals can be represented in the general form by equation 4.19 (which results from the expansion of equation 3.8), and whose periodicity condition is met by T in equation 4.20.

$$R_{xx}\left(t,\tau\right) = \lim_{T\to\infty} \frac{1}{T} \int_{-T/2}^{T/2} x\left(t - \frac{\tau}{2}\right) x\left(t + \frac{\tau}{2}\right) dt \tag{4.19}$$

$$E\left[x(t)x(t-\tau)\right] = R_{xx}(t,\tau) = R_{xx}(t+T,\tau) \tag{4.20}$$

When available for all values of t and τ the autocorrelation function is able to provide all the information regarding second-order cyclostationary components of the signal. However, displaying this information in the frequency domain may illustrate better the structure of the signal. The Spectral Correlation function can be estimated by the expression 4.21.

$$S_{xx}\left(\alpha, f\right) = \lim_{W\to\infty} \frac{1}{W} \int_{\mathbb{R}} \int_{-W/2}^{W/2} R_{xx}\left(t,\tau\right) e^{-j2\pi(f\tau+\alpha t)} dt d\tau \tag{4.21}$$

This technique involves two frequency variables with distinct meanings. Frequency f appears as a dual of the time-lag τ and represents the carrier frequency. On the other hand, frequency α is the dual of time t and represents the modulation frequency. This last parameter is also known as "cyclic frequency", and will represent our frequencies of interest, such as fault signature frequencies, whereas f can be seen as a high-frequency range, as if you were analysing a spectrum, where the cyclic frequency is modulated. The same result could be obtained by correlating the spectrum with itself, hence the name "spectral correlation" [12].

As such, it is logical to assume that the CSC presents the level of correlation of the signal at different frequencies, thus revealing the (cyclic) frequencies of interest.

Another interesting aspect is the fact that the method allows for a correct estimation of filter parameters, by selecting a frequency range, based on a magnitude threshold (typically, very close to and containing the maximum value). This procedure can be implemented in a fully automated way, or in a semi-automated one, depending on the case.

The representation of the CSC map can be done by a three-dimensional plot, or as a typical representation of the time-frequency domain, with the cyclic frequency α represented in the abscissa, the spectral frequency f in the vertical axis, and magnitude represented by a colour scale.

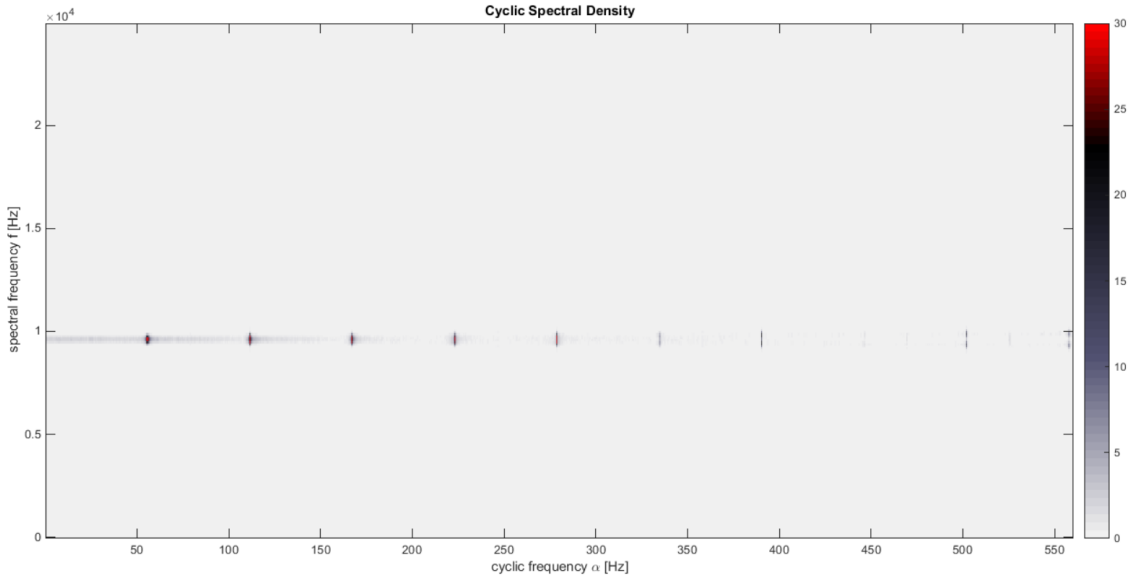

Figure 4.8: Example of a CSC map representation: cyclic frequency of 55 Hz and carrier of 10 kHz.

Figure 4.8 presents the spectral correlation map for a signal resulting from the multiplication of frequency modulated signals. Note that the cyclic frequency of 55 Hz and its harmonic components are modulated, and present higher magnitudes at the spectral carrier frequencies around the 10 kHz range. This practically matches the established parameters. There is a small shift however, due to a random component that was introduced.

Despite the potential of this procedure, its order of application in the processing must be carefully done. After performing demodulation of the signal, the modulation-related information that the spectral correlation presents is lost, with only the low frequencies presented. When a low range of frequencies, of the order of the cyclic frequencies is presented, no relevant information regarding modulations in the signal can be extracted.

However, it is an excellent analysis element to use prior to the application of envelope analysis, where it plays an important part in determining an adequate frequency band for filtering the signal.

4.3.4 Kurtogram

The Kurtogram is another tool employed to help estimate filter parameters.

The concept behind this tool is an imposed band-pass structure, focusing only on the estimation of two parameters: a central frequency, F_c, where the highest spectral kurtosis (SK) value is located; and a bandwidth B_w, that should achieve an optimum compromise between a too wide filter and a too narrow one. A excessively wide filter can alter the signal-to-noise ratio, whereas a too narrow filter has a very long impulse response that could alter the impulsive nature of the filtered signal [26]. Figure 4.9 shows an example of a kurtogram, where N_W represents the kurtogram window length that defines spectral resolution [3].

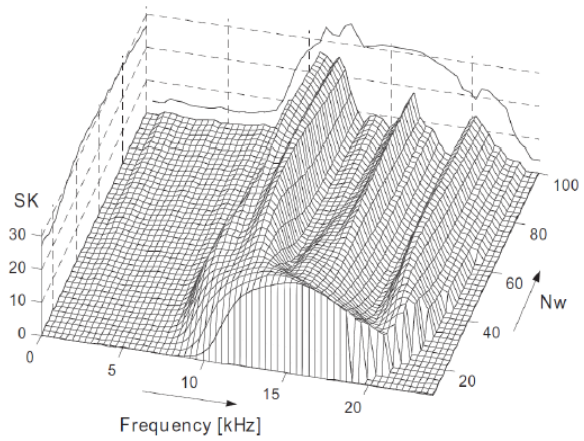

Figure 4.9: Example of a Kurtogram representing an outer race fault [12].

This approach is based on the fact that a band-pass filter is a good tool for selecting a frequency band where the signal-to-noise ratio is maximum. By decomposing the signal into successively narrower frequency bands, it may be possible to detect the frequency band(s) where the signal best presents its impulsive nature, in cases where there is more than one source. Applying a filter to the signal is fundamental, prior to performing its demodulation.

As such, pre-establishing filter parameters makes the filter independent from the assumed validity of the model [26].

Covering every possible combination of centre frequency and bandwidth by computation of the full kurtogram is very costly. So, a number of more efficient alternatives have been proposed. The most often used one is the fast kurtogram, which is based on the application a series of digital filters to the signal. It basically consists of progressively dissecting the frequency range into narrower bands that are half of the width of the previous one. The resulting combinations of centre frequency and bandwidth are illustrated in figure 4.10 [3].

However, it has been referred in section 2.2.3 that VFDs generate broadband impulsive signals. This poses as a severe limitation for the kurtogram application for condition monitoring purposes. The drive's signals interfere with the sensors, thus transmitting their impulsive nature to the acquired signals, as electromagnetic interference (EMI).

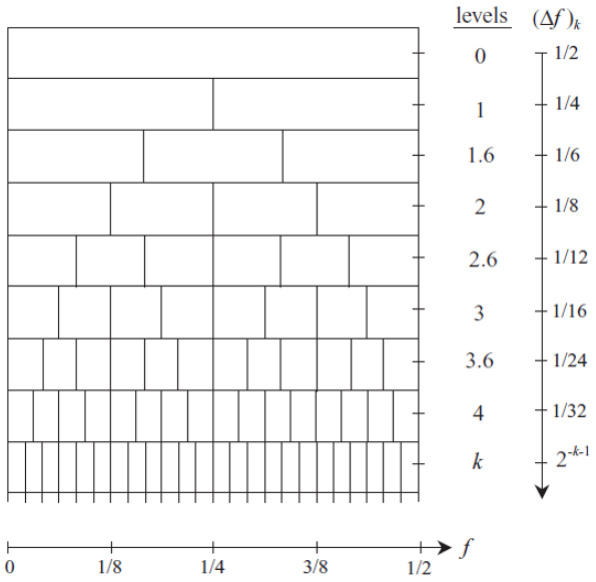

Figure 4.10: Example of a Fast Kurtogram [3].

In recent case studies, Smith [27], [28], studied this effect and proposed the application of an optimised spectral kurtosis tool for application in such cases where EMI severely affects the measured signals. This tool was not available at the time of development of this text. However, one of the main conclusions drawn from the author is that by applying a band-pass filter over a sufficiently narrow frequency band would be a good way of maximizing the signal-to-noise ratio. In [27] three filters were applied to three different frequency ranges (500, 2000 and 5000 Hz), with the two that were applied to the narrower bands gave clear results of the fault signature presence.

4.4 Adaptive Filtering

4.4.1 Adaptive Noise Cancellation

"Adaptive noise cancellation (ANC) is a procedure whereby a (primary) signal containing two uncorrelated components can be separated into those components by making use of a (reference) signal containing only one of them" [12].

There is no need for the reference signal to be identical to its corresponding part in the primary one, as long as the are related by a linear transfer function. This technique adaptively determines that transfer function and is then able to subtract the modified reference from the original signal, leaving the remaining signal untouched. ANC was proposed several years ago for extracting a faulty bearing signature in cases where the primary signal could for example be measured on the faulty bearing of a gearbox. The reference signal would be acquired on another remote bearing with no contamination from the faulty component. In spite of this, it relies on being able to acquire an uncontaminated reference signal, which may not be possible in some cases.

Self-Adaptive Noise Cancellation

When one of the two signal components are separated, where one is of deterministic nature, and the other one random, a reference signal can be reproduced as a delayed version of the

original signal. This is possible because if the delay is longer than the correlation length of the random part, the adaptive filter does not recognise the relationship and will be able to determine the transfer function between the deterministic component and the delayed reproduced reference. Thus, separation can be accomplished by using only one signal, and this procedure is called Self-Adaptive Noise Cancellation (SANC). The procedure is illustrated in figure 4.11, applied to the separation of bearing and gear components in the same signal. This filter is recursive and updates its parameters at each iteration, which means that it is able to react to slow changes in the system that generated the measured signal [12].

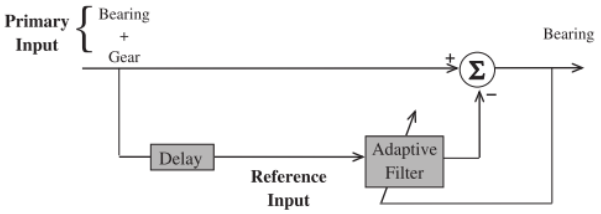

Figure 4.11: Schematic diagram of SANC used for removing periodic interference (gear) leaving random signal (bearing) [12].

4.4.2 Minimum Entropy Deconvolution

The Minimum Entropy Deconvolution (MED) is a processing method whose goal is to minimise the spread of impulse-response filters to obtain a signal closer to the impulsive nature one generated at its source. It was primarily used to enhance reflections from distinct subterranean layers in seismic analysis. The concept behind it is to determine the inverse filter that counteracts the effect of the transmission path of the structure, based on the assumption that the original excitation is impulsive, thus having high kurtosis.

The name derives from the fact that increasing entropy corresponds to increasing disorder, whereas impulsive signals are very structured. It is also required that all significant frequency components must have zero phase at the time of each impulse's generation. This allows for minimization of the entropy, maximizing the structure of the signal, which is an equivalent way of saying that the kurtosis of the inverse filter output (corresponding to the original input to the system) is maximized. The MED could just as well be called "maximum kurtosis deconvolution", as the criteria used to optimise the coefficients of the inverse filter is maximisation of the kurtosis (impulsiveness) of the inverse filter output.

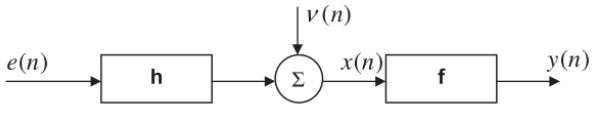

Figure 4.12: Schematic diagram of the MED algorithm [12].

Figure 4.12 illustrates the basic conceptualization of this method. The forcing signal $e(n)$ passes through the structural filter **h** whose output is crossed with noise $v(n)$ to generate the measured output $x(n)$. The inverse filter **f** then produces the output $y(n)$, which must be as close as possible to the original input $e(n)$. Though the input $e(n)$ is unknown, it is assumed to be as impulsive as possible. This procedure is achieved iteratively, when the filter coefficients of **f** converge within a specified tolerance [12].

However, the main disadvantage of this method is related to the fact that it tends to enhance every impulsive component that occurs in the signal, regardless of the frequency

at which such component occurs. In addition, filter parameters need to be established upfront. If one is not properly familiarized with the method it can be severely time-costly.

4.5 Envelope Analysis

Envelope analysis has been the most commonly applied signal processing method to extract bearing diagnostic information for decades.

The basic theory behind this concept is that when a vibration impulse is generated, from a strike of a localised bearing fault with another bearing surface, this strike has an extremely short duration in time, when compared to the time between pulses. Due to this fact, the energy that is released is distributed along a vast frequency range, thus exciting resonant modes of the surrounding mechanical structure. These excitations will tend to occur repetitively, as the contacts between the fault and mating surfaces will normally occur in a repetitive manner during the bearing's operation. The frequency of those impulses will be one of the aforementioned fault characteristic frequencies that were already approached in the previous chapter. For this analysis, the resonance is considered to be amplitude modulated at the fault characteristic frequency, making it possible (by applying this technique) to detect the presence of a fault, as well as its location on the physical component of the bearing.

Raw signal spectra often present very little diagnostic information about the faults. Envelope analysis consists of performing a band-pass filter on the high-frequency band excited by the fault signature. The signal is then amplitude-demodulated by applying a Hilbert transform (HT) to remove the effect of the carrier frequencies. Finally, relevant diagnostic information can then be visualized in the enveloped signal's spectrum [12].

The main challenge in performing proper envelope analysis is to determine precisely the high-frequency band that is excited by the fault's impacts [20]. For this purpose, the tools that were presented throughout this section (except for Adaptive Filters) can be used as filter detection tools, as they often provide information on which bands are most excited in the signal, and in which demodulation should be applied.

Figure 4.13 presents an illustration of how envelope analysis is usually performed.

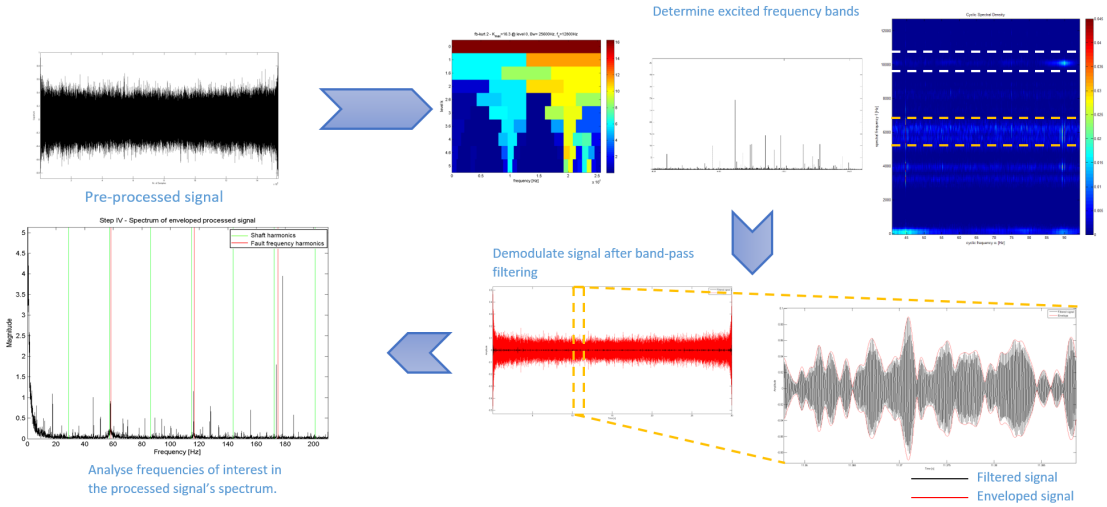

Figure 4.13: Schematic representation of envelope analysis.

Since the beginning of envelope analysis, there has been a strong debate on which would be the most appropriate way of determining an optimum frequency band for demodulation. Some authors propose the hammer-tap test for detecting resonances of the bearing housing, However, nowadays this issue can largely be solved by applying SK-based signal processing tools, or others seen throughout this chapter [3].

4.6 Adopted Procedure

The adopted procedure for the present work will be presented in several stages.

The first stage consisted on gaining a better insight into the components present in both signals. As such, visualization of the raw signals' spectra as well as the spectra of the enveloped raw signals was a fundamental first approach for this purpose.

Secondly, a pre-established procedure with proven results was applied, where the signals were first pre-processed with Cepstrum to remove discrete frequency components. Afterwards, both the fast kurtogram and CSC were applied to determine optimum bands for filtering. Finally, envelope analysis was performed to acquire fault related information.

In a final stage, the MED was applied right after the Cepstrum, to try to evaluate the filter's influence in the methodology proposed in the previous stage.

The scheme represented in figure 4.14 best demonstrates the structure of the present work. A preliminary analysis stage was implemented, whose goal was to determine which frequency bands were most excited in the signal, and thus, most likely to carry fault-related information. The second stage is dedicated to the application of envelope analysis with the parameters pre-established in the preliminary analysis.

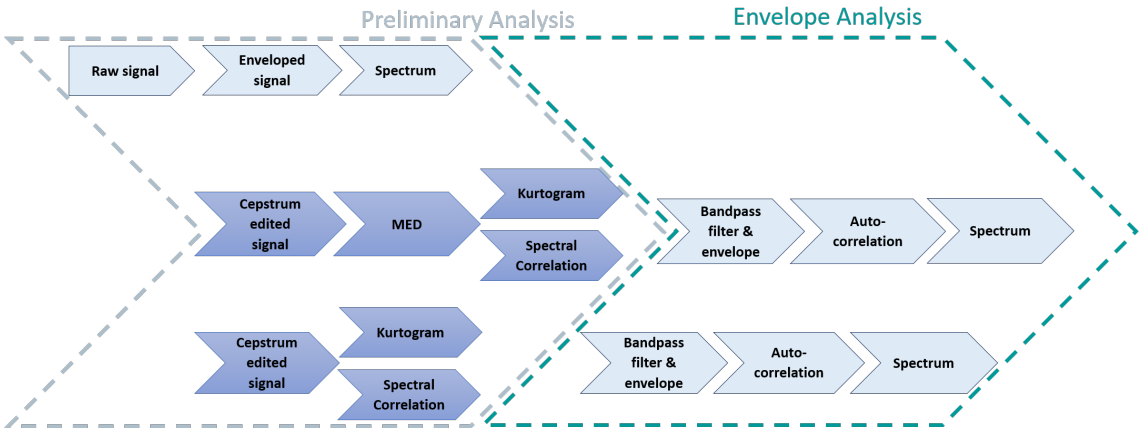

Figure 4.14: Schematic representation of the adopted analysis procedure.

As a side note, it is also worth mentioning that most of the software tools that were used in this procedure were provided by Siemens SISW. The Cyclic Spectral Correlation algorithm, however, was made available at a Mathworks online forum by Antoni. Personally, the role of my work was mostly related to integrating the blue blocks from the previous scheme (in the pre-processing stage) in a way that would best serve the goal of this work: diagnosis of the bearing fault. Ultimately, my personal contribution culminated in integrating these tools in a Matlab program capable of performing this analysis in a semi-automated manner. For this purpose, close guidance and insights provided by Siemens' experts proved very important throughout this work.

CHAPTER 5

Experimental Tests and Results

This chapter aims to elucidate the reader on how applying the previously established procedure is possible to diagnose motor bearing faults. For this purpose, a series of measurements were performed on the SpectraQuest Machine Fault Simulator (MFS) at Siemens SISW facilities in Leuven, Belgium, where the present work was developed. Siemens SISW is leading provider of product life-cycle and manufacturing operations management software worldwide. It aims to optimize its clients processes by proper planning and development of manufacturing operations and support. SpectraQuest (SQ) is a company that focuses on mechanical structures built for the singular purpose of mechanical damage study and assessment.

5.1 Experimental Setup

Figure 5.1 shows the test rig provided by SpectraQuest, along with the sensors in place for the performed measurements. The test rig in use for the present work allows researchers to run small machinery pieces under both healthy and faulty conditions so that afterwards diagnosis through signal processing can be further investigated.

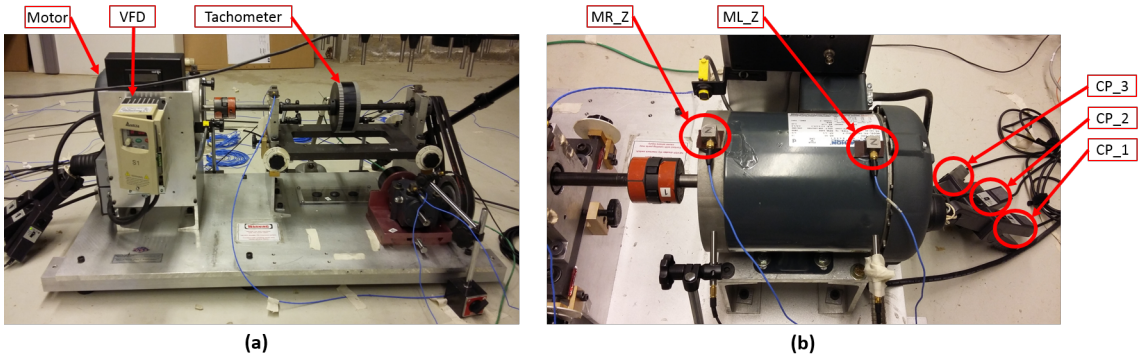

Figure 5.1: Experimental Setup: (a) Test rig; (b) Sensors to analyse.

The sensor cases that were analysed in the present text refer to the accelerometer placed on top of the left side of the motor (from the front view on (a)) from here on designated as MLz, and the three current probes (designated as CP1, CP2 and CP3), placed on the motor supply cables. For analysis of motor bearing faults, two motors were provided with this test bench: one healthy motor and one with an undetermined bearing fault. Hence, for

determining the exact fault condition signal processing will be performed on the measured signals.

To investigate fault conditions it is usual to resort to features, or Condition Indicators (CI). For bearings, the indicators analysed were their characteristic fault frequencies in the Fourier spectrum and the Cyclic Spectral Correlation map. The bearing characteristic fault frequencies can be calculated once their geometric properties are known. Regarding the operational conditions of the testing, the measurements were taken for speeds ranging from 300 rpm to 2700 rpm, with increments of 240 rpm, making a total of 11 cases, though only 6 were chosen for the present analysis. It was considered in an initial stage that the higher rotational speeds would provide better results for the performed analysis. For the particular case in which the motor was operating at 1980 rpm (33 Hz), it was found that an extreme level of vibration occurred in the test rig. As such, considering the possibility that this operating condition could excite a resonance of the whole structure, this particular case was disregarded. For this bearing's particular case, its properties and fault frequencies for each analysed speed are listed as follows:

Bearing Model	NSK 6203
Type of Rolling Element	Ball
Nr. of Rolling Elements	8
Diameter of Rolling Element [cm]	0.266
Diameter Pitch [cm]	1.142
Contact Angle [°]	0

Table 5.1: Bearing Properties

Speed [rpm]	Speed [Hz]	BPFO [Hz]	BPFI [Hz]	FTF [Hz]	BSF [Hz]
1260	21	64.434	103.566	8.054	42.633
1500	25	76.708	123.292	9.588	50.754
1740	29	88.981	143.019	11.123	58.874
2220	37	113.527	182.473	14.191	75.116
2460	41	125.800	202.200	15.725	83.236
2700	45	138.074	221.926	17.259	91.357

Table 5.2: Bearing Fault Frequencies

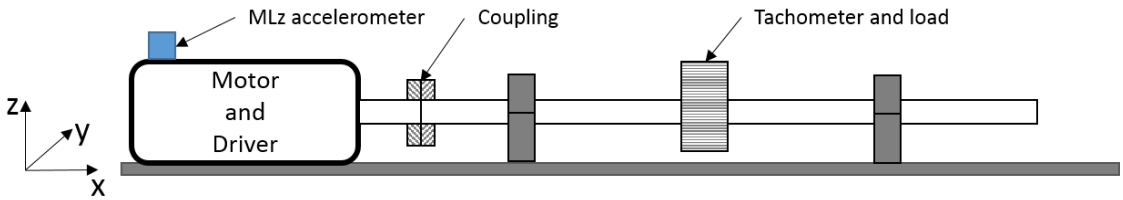

Figure 5.2: Test bench schematic: Axis definition.

Though there are two triaxial accelerometers placed on the motor, the one selected for analysis was MLz. The reason for this will be presented in the preliminary analysis. The z term in its designation refers to the z direction that was analysed, as it was perpendicular to the motor housing surface. The accelerometer axes directions can be viewed in figure 5.2.

For electric isolation purposes, the accelerometers were first glued on to a small wooden plaque covered in varnish, which was then glued on to the motor. Another purpose of the present investigation was to compare the processing results of the current signals to that of the accelerometer signals to check if they would provide viable information regarding the fault condition and to try to understand to what extent the same signal processing stages could be applied to both sets of signals. The following sections refer to a sequence of analysis stages performed during the present work.

5.2 Preliminary Analysis

As mentioned in the beginning of the present chapter, the bearing fault in the motor was undetermined, meaning that there was no previous knowledge of which was the faulty bearing, nor what kind of fault had been planted. As bearings on each end of the motor are of identical geometrical characteristics, hence, current signals were not found useful in determining which was the faulty bearing, as they are not able to perform such a distinction. As such, and because accelerometers were placed *in loco*, their signals were compared for several measurements, to try to find relevant changes in condition of the bearings on each end of the motor.

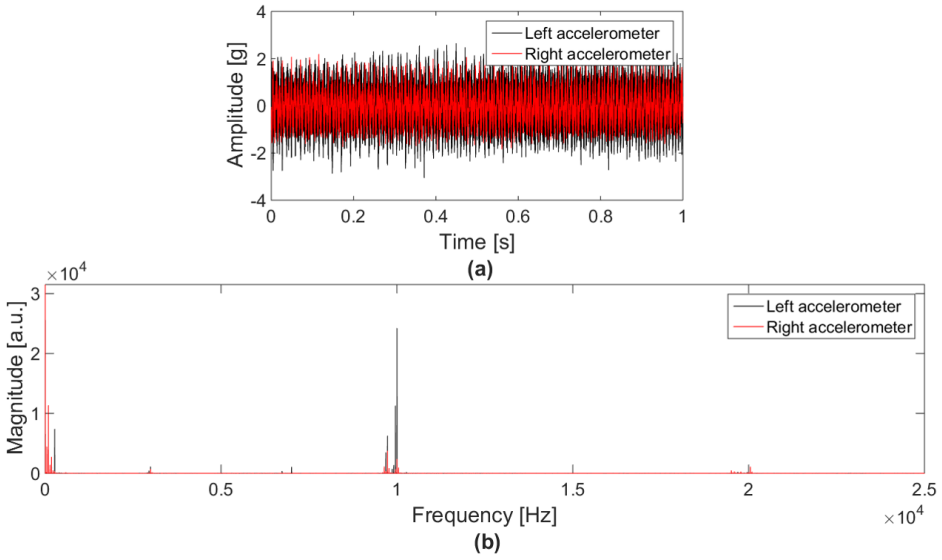

Figure 5.3: Accelerometers' signals comparison: (a) Time-domain signals; (b) Spectra of the signals.

Figure 5.3 presents the results for accelerometer MLz and MRz compared when the motor was running at 2700 rpm. This can be considered a representative case, as what is presented in the time domain signal plot was also confirmed for several other measurements. In these plots, the MLz signal proved to have higher amplitude components, and thus, assumed that it was closer to the faulty bearing.

5.2.1 Spectra

After determining which sensors should be analysed, the preliminary analysis took place. First, we began by plotting the spectra of both raw signals and then of the enveloped

raw signals. In the raw signals' spectra one can often visualize some excitations in high-frequency ranges. In some of those high-frequency ranges, modulation components can sometimes be seen. The terminology *enveloped signal* refers to the signal demodulated by applying a Hilbert transform to remove the carrier frequency effect. Thus, it is sometimes possible to observe in enveloped signals' spectra, the characteristic fault frequencies in low frequency ranges.

However, just by applying demodulation on the signal, relevant diagnostic information could not be extracted. The raw spectra, on the other hand, were quite useful for excited bands' identification.

Some examples are shown in figure 5.4.

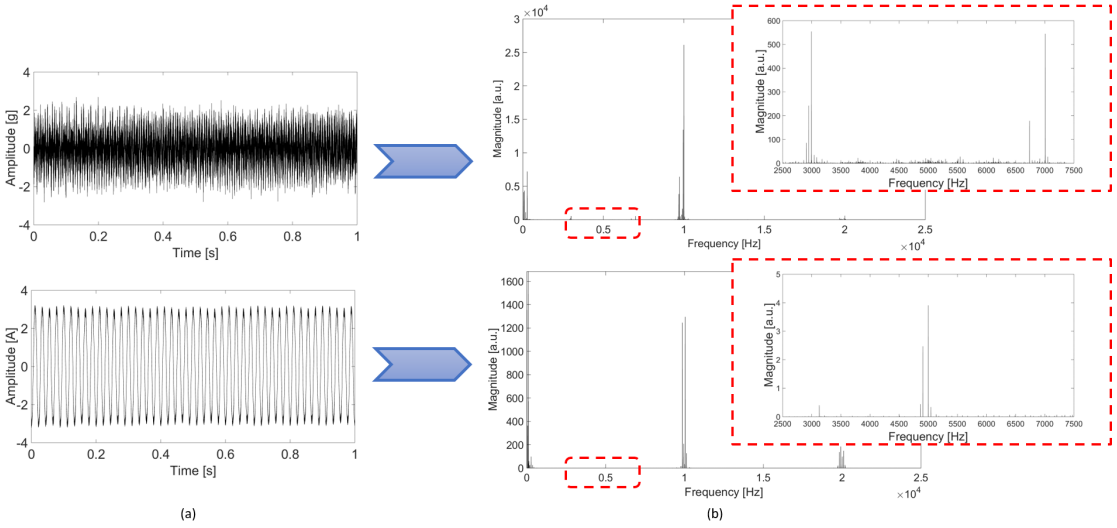

Figure 5.4: Spectra evaluation for excited bands: (a) Time-domain acceleration and current signals; (b) Spectra of the respective signals.

Note that in both spectra, but mainly in the one of the current signal, the 5 kHz region is severely excited, as well as at 10 kHz. These regions were considered to be under electromagnetic influence, with the 10 kHz component being the main contribution, as it is of common choice, and the 5 kHz as being a sub-harmonic of the 10 kHz. Hence, for analysis purposes these regions of the spectrum were disregarded for most of the present work. The presence of BSF and shaft modulations appears to be seen in some ranges.

The figures present the signals analysed for the accelerometer signal of the faulty motor running at 2700 rpm.

5.2.2 Pre-processing

Pre-processing techniques like the Cepstrum offer severe advantages in terms of reducing discrete frequency components that often mask bearing information in the signal. A representation of the signals before and after cepstral editing is shown in figure 5.5. Note that in this figure there are noticeable periodic components in the original signal that are removed after cepstral editing is performed.

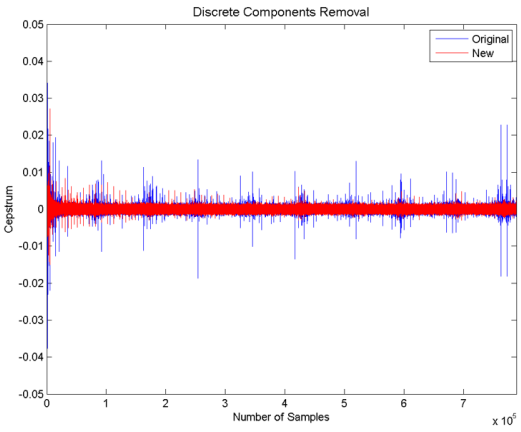

Figure 5.5: Cepstral editing: before and after.

These benefits are also clearly visible once the signals' spectra are plotted. Remember that after cepstral editing is performed, the time domain signal can be retrieved. Thus, figure 5.6 presents both spectra: before and after cepstral editing. This procedure accounts for a severe reduction in discrete frequency components, as well as their side-bands. This allows us to obtain a residual signal carrying the bearing fault related information.

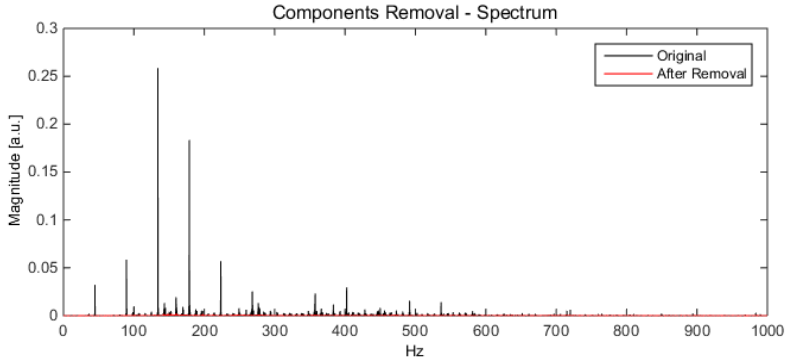

Figure 5.6: Spectrum of cepstral edited signal.

The figures present the signals analysed for the accelerometer signal of the faulty motor running at 2700 rpm.

5.2.3 Determining Optimum Filtering Band

After the pre-processing of the signal, it is usual to apply a tool to detect which frequency bands are most excited. Now that discrete frequency components have been removed, their effect in detection of those bands should not be a factor of influence.

Kurtogram

The fast kurtogram was a tool that was used throughout most of this work. Some representative results are shown in figures 5.7 and 5.8.

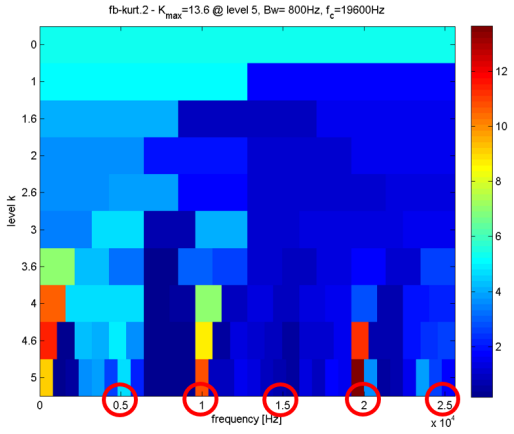

Figure 5.7: Kurtogram of the accelerometer signal.

Results shown from the kurtogram applied to the accelerometer signal proved that the signal is still affected by electromagnetic interference. The regions circled in red represent areas in which electromagnetic interference is expected, and the maximum kurtosis value is represented in precisely one of those areas.

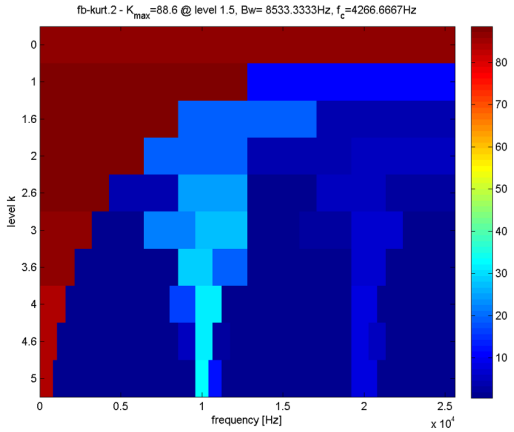

Figure 5.8: Kurtogram of the current signal.

The current signal however, appears to keep its regular nature. Remember that, though the measured signal may appear sinusoidal, by the way it is generated it still consists of pulses. Even though, in theory, the application of the Cepstrum is suppose to remove discrete frequency components, in practice that does not happen when processing the PWM signals. Hence, they maintain their broadband impulsiveness. It is also important to point out that, although the maximum kurtosis does not occur in the first level of the kurtogram, the kurtosis value presented at that level by the current signal is still very high (pretty close to the maximum value). In such cases, the signal can be classified as broadband impulsive, with no distinctive frequency bands of interest to be identified. In such cases, filtering is not performed, and we would resort to the demodulation of the signal by obtaining its envelope.

Overall, the kurtogram proved to be an ineffective filter detection tool when faced with electromagnetic interference due to the PWM effect.

Cyclic Spectral Correlation

The Cyclic Spectral Correlation was applied in the same stage as the fast kurtogram. Since they are both tools that are able to present high-frequency excitations, their application here seems obvious. The goal of this technique remains the same of the kurtogram: being able to identify excited frequency bands for applying envelope analysis. A major setback of this method however is that its computation is severely costly, in case one does not strict to a narrow frequency range. Bearing this in mind, the first processed plots only ranged up to 30 Hz in the x axis (representing cyclic frequencies).

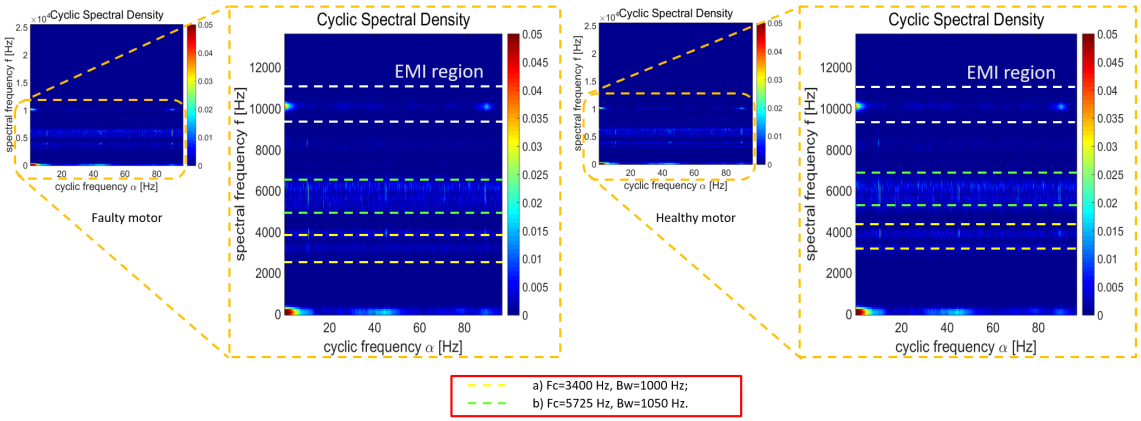

Figure 5.9: CSC maps representation for both faulty and healthy cases.

Figure 5.9 presents the results. The case of application remains the same: accelerometer signal of the faulty motor at 2700 rpm. Modulation bands at higher frequencies are clearly visible in both CSC maps.

As such, two filters were identified by this procedure: filter a), with centre frequency of 3400 Hz and band-width of 1000 Hz, and filter b) of centre frequency 5725 Hz and bandwidth 1050 Hz. Determining these values was possible after analysis of all six cases referred in section 5.1.

Note that the PWM effect still appears to be present in the CSC maps at 10 kHz.

5.3 Analysis of Processed Signals

After being able to identify modulated frequency bands, envelope analysis was performed on the signals. Hence, band-pass filters were applied according to the previously established parameters, in order to improve the signal-to-noise ratio in those bands. The signals were then demodulated and their envelopes' spectra were analysed. These spectra can be observed in figures 5.10 and 5.11.

Markers were included in the spectra plots, where green markers represent the shaft rotation frequency and its harmonics, whereas the red markers represent the fault frequency and its harmonics. The real rotational speed measured in the raw signal's spectrum was

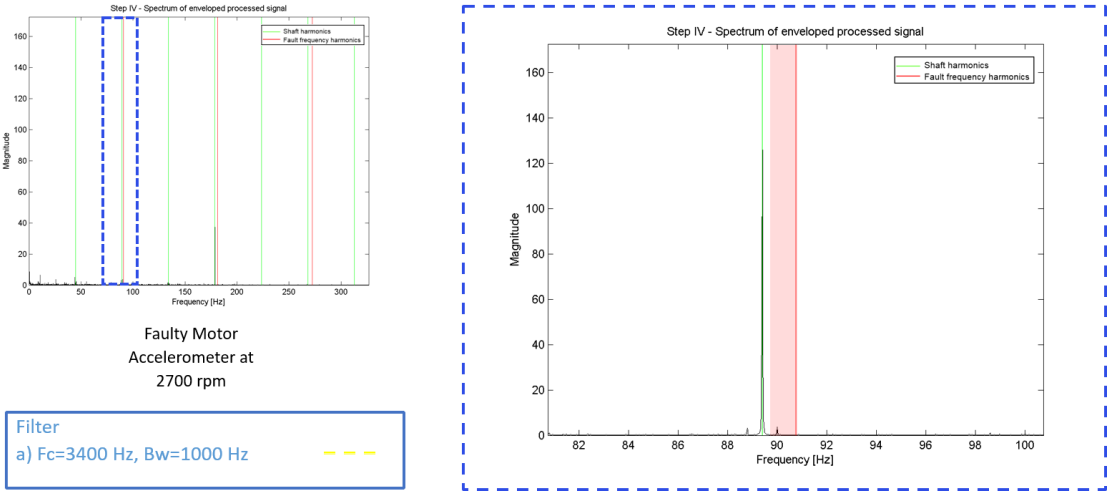

Figure 5.10: Signal processed with filter a) spectrum.

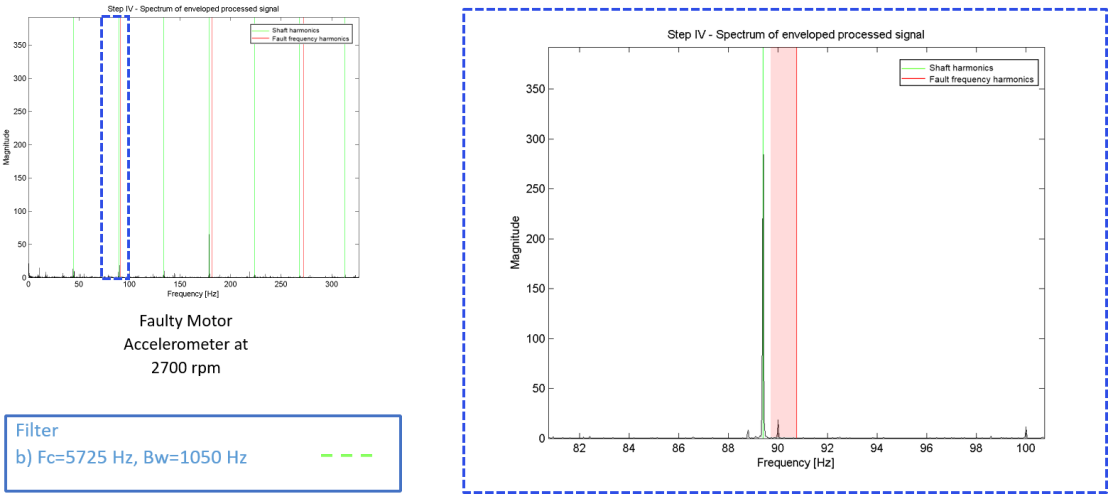

Figure 5.11: Signal processed with filter b) spectrum.

used for this calculation. However, remember that the bearing fault frequencies calculations are based on pure kinematic relations. In practice, it is duly noted in the literature that an average $1-2\%$ deviation from the frequencies' calculated values can occur due to the bearing slip [12]. A 2% deviation is represented by the red shadow area.

However, by analysing these spectra, we cannot visualize any relevant information related to the fault presence, even though one can notice a slight increase in amplitude at 90 Hz from filter *a)* to filter *b)*. So, at this point it is only logical for one to wonder what has happened during the performed analysis.

When confronted with such cases, it is often good practice to take a step back in the analysis to check what could have been missed during the processing stage. Therefore, by taking a closer look into the faulty case represented in figure 5.9, the results presented in figure 5.12 were found.

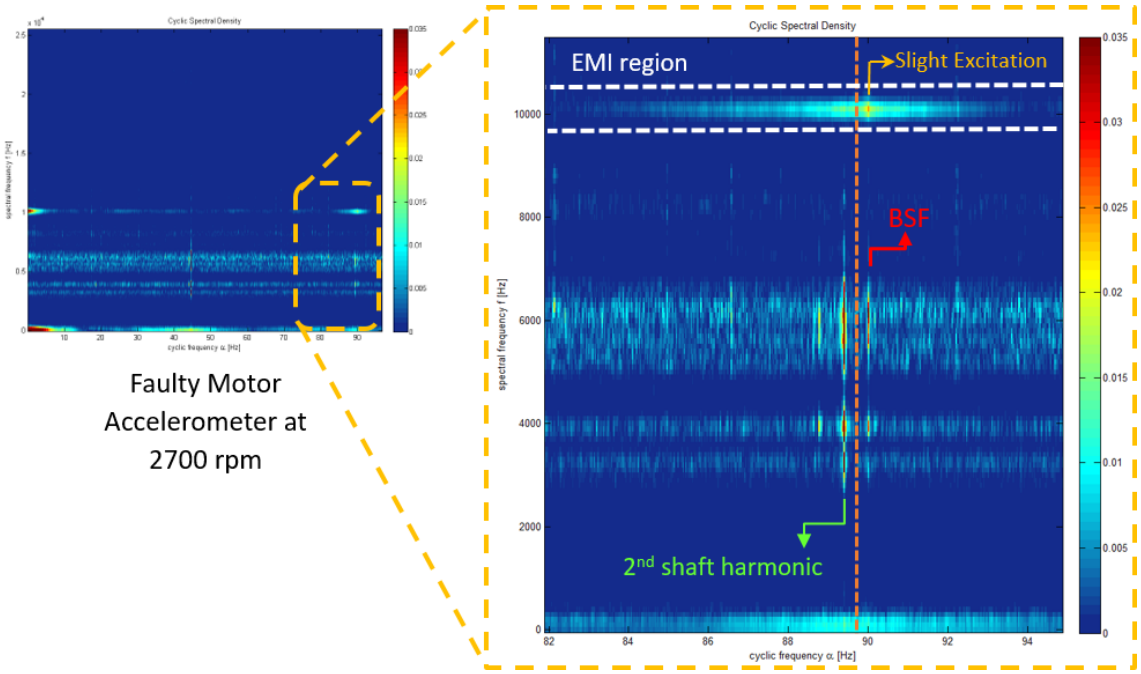

Figure 5.12: CSC map representation for faulty motor's accelerometer at 2700 rpm.

Note that the BSF can be distinguished from the second harmonic of the shaft speed. However, they are modulated in the same frequency band, with the shaft component being much higher in magnitude, leading to the previously seen result in the spectrum, after applying filter b). However, there is a slight excitation in the EMI affected region. Thus, this region was now selected for analysis. The spectral correlation maps were once again analysed for all cases to determine filter parameters. The parameters established for this case are: centre frequency of 10 kHz and band-width of 1000 Hz.

Results of CSC maps and spectra are now presented for some cases from figure 5.13 to figure 5.18. On a final note, for establishing filter parameters in the present analysis, it was taken into consideration a stated fact in [27] where it is said that narrower frequency bands help to enhance signal-to-noise ratio in envelope analysis in cases where EMI is a factor of influence.

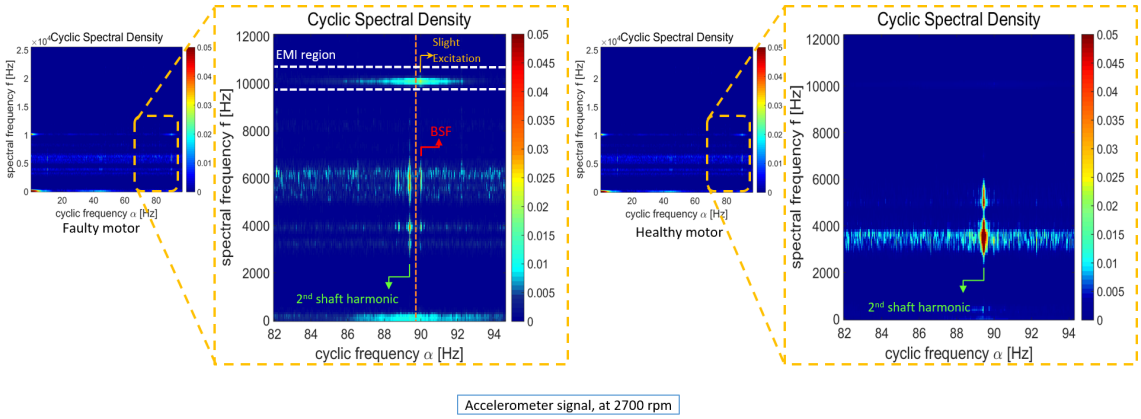

Figure 5.13: CSC map for accelerometer signal at 2700 rpm.

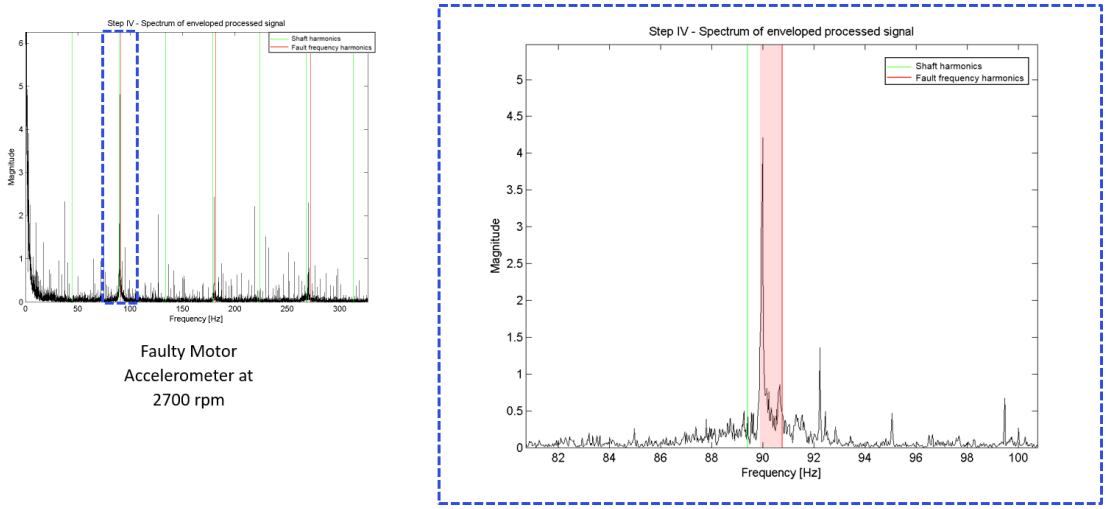

Figure 5.14: Feature analysis for accelerometer signal at 2700 rpm.

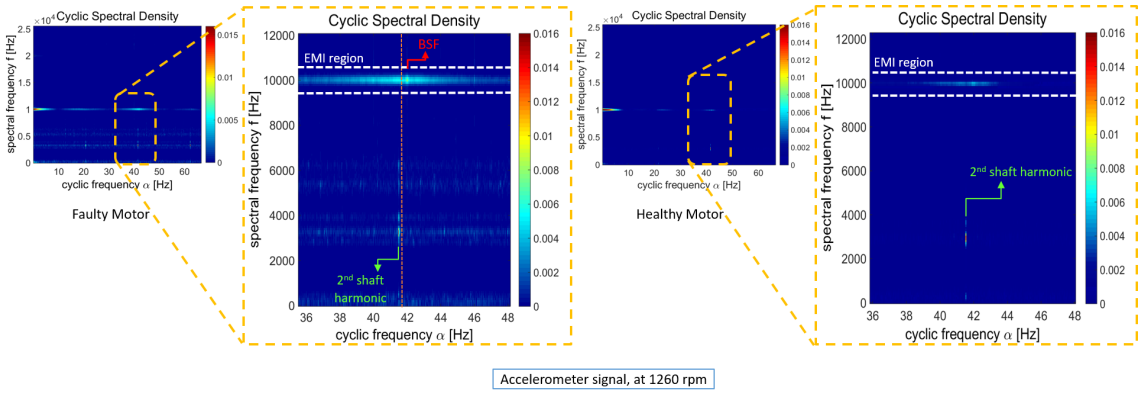

Figure 5.15: CSC map for accelerometer signal at 1260 rpm.

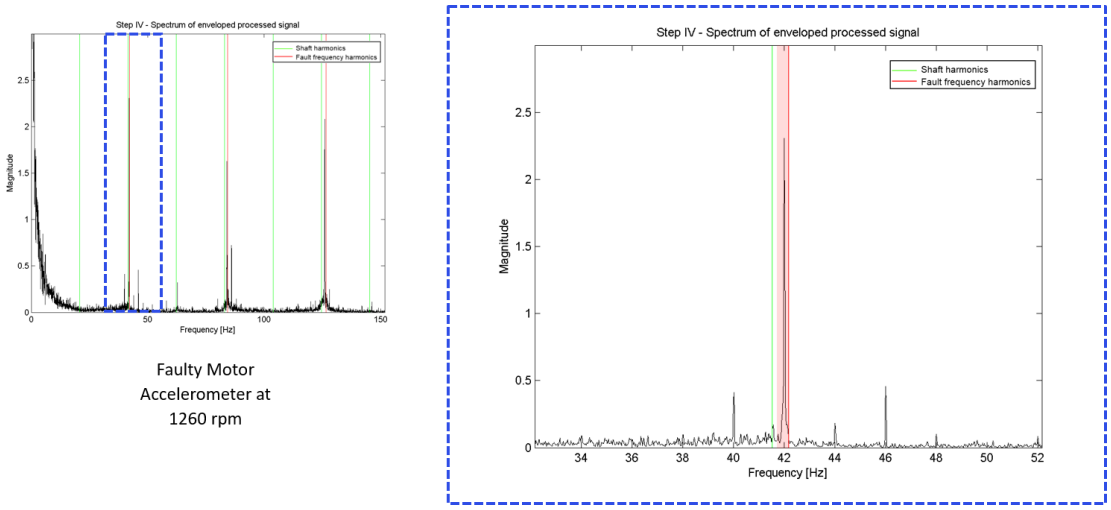

Figure 5.16: Feature analysis for accelerometer signal at 1260 rpm.

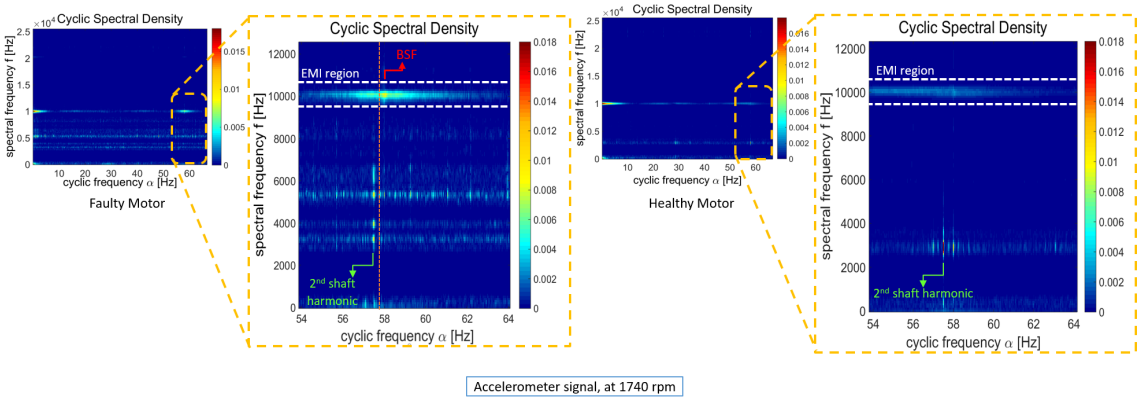

Figure 5.17: CSC map for accelerometer signal at 1740 rpm.

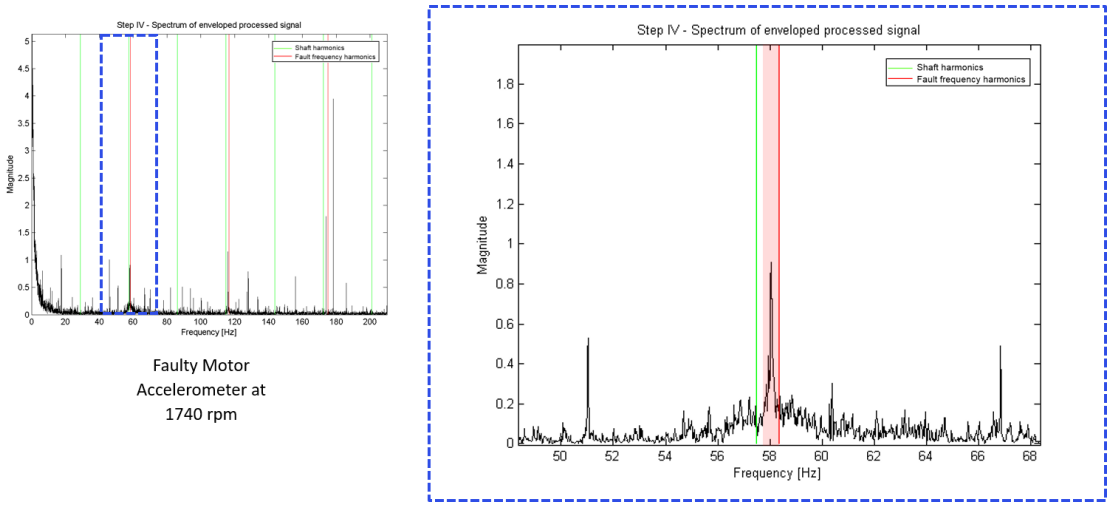

Figure 5.18: Feature analysis for accelerometer signal at 1740 rpm.

There are some noteworthy considerations to be made regarding the presented results. Note that the fault frequency in the spectrum corresponding to the BSF is now inside the $1-2\%$ frequency deviation range. Plus, that component matches exactly the one observed in the CSC map, in the cyclic frequency axis.

As this was proven to be the most effective procedure, it was also applied to the current probe signals. The results for the case in which the motor was running at 2700 rpm are shown in figures 5.19, 5.20 and 5.21. Note that this time, there is no modulation represented in the cyclic spectral correlation map. Besides, the 90 Hz in this case is considered to be the second harmonic of the shaft rotation speed instead of the fault frequency. Why? For the simple reason that 90 Hz is exactly twice of the set speed on the drive. Notice that for the accelerometer case at this speed, the second harmonic of the shaft frequency was $89,4$ Hz and the BSF of 90 Hz. The rotational speed is slightly lower due to the rotor slip, thus also resulting in a slight reduction of the estimated fault frequency. The electrical response however, is practically instantaneous. Additionally, there are no modulation effects visible in the current probe's CSC maps, and no fault-related information as well. By visualizing the spectra, this analysis is confirmed. Note that new markers have been included in the spectra, represented in blue. These markers are related to characteristic bearing fault frequencies that were found in [29] and are described by equation 5.1:

$$f'_{bf} = |f_s \pm f_r \pm k \times f_{bf}| \tag{5.1}$$

where f_s is the supply frequency (50 or 60 Hz), f_r corresponds to the shaft rotation frequency, f_{bf} is a bearing fault characteristic frequency, and k an integer.

It is clear that these components appear in the spectra of raw current signals. However, their combination was not clear after the processing was performed.

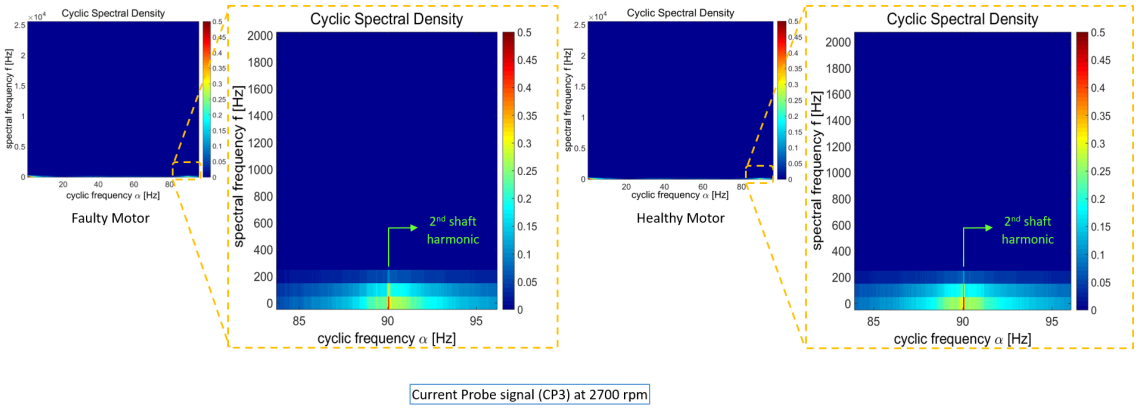

Figure 5.19: CSC map for CP3 signal at 2700 rpm.

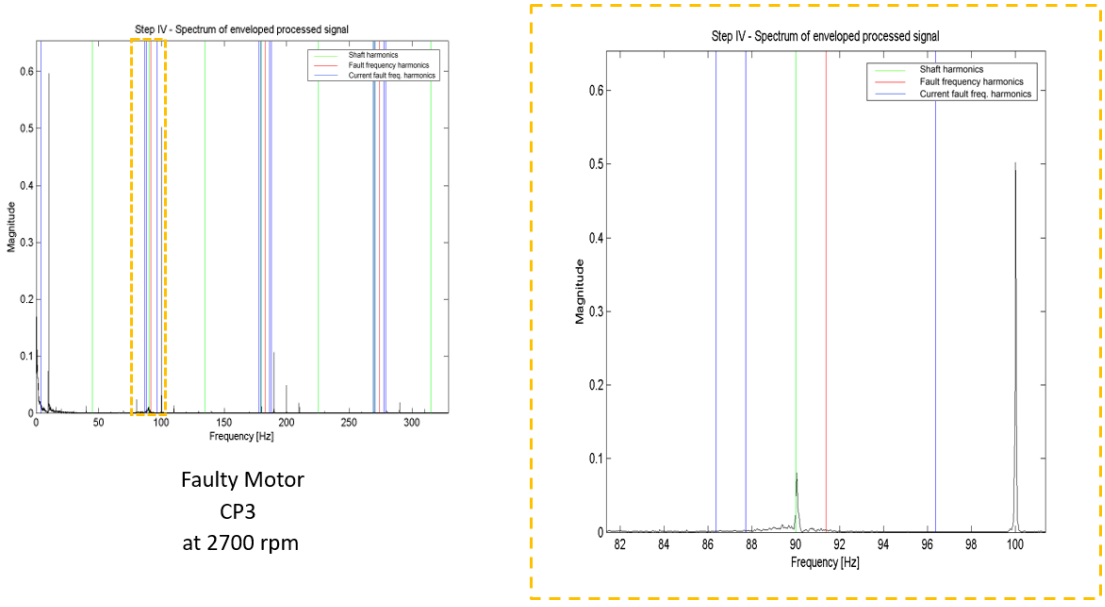

Figure 5.20: Feature analysis for CP3 signal at 2700 rpm (faulty motor).

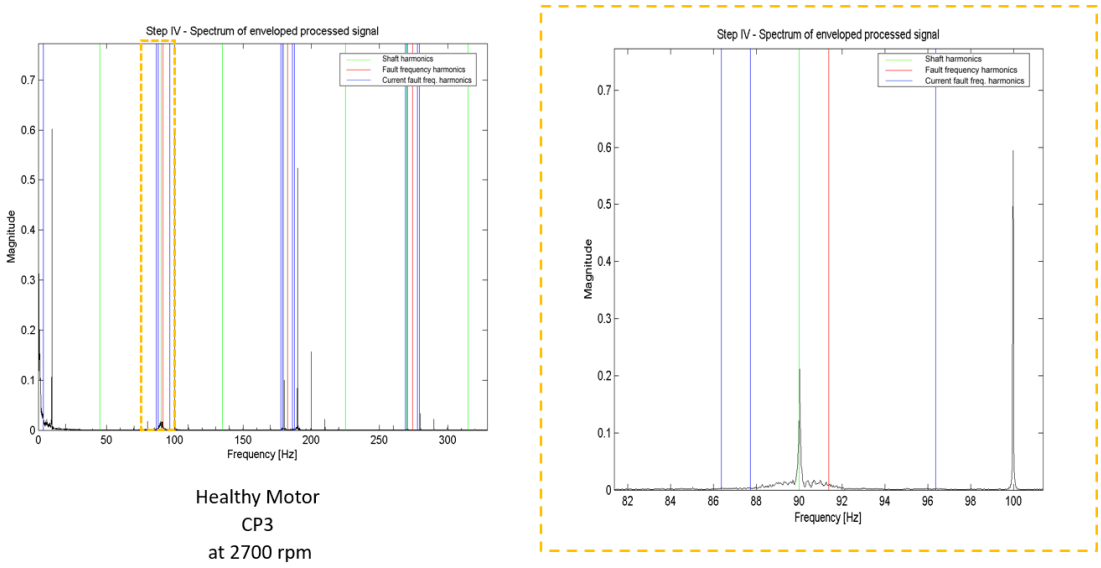

Figure 5.21: Feature analysis for CP3 signal at 2700 rpm (healthy motor).

5.4 MED influence

One of the purposes of the present work was also to assess to what extent the inclusion of an adaptive filter for our analysis could be beneficial. Therefore, the MED filter was included right after our pre-processing stage, but prior to the application of filter detection tools such as the fast kurtogram and the cyclic spectral correlation. Afterwards, envelope analysis was also performed.

The effect of the MED filter on the fast kurtogram and on the CSC can be seen in figures 5.22 and 5.23, respectively.

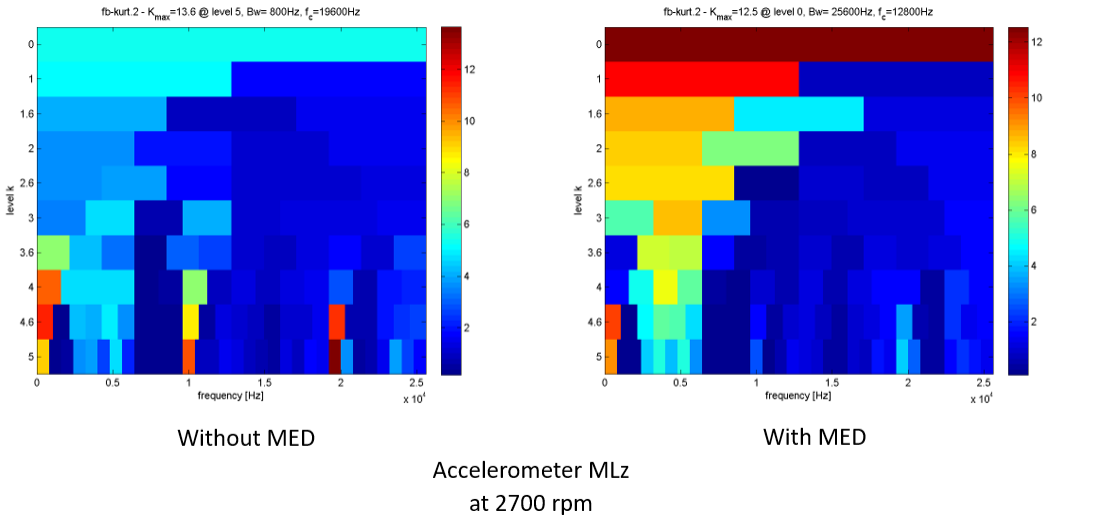

Figure 5.22: Kurtogram results for accelerometer signal at 2700 rpm.

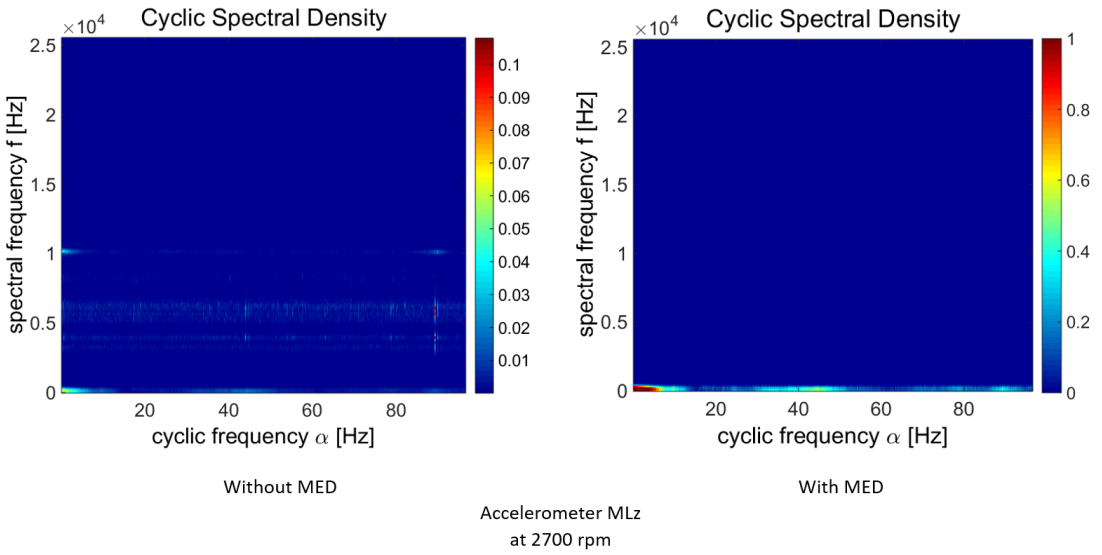

Figure 5.23: CSC results for accelerometer signal at 2700 rpm.

Notice that when the MED is applied, the kurtogram shows maximum kurtosis values at the first level, meaning that the signal is overall impulsive. On the spectral correlation maps, modulation effects may become less clear.

The inverse filter response of the MED algorithm is based on the assumption that the original signal is as impulsive as possible and tries to retrieve it. In the case of bearing fault detection, characteristic frequencies are usually low, but modulated at high frequencies. In the case presented for the faulty motor's accelerometer, with the motor running at 2700 rpm, modulation effects were no longer noticeable. This was, however, a particular case. There are others, such as those presented in figures 5.24 and 5.25, where some modulations can be seen, especially in the EMI affected region, although the fault related information becomes less obvious. Overall, the most significant loss of information was related to shaft speed harmonics after applying the MED. Consequently, for the present analysis, the CSC maps obtained after applying the MED filter were not of much use in detecting the bearing fault information, by themselves alone.

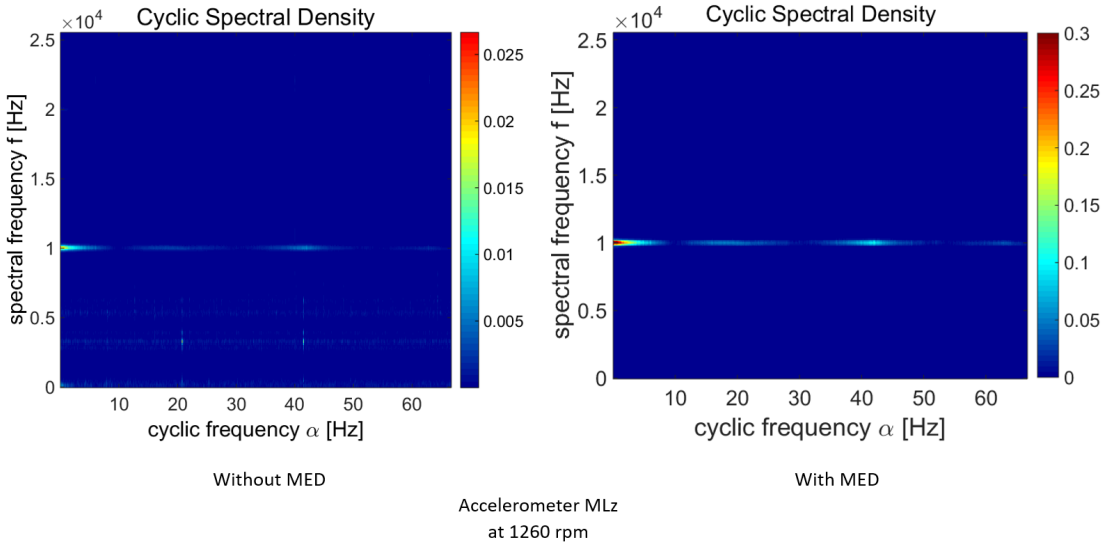

Figure 5.24: CSC results for accelerometer signal at 1260 rpm.

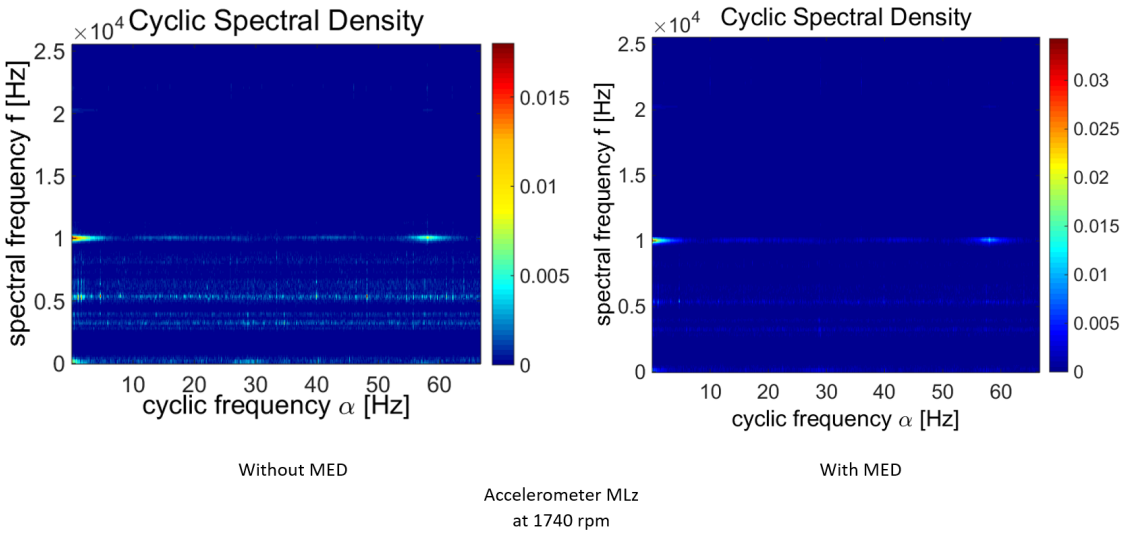

Figure 5.25: CSC results for accelerometer signal at 1740 rpm.

Since the fast kurtogram initially showed the signal to be broadband impulsive, the signal was not filtered, but only subject to demodulation. Two spectra are compared for different filter parameters in figure 5.26. These signals are relative to the faulty motor.

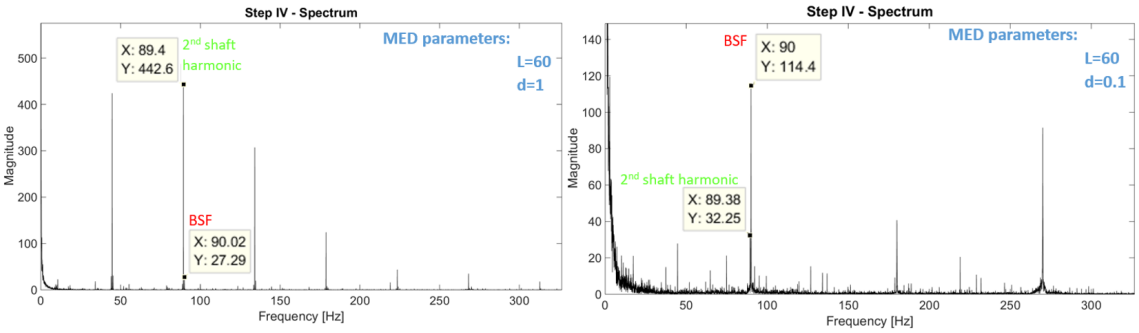

Figure 5.26: Feature analysis for accelerometer signal at 2700 rpm (faulty motor).

A clear difference can be seen between both spectra. When the correct filter parameters are inserted, fault information can be revealed. Parameter L refers to filter length, and d is a delta term that represents the difference in kurtosis between iterations allowed for stopping the iterative process. However, if one is not familiarized with the method, parameter study by trial and error is very time consuming, and there are probably analysis tools available that would not justify this additional effort. Additionally, the MED algorithm computation can prove to be very time-costly, depending on the nature of the signal one is analysing, and also on the filter parameters that are set.

CHAPTER 6

Conclusion

6.1 Conclusions

At the end of the present work, some important conclusions are now mentioned:

- Pulse-width modulated (PWM) signals from variable-frequency drives mirror the main characteristics of fault signatures: periodicity and impulsiveness. As such, for bearing diagnostic purposes, they can pose a severe limitation.
- High electromagnetic interference (EMI) around 5kHz, 10kHz and 20kHz poses as limitation for applying the fast kurtogram.
- Even though the Cyclic Spectral Correlation (CSC) is also affected by EMI, it is still a very powerful tool for analysing cyclostationary signals, such as those produced by bearing faults.
- Application of the Minimum Entropy Deconvolution (MED) algorithm before using filter detection tools was ineffective, for the selected filter parameters. It enhances all impulsive components in the whole signal, making it more difficult (or even unnecessary) to determine an optimum filtering band.
- Application of Cepstrum significantly reduces the presence of discrete frequency components present in the signal, as well as their side-bands. However, it is not able to remove them completely.

  The justification for this fact is that, when in presence of EMI generated by variable frequency drives (VFDs), discrete components, such as that of the shaft rotation, can be modulated by the EMI due to large line to ground voltage transients that occur in the VFD. Several transients line up in phase, generating a signal of high-order cyclostationarity [27].
- Possible misalignment of the shaft may lead to an increase of the shaft speed harmonics' amplitudes.
- It is possible that because the supposed eccentricity generated by the fault impulse is very small in amplitude, the changes of inductances will not produce a visible current frequency when compared to other components of the spectra.
- At this point of the present work, no viable diagnostic information regarding the bearing fault could be extracted from the current signals.

6.2 Future works

After conclusion of this work, some future developments on this topic are now suggested:

- Further investigation of the MED filter's parameters is required, for proper detection of fault signatures.
- Further understanding of the nature of the VFD, as well as of the current signals should be investigated to confirm this analysis and identify other components present in the spectra.
- Application of an optimized spectral kurtosis tool for filter detection, under EMI conditions could be tested to help validate a new filter detection alternative [27].
- Analysis of cyclostationarity indicators has also been proven of interest and more effective, even under EMI conditions [27].

Bibliography

[1] KU Leuven and K Gryllias. Condition Monitoring, 2015.

[2] ALcontrol. Benefits of Oil Analysis with ALcontrol.

[3] Robert Bond Randall. *Vibration-Based Condition Monitoring: Industrial, Aerospace and Automotive Applications*. 2010.

[4] Stephan J. Chapman. *Electric Machinaery Fundamentals*. Jones, Elizabeth A., 4th edition, 2005.

[5] Subrata Karmakar, Surajit Chattopadhyay, Madhuchhanda Mitra, and Samarjit Sengupta. *Power Systems Induction Motor Fault Diagnosis Approach through Current Signature Analysis*. 2016.

[6] VIBES Corp. and Garret Sandwell. Electrically Induced Bearing Damage & Shaft Currents. Technical report, 2016.

[7] FAG. Rolling Bearing Damage: Symptoms, Causes, Remedies, 2011.

[8] International Conference, Optimization Techniques, Power Electronic, and Technology Hyderabad. Control of Induction Motor Drive using Space Vector. 3(4):3344–3351, 2016.

[9] R Keith Mobley. *An Introduction to Predictive Maintenance (Second Edition)*. Butterworth-Heinemann, 2002.

[10] Amiya R Mohanty. *Machinery Condition Monitoring Principles and Practrices*. CRC Press, 2015.

[11] ALENA; BILOŠOVÁ and JAN BILOŠ. *VIBRATION DIAGNOSTICS*. 2012.

[12] Robert B. Randall and Jrme Antoni. Rolling element bearing diagnostics-A tutorial. *Mechanical Systems and Signal Processing*, 2011.

[13] Paulo Jorge Nascimento and Morais Porto. Condition Monitoring of Bearings under Low and Medium Speed Rotation. Master's thesis, 2016.

[14] Jérôme Antoni. Cyclostationarity by examples. *Mechanical Systems and Signal Processing*, 23(4):987–1036, 2009.

[15] Kihong Shin and Joseph K Hammond. *Fundamentals of signal theory*, volume 270. 1960.

[16] J Antoni, D Abboud, and G Xin. Cyclostationarity in Condition Monitoring: 10 years after. In *PROCEEDINGS OF ISMA*, 2016.

[17] B Kiran Kumar, G Diwakar, and M R S Satynarayana. Determination of Unbalance in Rotating Machine Using Vibration Signature Analysis. *International Journal of Modern Engineering Research*, 2(5):33415–33421, 2012.

[18] KU Leuven and K Gryllias. Condition Monitoring, 2015.

[19] WA Gardner. *Statistical Spectral Analysis A Nonprobabilistic Theory*. Englewood Cliffs, New Jersey 07632, 1988.

[20] Ian Howard. *A review of rolling element bearing vibration:detection, diagnosis and prognosis*. DSTO Aeronautical and Maritime Research Laboratory, Melbourne Victoria 3001, Australia, 1994.

[21] Carina Freitas, Paulo Morais, Jacques Cuenca, Agusmian Partogi Ompusunggu, Mathieu Sarrazin, and Karl Janssens. Condition monitoring of bearings under medium and low rotational speed. In *8th European Workshop On Structural Health Monitoring (EWSHM 2016)*, Bilbao, 2016.

[22] Luisa F. Villa, Aníbal Reñones, Jose R. Perán, and Luis J. De Miguel. Angular resampling for vibration analysis in wind turbines under non-linear speed fluctuation. *Mechanical Systems and Signal Processing*, 25(6):2157–2168, 2011.

[23] Eric Bechhoefer and Michael Kingsley. A review of time synchronous average algorithms. *Annual Conference of the Prognostics and Health Management Society*, pages 1–10, 2009.

[24] Z. K. Peng and F. L. Chu. Application of the wavelet transform in machine condition monitoring and fault diagnostics: A review with bibliography. *Mechanical Systems and Signal Processing*, 18(2):199–221, 2004.

[25] R.B. RANDALL, J. ANTONI, and S. CHOBSAARD. The Relationship Between Spectral Correlation and Envelope Analysis in the Diagnostics of Bearing Faults and Other Cyclostationary Machine Signals. *Mechanical Systems and Signal Processing*, 15(5):945–962, 2001.

[26] Jérôme Antoni and R. B. Randall. The spectral kurtosis: Application to the vibratory surveillance and diagnostics of rotating machines. *Mechanical Systems and Signal Processing*, 20(2):308–331, 2006.

[27] Wade A Smith, Dikang Peng, Zhongxiao Peng, and R B Randall. Electromagnetic interference in vibration signals and its effect on bearing diagnostics. In *11th International Conference on Vibrations in Rotating Machinery*, Manchester, 2016.

[28] Wade A Smith, Zhiqi Fan, Zhongxiao Peng, Huaizhong Li, Robert B Randall, and Robert B. Smith, Wade A.;Fan, Zhiqi;Peng, Zhongxiao; Li Huaizhong; Randall. Optimised spectral kurtosis for bearing diagnostics under electromagnetic interference. *Mechanical Systems and Signal Processing*, 75:371–394, 2016.

[29] Ahmed Alwodai, Tie Wang, Zhi Chen, Fengshou Gu, Robert Cattley, and Andrew Ball. A Study of Motor Bearing Fault Diagnosis using Modulation Signal Bispectrum Analysis of Motor Current Signals. *Journal of Signal and Information Processing*, 4:72–79, 2013.